

NAVAL POSTGRADUATE SCHOOL

Monterey, California



THESIS

ELECTRICALLY PROPELLED HANG GLIDER FOR SMALL UNIT BATTLEFIELD MOBILITY

by

Rodney S. Nolan

June 1999

Thesis Advisor:

Xiaoping Yun

Approved for public release; distribution is unlimited.

REPORT DOCUMENTATION PAGE			Form Approved OMB No. 0704-0188	
Public reporting burden for this collection of information is estimated to average 1 hour per response, including the time for reviewing instruction, searching existing data sources, gathering and maintaining the data needed, and completing and reviewing the collection of information. Send comments regarding this burden estimate or any other aspect of this collection of information, including suggestions for reducing this burden, to Washington Headquarters Services, Directorate for Information Operations and Reports, 1215 Jefferson Davis Highway, Suite 1204, Arlington, VA 22202-4302, and to the Office of Management and Budget, Paperwork Reduction Project (0704-0188) Washington DC 20503.				
1. AGENCY USE ONLY (Leave blank)		2. REPORT DATE June 1999		3. REPORT TYPE AND DATES COVERED Master's Thesis
4. TITLE AND SUBTITLE ELECTRICALLY PROPELLED HANG GLIDER FOR SMALL UNIT BATTLEFIELD MOBILITY			5. FUNDING NUMBERS	
6. AUTHOR(S) Nolan, Rodney S.				
7. PERFORMING ORGANIZATION NAME(S) AND ADDRESS(ES) Naval Postgraduate School Monterey, CA 93943-5000			8. PERFORMING ORGANIZATION REPORT NUMBER	
9. SPONSORING / MONITORING AGENCY NAME(S) AND ADDRESS(ES) Space and Naval Warfare System Center - San Diego San Diego, CA 92152-5001			10. SPONSORING / MONITORING AGENCY REPORT NUMBER	
11. SUPPLEMENTARY NOTES The views expressed in this thesis are those of the author and do not Reflect the official policy or position of the Department of Defense or the U.S. Government.				
12a. DISTRIBUTION / AVAILABILITY STATEMENT Approved for public release; distribution is unlimited.			12b. DISTRIBUTION CODE	
13. ABSTRACT (maximum 200 words) On the high speed, info-centric, dispersed battlefield of the future, information dominance will require increased small unit battlefield mobility. The trend of the future will be towards smaller units responsible for scouting, securing, and shaping the battlefield prior to a larger, heavier force being injected at the crucial time and place to decisively engage the enemy. This light scouting, shaping force has a need for some type of vehicle to provide battlefield mobility, insert, extract, escape and evasion, and re-supply. This thesis explores the possibility of using an electrically powered hang glider for small unit battlefield mobility. This platform is not envisioned to replace other means of insertion such as helicopter, rubber boat, etc. This platform is envisioned to provide mobility for these small units once they have been inserted, especially over terrain that is difficult for foot mobility. This thesis discusses the research concept used to conduct the vehicle design. A proposal for an optimal system design using commercially available components is given along with a description of the capabilities and limitations of the platform.				
14. SUBJECT TERMS Information Dominance, Reconnaissance, Battlefield Mobility, Aerial Vehicle.			15. NUMBER OF PAGES 172	
			16. PRICE CODE	
17. SECURITY CLASSIFICATION OF REPORT Unclassified	18. SECURITY CLASSIFICATION OF THIS PAGE Unclassified	19. SECURITY CLASSIFICATION OF ABSTRACT Unclassified	20. LIMITATION OF ABSTRACT UL	

Approved for public release; distribution is unlimited

**ELECTRICALLY PROPELLED HANG GLIDER FOR SMALL UNIT
BATTLEFIELD MOBILITY**

Rodney S. Nolan
Major, United States Marine Corps
B.A., Auburn University, 1979


Submitted in partial fulfillment of the
requirements for the degree of

MASTER OF SCIENCE IN ELECTRICAL ENGINEERING


from the

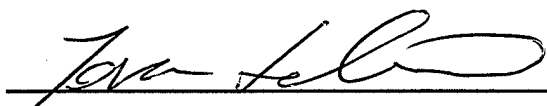
**NAVAL POSTGRADUATE SCHOOL
June 1999**

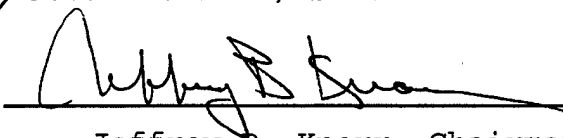
Author:


Rodney S. Nolan

Approved by:


Xiaoping Yun, Thesis Advisor


Jovan Lebaric, Second Reader


Jeffrey B. Knorr, Chairman
Department of Electrical and
Computer Engineering

ABSTRACT

On the high speed, info-centric, dispersed battlefield of the future, information dominance will require increased small unit battlefield mobility. The trend of the future will be towards smaller units responsible for scouting, securing, and shaping the battlefield prior to a larger, heavier force being injected at the crucial time and place to decisively engage the enemy. This light scouting, shaping force has a need for some type of vehicle to provide battlefield mobility, insert, extract, escape and evasion, and re-supply. This thesis explores the possibility of using an electrically powered hang glider for small unit battlefield mobility. This platform is not envisioned to replace other means of insertion such as helicopter, rubber boat, etc. This platform is envisioned to provide mobility for these small units once they have been inserted, especially over terrain that is difficult for foot mobility. This thesis discusses the research concept used to conduct the vehicle design. A proposal for an optimal system design using commercially available components is given along with a description of the capabilities and limitations of the platform.

TABLE OF CONTENTS

I. INTRODUCTION.....	1
A. GENERAL	1
B. PROBLEM STATEMENT	2
C. OUTLINE OF THE THESIS	3
II. RESEARCH CONCEPT	5
A. MISSION REQUIREMENTS.....	5
1. <i>Constraints</i>	6
2. <i>Requirements</i>	6
B. START WITH WHAT IS ALREADY KNOWN	7
III. AERODYNAMICS	9
A. WHAT IS REQUIRED TO FLY	9
IV. ELECTRICAL COMPONENTS.....	23
A. GENERAL ELECTRIC MOTOR DESIGN	23
B. PERMANENT MAGNET MOTOR	25
C. PERMANENT MAGNET BRUSHLESS DIRECT CURRENT MOTOR.....	26
V. POWER SOURCE.....	31
A. GENERATING CURRENT.....	31
B. BATTERIES	32
C. FUEL CELL.....	34
D. GENERATORS	35
VI. OPTIMAL DESIGN	37
A. OPTIMIZING THE SYSTEM.....	37
B. FOOT LAUNCHED MICRO LIGHTS (FLML)	37
1. <i>Major Types</i>	37
2. <i>Placement of Motor and Propeller</i>	41
C. MOTOR AND PROPELLER.....	47
1. <i>FLML Flight Parameters</i>	47
2. <i>Motor and Propeller Tradeoffs</i>	49
D. POWER SOURCE CONSIDERATIONS.....	59
1. <i>Battery</i>	59
2. <i>Fuel Cell</i>	61
3. <i>Generator</i>	61
4. <i>Analysis of Power Requirement for Electrically Propelled Hang Glider</i>	62
VII. DESIGN PROPOSAL FOR A RECONNAISSANCE AND INTELLIGENCE DELIVERY EQUIPMENT (RIDE) SYSTEM.....	69
A. HANG GLIDER DESIGN	69
B. METHOD OF MOUNTING THE MOTOR AND PROPELLER	72
C. MOTOR, CONTROLLER AND PROPELLER	73
D. POWER SOURCE SELECTED	76
1. <i>Tradeoffs for Different Power Sources</i>	76
VIII. CONCLUSIONS AND FOLLOW ON RESEARCH	79

A. CONCLUSIONS	79
B. FOLLOW ON RESEARCH	81
LIST OF APPENDICES	85
A. PROPELLER THEORY [REF. 6]	85
B. PARASITE DRAG COEFFICIENT DERIVATION [REF. 13]	113
C. BATTERY TECHNOLOGY [REF. 15 & 16]	117
D. SCHEMATICS OF MOTOR AND CONTROLLER [REF. 8 & 18]	125
E. FUEL CELL TECHNOLOGY [REF. 17]	151
LIST OF REFERENCES	157
INITIAL DISTRIBUTION LIST	159

LIST OF FIGURES

Figure 1 Hang Glider Frame Pagen [Ref. 11]	15
Figure 2 Forces Acting on the Glider Pagen [Ref. 11]	16
Figure 3 Pancake Motor for Wheel Chair [Ref. 18]	28
Figure 4 Shell Type Armature Motor for Antenna Adjustment	29
[Ref. 18]	29
Figure 5 Inside Out Motor [Ref. 18]	29
Figure 6 Beginner Hang Glider, Single Surface, Low Aspect Ratio Pagen	
[Ref. 19]	39
Figure 7 Novice Hang Glider, Double Surface, Higher Aspect Ratio Pagen	
[Ref. 24]	40
Figure 8 Expert Hang Glider, Double Surfaced, Very High Aspect Ratio Pagen	
[Ref. 24]	40
Figure 9 Front Mounted Motor [Ref. 20]	43
Figure 9a Take Off With Front Mounted Motor [Ref. 20]	43
Figure 10 Rear Mounted Motor on Keel [Ref. 21]	44
Figure 11 Rear Mounted Motor on Pod [Ref. 22]	44
Figure 11a Take Off With Rear Mounted Motor on Pod [Ref. 22]	45
Figure 12 Motor Mounted on Down Tubes [Ref. 23]	47
Figure 13 Battery Comparison [Ref. 15]	60
Figure 14 Fisher 8 HP Motor [Ref. 18]	74
Figure 15 H-Power Fuel Cell [Ref. 17]	77

ACKNOWLEDGEMENTS

I would like to acknowledge the financial support of the Space and Naval Warfare System Center-San Diego (SPAWARSYSCEN SD) Research Fellowship Program. Because of this program the purchase of necessary equipment was possible.

I would like to thank my thesis advisor, Professor Xiaoping Yun, NPS ECE Department, for his support, patience, guidance and encouragement. Working with him was thought provoking, rewarding, and enriching.

Many thanks to my second reader Dr. Jovan Lebaric, NPS ECE Department, his expertise with permanent magnetic brushless direct current motors and battery technology was priceless. It was a pleasure to work with an expert from the solar powered car races.

Many thanks to Commander Rob King, NPS AA Department who was very supportive with his advice concerning aerodynamics and propeller theory.

Thanks to Dr. Mark Drela of the Massachusetts Institute of Technology for the introduction to his XROTOR computer program. Without this program it would have been impossible to rapidly generate different propeller geometries.

Thanks to Lieutenant Commander Shipley, NPS PH Department and Dr. Mike Shields, NPS ECE Department for

taking the time to share their knowledge of hang gliding and giving much good advice from the pilots perspective.

I would like to acknowledge the love, patience and support of my lovely wife Beate, and my son and daughter, Russell and Breena; who once again put up with my long hours at work and inattention to family matters.

I would like to dedicate this thesis to the Marines, past and present, involved in Scout Sniper and Reconnaissance activities. I believe your future will be busy. The boy scouts got it right - be prepared.

I. INTRODUCTION

A. GENERAL

Information dominance is a tenant of information warfare. A successful commander must make informed decisions faster than his adversary in order to force the enemy to react to his actions. Obviously, to do this the commander needs the right information. Much of this information is provided by National and Theater electronic assets, however; the critical gaps in this information will have to be filled by Reconnaissance personnel working in small units inside the enemy's area of operations. On the high speed, info-centric, dispersed battlefield of the future, this information dominance will require increased small unit battlefield mobility.

As last year's Hunter-Warrior war fighting experiment has shown, the ongoing trend on the future battlefield will be towards smaller units responsible for scouting, securing, and shaping the battlefield prior to a larger, heavier force being injected at the crucial time and place to decisively engage the enemy. This light scouting, shaping force has a need for some type of vehicle to provide battlefield mobility, insert, extract, escape and evasion, and re-supply. This need will become greater as these trends are

further developed. A one-man, electrically powered hang glider that is capable of unassisted take-off and cruise flight could provide this capability.

This thesis explores the possibility of using an electrically powered hang glider for small unit battlefield mobility by modeling and simulating a commercially manufactured hang glider that will be modified to mount an electric motor, power supply, and propulsion system.

B. PROBLEM STATEMENT

In the near future the United States Marine Corps will field a tilt rotor aircraft, the MV-22 Osprey, and the new Advanced Amphibious Assault Vehicle (AAA Vehicle). These new platforms will provide a tremendous capability to move relatively large numbers of Marines around the battlefield in a short period of time. Reconnaissance personnel will be able to use these and other more conventional insertion platforms such as parachutes and small boats to initially enter the area of operations, but; they will then have to rely on foot mobility, or be extracted and re-inserted by some other platform, in order to move some distance to provide reconnaissance support in a different geographical area. The heavy units using one of the new mobility platforms that the Marine Corps will soon possess will rapidly outrun the reconnaissance personnel. The

reconnaissance personnel of the future are going to have a hard time keeping up with the new mobility of these units.

There are several reasons that support the concept demonstration for battlefield mobility on an electrically powered aerial vehicle. The electric motor will be quiet. By using an electric motor the power supply can be re-charged using a solar panel, thus no gasoline re-supply is required. A hang glider is one of the lightest and most efficient platforms available that can provide the lift required to move a combat loaded Marine over any terrain, for some distance, in a reasonable period of time. This platform is not envisioned to replace other means of insertion such as helicopter, rubber boat, etc. This platform is envisioned to provide mobility for these small units once they have been inserted, especially over terrain that is difficult for foot mobility. Other capabilities that this platform could provide are the ability to move from the ground to a roof top in order to secure a helicopter landing zone, an escape and evasion platform if a small unit is compromised, scouting platform, and a re-supply platform.

C. OUTLINE OF THE THESIS

Chapter II provides a description of the research concept used to conduct the vehicle design. Chapter III discusses the aerodynamics considered in the design, while Chapter IV examines the motor and controller required for

the propulsion system. Chapter V contrasts and compares different power sources that could be used. Chapter VI discusses how to put the components together to create the aircraft. Chapter VII presents the proposal for an optimized system design using commercially available components and what mission requirements can be met. Chapter VIII presents conclusions and recommendations for future study.

II. RESEARCH CONCEPT

A. MISSION REQUIREMENTS

For the purpose of the proof-of-concept demonstration there are a number of specific research areas to be explored including:

- How much thrust must the motor and propulsion system generate to provide unassisted take-off and cruise flight capability for a combat loaded Marine weighing between 200 and 250 pounds?

- What modifications to the glider will be required to mount the motor, power supply, and propulsion system without adversely altering the gliders flight characteristics?

- How do we maximize the lift capability of the glider?

- How do we minimize the weight of the glider itself?

- How large an area will be required to take-off and land the glider?

- How do we minimize the size of the glider when it is broken down for transport?

- What is the best way to model this system as an optimal control problem?

Commercially available equipment will be modified and configured as a transportation system. This system will be modeled and simulated to find the optimal configuration based on a list of mission constraints and operational requirements.

1. Constraints

- Maximum weight of the aircraft without a pilot is between 90 to 130 pounds.

- Dimensions of the aircraft when broken down for ground transportation is 6 to 9 feet in length.

- Power supply must be re-chargeable with solar panel.

2. Requirements

- System must be capable of unassisted take-off and cruise flight.

- Power supply must have 2 to 4 hour endurance capability.

- Glider must climb at a minimum of 300 to 400 feet per minute.

- Glider must have a range of 40 to 75 miles.

- Glider must be able to lift a minimum of 300 pounds to include the weight of glider.

- Glider must be capable of between 25 and 35 mph airspeed in straight and level flight.

B. START WITH WHAT IS ALREADY KNOWN

The sport of Hang Gliding relies on rising air or thermals, to provide lift to the aircraft that allows flight. Foot Launched Micro Light (FLML) aircraft are simply hang gliders using gasoline fueled reciprocating engines to provide propulsion to enable a foot launched hang glider to climb unassisted to some altitude where the pilot can then rely on thermally derived lift. There are several different models commercially available today. We will look at these models and reverse engineer these systems as a starting point for our own design. This approach has many advantages. First we know that these FLML will fly. Second we know the approximate performance standards they meet with known engine and propeller sizes. Third since we know the design of each of these models such as the engine placement, etc.,

we can look at the trade-offs concerning our requirements for unassisted flight using electric motors. We can then optimize our design based on minimum performance required of each of the major components with the purpose of optimizing the entire SYSTEM using our stated mission requirements to drive the design by trading off certain advantages and disadvantages of each of the major components. We will look at flight controllability versus optimal motor placement, engine power required versus thrust required for a specific rate of climb, total system weight versus endurance, and propeller geometry and size versus propeller thrust. The major components of our system will be the hang glider, electric motor and controller, propeller, and the power system. Each of these will be considered in detail.

III. AERODYNAMICS

A. WHAT IS REQUIRED TO FLY

The study of aerodynamics is the study of fluid flow. In our case the fluid is air. The physical laws governing this flow are rather involved. In Finbar Sheehy's book "The Hang Glider's Technical Notebook", an excellent description of these laws and how they relate to flight is provided. While his descriptions of these laws are somewhat simplistic and not absolutely aerodynamically correct, he paints a word picture that makes the flight process easy to visualize. "To understand how a hang glider flies we will begin with a look at Newton's laws of motion.

- An object at rest tends to remain at rest, and a moving object tends to continue moving at a steady speed in a straight line, unless acted on by a force.

- When an object is acted on by a force, it accelerates in the direction of the force. The acceleration is proportional to the force, and is inversely proportional to the mass of the object.

- When one object applies a force to a second object, the second object applies an equal and opposite force to the first object.

If we can build a machine or a wing, which can push air downward, then the air will push the machine upward. A wing in an airflow deflects the air downward. In doing so it pushes down on the air, so that the air pushes the wing upward. This is how the wing develops the necessary LIFT force." Sheehy [Ref. 1].

We know that we need to push air downward in order to stay up. If we hold a flat plate at an angle to an airflow, the plate deflects the airflow. If it deflects the flow downward, the air will try to move the plate upward, providing lift. It is possible to improve this result if the plate is curved. "Newton's second law tells us that the air molecules will flow in a straight line unless some force deflects them." Sheehy [Ref. 1]. If they are flowing in a path that curves downwards then something must be pushing them down. In the case of a fluid, such as air, the only thing that can push, is the pressure. The pressure of the air flowing on the bottom of a curved plate must be higher than the pressure on the top of the plate. This means that the pressure directly below the plate is higher than the pressure above the plate. The sum of the pressures across the entire area of the plate are pushing on the plate, so the pressure difference is trying to push the plate upwards. We can also round off the sharp corners of our plate by giving it an airfoil cross section. This helps to prevent the moving air from separating or leaving the surface of our

the moving air from separating or leaving the surface of our plate which now looks like a wing. In fact, the pressure on the top curved surface of the plate or airfoil is now actually less than the atmospheric pressure because it is accelerating, which further increases the pressure difference between the top and bottom of the wing. The angle of the wing relative to the airflow is called the Angle of Attack. The bigger the angle of attack, the harder the plate pushes the air downward as it flows past, and more lift is developed, up to a point. Beyond this point the air is being asked to turn too quickly. It cannot do so and the airflow separates from the upper surface of the wing and lift is rapidly decreased causing the wing to stall. "At any angle of attack the lift force varies as the square of the airspeed, so at higher airspeeds we can use a lower angle of attack to generate the required lift to maintain flight." Sheehy [Ref. 1]. The amount of the lift force L , is computed as follows from Anderson [Ref. 9 & 10]:

$$L = C_L \rho V^2 S / 2$$

where

L = LIFT

ρ = AIR PRESSURE

V = AIRSPEED

S = SURFACE AREA OF WING

$C_L = 2W/\rho V^2 S$ = LIFT COEFFICIENT

W = WEIGHT OF AIRCRAFT

For an aircraft to be in straight and level flight, lift must equal weight.

As a wing is moving through the air another force opposes its forward motion. This force is called drag. We need to consider two types, parasite and induced. Parasite drag is basically skin friction drag. It is created by the friction the air creates as it moves along the surface of the wing. Parasite drag rapidly gets worse as airspeed increases. The second kind of drag is called induced drag. It is the price we pay for creating lift. "When the wing deflects air down, it turns some of the air's horizontal speed into vertical speed. The vertical speed provides the lift force, but the lost horizontal speed causes a drag force. The bigger the angle of deflection, the more horizontal speed the air loses and the bigger this drag force becomes. If the airspeed is low then a large angle of deflection is needed to create enough lift to maintain flight but the induced drag is also large. On the other hand, if the airspeed is high then only a small deflection angle is needed to get the required lift, and so the induced drag is also small. This means that the induced drag

decreases when the airspeed increases, if the lift force is kept constant. Induced drag can also be decreased by making the wing longer." Sheehy [Ref. 1]. The amount of the drag force D , is computed as follows from Anderson [Ref. 9 & 10].

DRAG = PARASITE DRAG + INDUCED DRAG

DRAG COEFFICIENT = PARASITE + INDUCED = $C_D = C_{D0} + C_{Di}$

$$C_D = C_{D0} + C_L^2 / \pi \epsilon AR$$

where

C_{D0} = PARASITE DRAG COEFFICIENT

AR = ASPECT RATIO = b^2/S

b = WING SPAN OR LENGTH

ϵ = WING EFFICIENCY FACTOR < 1

For straight and level flight thrust must equal drag.

A hang glider is basically a wing with a pilot hanging below it. The pilot controls the hang glider by shifting his body weight around the center of gravity, located approximately 12 inches above the pilot's back, thus allowing the hang glider to turn, climb and descend. In sport hang gliding thrust is obtained by trading altitude

for airspeed which gives us the airflow over the wing to generate lift. Thrust is opposed by the drag forces. For parasite drag, air resists anything moving through it. This includes not just the wing but anything attached to it. A hang glider wing has a lot attached to it, such as the pilot, the wire rigging, king post and control frame (Figure 1). As we have just seen, induced drag decreases as the airspeed increases, assuming a constant lift force. "From Newton's first law, if the glider is moving at a steady speed in a straight line, the total force acting on it must be zero. Since we know of three forces acting on it, lift, drag, and weight, these must cancel out" Sheehy [Ref. 1]. The lift is at right angles to the glider's path through the air and drag is acting backwards along the glider's path. Weight always pulls straight down (Figure 2).

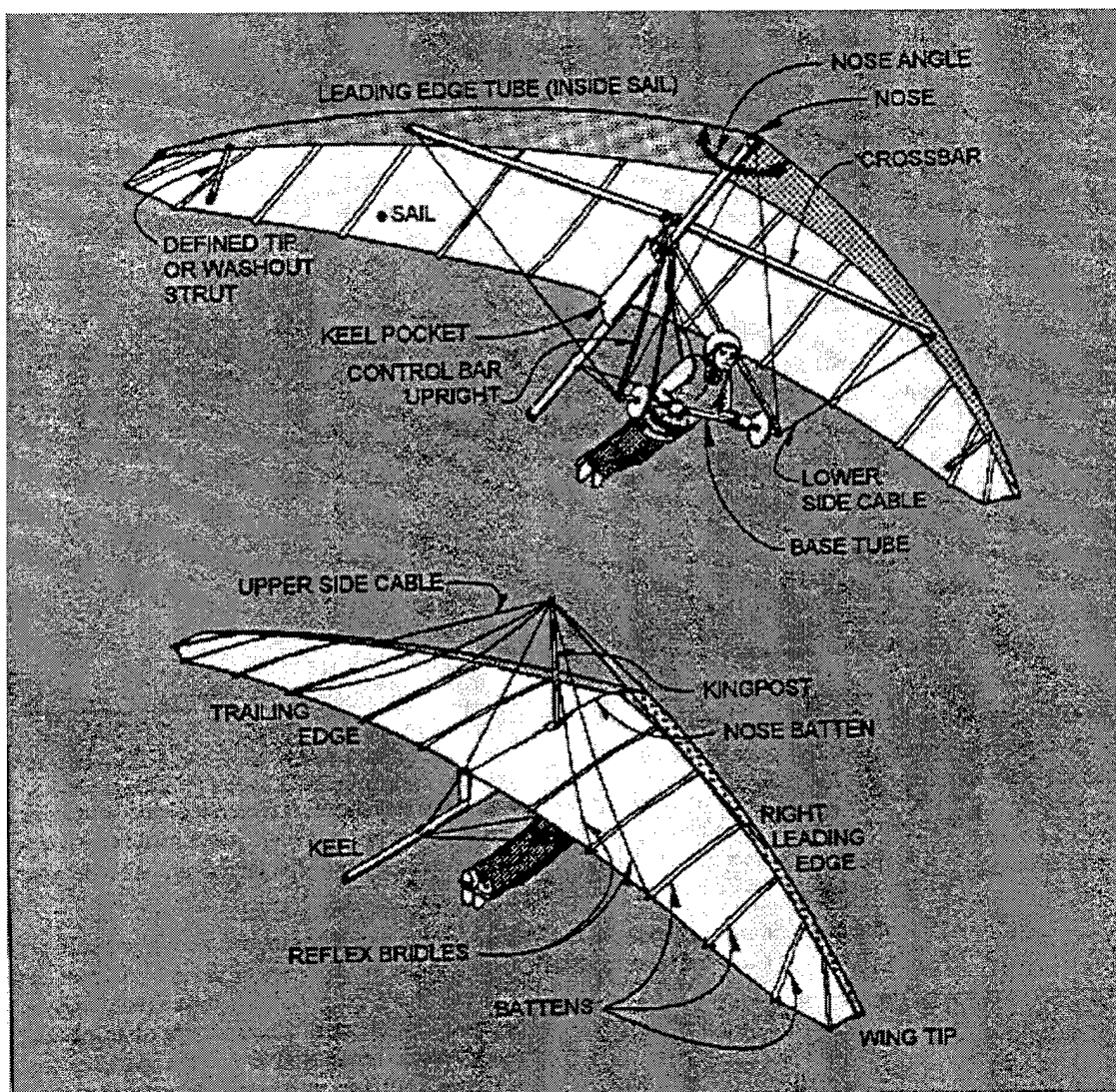


Figure 1 Hang Glider Frame Pagen [Ref. 11]

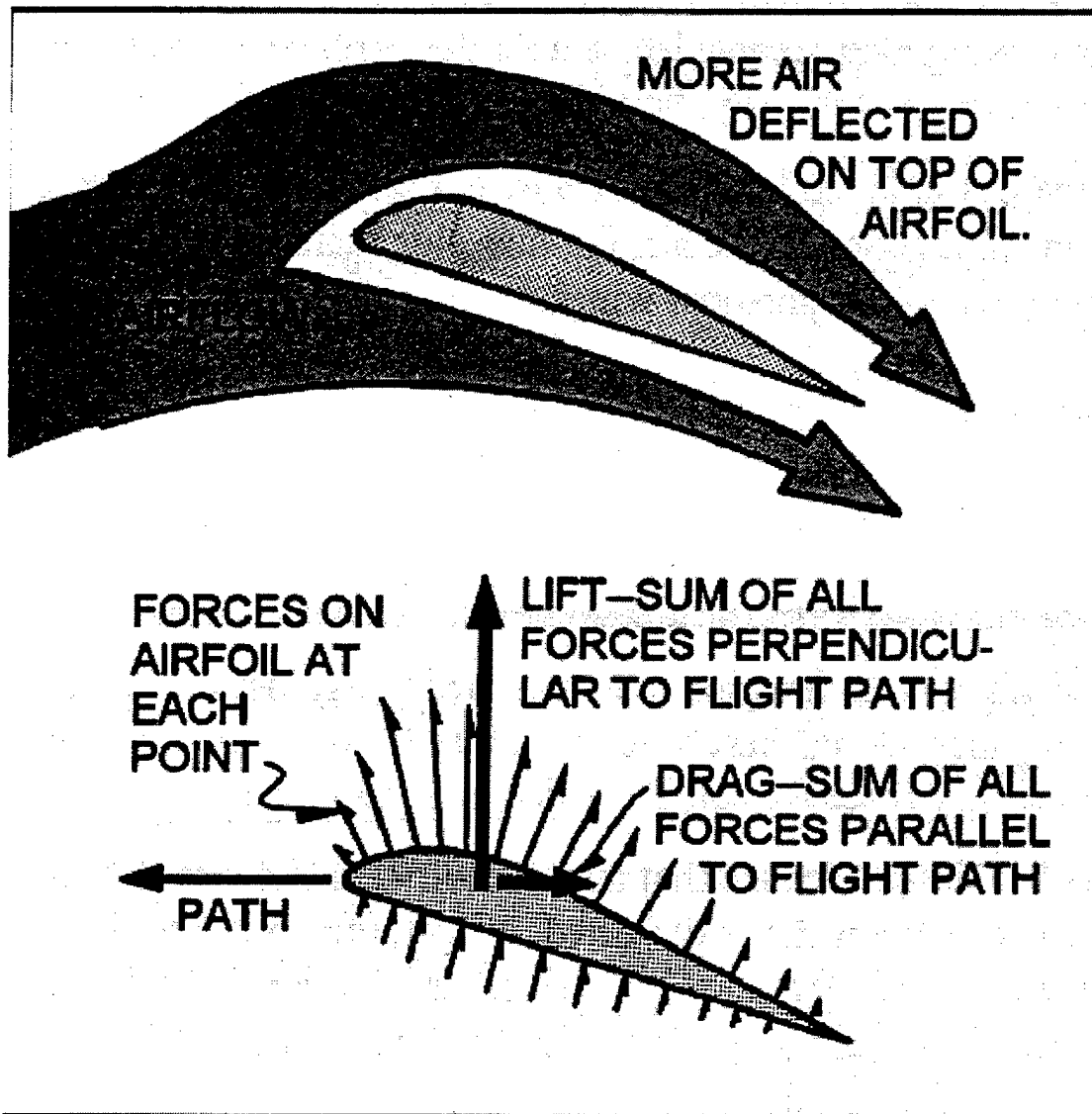


Figure 2 Forces Acting on the Glider Pagen [Ref. 11]

The glider equation in vector form is given below.

$$\text{LIFT} + \text{DRAG} + \text{WEIGHT} = 0$$

The distance traveled forward over the ground divided by the distance traveled down or the loss of altitude is

equal to the best lift to drag ratio or L/D. For the glider to travel the maximum distance forward through the air for a given loss of altitude it should fly at whatever speed gives the maximum L/D ratio. Since the induced drag is highest at low airspeed, and the parasite drag is highest at high airspeed, there is an airspeed that results in minimum total drag. This happens when the two types of drag have the same value. Any slower, and induced drag becomes the big problem. Any faster, and parasite drag takes over.

PARASITE DRAG = INDUCED DRAG

$$C_{D0} = C_{Di}$$

where

$$C_{Di} = C_L^2 / \pi \epsilon AR$$

The sink rate is the vertical airspeed or the rate at which the glider loses altitude. The sink rate depends on the glider's forward airspeed and angle of attack. The minimum sink rate is the forward airspeed and angle of attack that is just above the stall speed, which gives the minimum loss of altitude. "A good L/D ratio can still result in a high sink rate if the glider moves fast enough. The best sink rate happens at a lower speed than the one giving the best L/D ratio", Sheehy [Ref. 1]. This means that the wing is operating in the range where the induced drag is the

main source of drag. This is where the glider's aspect ratio is most important. All other things being equal, a glider with a high aspect ratio, or long thin wings; will have lower induced drag and will have a lower sink rate at a given airspeed. This becomes most important at the minimum sink speed, where the induced drag is the important source of drag. We see that lift increases with an increasing angle of attack. "There is a critical angle of attack, however, the stalling angle of attack, and when the angle of attack exceeds this value the lift decreases." Sheehy [Ref. 1]. When the wing is operating at this angle it is developing its maximum lift for that airspeed. The only way to increase the lift is to increase the airspeed. If the glider is flown more slowly, it loses lift because of the decreasing airspeed. To generate enough lift as airspeed decreases to maintain altitude, the pilot increases the angle of attack. Eventually the angle of attack reaches the stalling angle. The airspeed at which this happens is called the stall speed. It is the lowest airspeed at which the wing can still develop enough lift to fly. As it slows below this airspeed, increasing the angle of attack further actually decreases the available lift. This causes the wing to fall. Recovery is possible only by pointing the wing down, reducing the angle of attack and letting the airspeed increase as gravity pulls the glider downward. Once the airspeed is high enough the wing can again develop enough lift and begin flying.

Looking at the performance of a non-stalled wing, we see that increasing the wing area does not help generate lift, and actually hurts performance a little by increasing the parasite drag. However, there is a minimum useful wing area. First, the wing area must be big enough to keep the stall speed below the calculated speed for minimum sink, so that the glider can actually get to minimum sink speed and still fly. Second, the stall speed must be low enough to allow safe takeoff and landing since we takeoff and land at the stall speed. "The stall speed depends on the square root of the wing loading, or the weight divided by the wing area. Once we know the maximum acceptable stall speed, the stalling angle of attack of the airfoil used, and the aspect ratio of the wing, we can compute the maximum wing loading. Given the maximum weight to be carried, we can find the minimum wing area needed. " Sheehy [Ref. 1].

Hang gliders have their best L/D at very low airspeeds. This means that the stall speed has to be even lower than the minimum sink speed and best L/D speed. As gliders have become aerodynamically CLEANER due to less wires and cables for lower drag, the L/D and minimum sink speeds have become higher. This has made higher stall speeds acceptable, and so there has been a trend among the newer, higher performance gliders to smaller wing areas with larger aspect ratios. However the higher stall speeds make takeoff and landing more difficult and the larger aspect ratios make the gliders

harder to control. The pilot causes the glider to turn by shifting his weight to one side or the other to force one wing tip down. The lift force is still being generated straight out from the wing and the glider is still moving forward through the air. This causes the glider to be pulled in the direction of the lower wing thus causing a turn. Climbing or descending is accomplished by the pilot shifting his weight forward or back to raise or lower the nose of the glider which increases or decreases lift. If the aspect ratio is too high, the pilots weight shift won't be able to accomplish the necessary raising and lowering of the wings or nose to steer the glider.

We can now understand our first set of tradeoffs. We want a small total wing area to reduce our parasite drag, but; we need a certain amount of wing area to keep our stall speed in the range that is attainable for takeoff while running with our hang glider. We want the largest aspect ratio we can get for the best L/D which means we can fly for the least amount of thrust and therefore power, but; this aspect ratio cannot be so great that the pilots weight cannot control or steer the hang glider in flight. The speed for best L/D is our most economical speed for cruise flight since it has the least drag and so requires the least thrust, but; the minimum sink speed will be better for climbing as it gives the most altitude gain per distance

traveled over the ground. We will see how these tradeoffs affect our design in future chapters.

IV. ELECTRICAL COMPONENTS

A. GENERAL ELECTRIC MOTOR DESIGN

All models of commercially available powered hang gliders use a gasoline powered reciprocating engine, rated at about 15 horsepower (HP), to turn a propeller to generate approximately 100 foot pounds of thrust, to climb at a rate of 300 to 400 feet per minute. We require an electric motor or motors, that can also generate 15 HP.

The basic theory behind the operation of a DC motor is that current in a conductor forms a magnetic field around that conductor. If this current-carrying conductor is located in a magnetic field at right angles to the current's field, a force will be exerted on this conductor. If the flux lines of the external magnetic field are in the same direction as the flux lines due to the conductor current (that is have the same polarity), they will repel each other. When the flux lines are in the opposite directions from one another, they will attract each other. This causes a net force on the conductor. If either the number of lines in the field or the current in the conductor is increased, the net force is also increased.

If a conductor is moved in a magnetic field, it does what is known as CUTTING FLUX that generates a voltage in the conductor. The more flux, or the faster the movement of the conductor, or cutting of flux, the higher the generated

voltage. This generated voltage in a motor is known as the electromotive force or EMF. If a U shaped metal bar is wrapped with a wire conductor, essentially an electromagnet, and placed in a magnetic field it will create a torque. If the coil is allowed to rotate, at some point the current must reverse for the torque to maintain the same direction. This can be done with brushes or in a brushless motor with electronic switching.

Therefore, electric motor operation is based on the interaction of magnetic forces repulsing or attracting each other. Continuous relative change of the magnetic forces is accomplished with electromagnets capable either of being turned on or off or of changing polarity due to reversal of current. In the case of the Direct Current or DC motor, the polarity is changed by reversing the current mechanically in the rotating member by a switch consisting of commutators and brushes. In the brushless DC motors, the currents in the windings are switched electronically.

For a motor with a two-pole construction the torque and EMF are computed as follows. Sokira and Jaffe [Ref. 2].

$$T = Z_a \Phi I_a = \text{TORQUE}$$

$$E_b = Z_a \Phi S = \text{EMF}$$

where

$$\Phi = \text{FLUX}$$

Z_a = NUMBER OF ARMATURE CONDUCTORS

I_a = ARMATURE CURRENT

S = REVOLUTIONS PER MINUTE

For a motor with any number of poles the equations are as follows. Sokira and Jaffe [Ref. 2].

$Z_a \Phi = T/I_a = K_t$ = TORQUE CONSTAN

$Z_a \Psi = E_b/S = K_e$ = VOLTAGE CONSTANT

$P_{Gout} = E_b \times I_a$

B. PERMANENT MAGNET MOTOR

The development of new magnet materials has made the permanent magnet motor popular due to its efficiency. Among the magnets used today are ceramic magnets and rare-earth magnets. New rapid heating and quenching techniques are used for manufacturing powerful magnets out of readily available materials. Ceramic magnets are the lowest cost. Rare-earth magnets offer improved motor performance over the ceramic types but are expensive. The new rapid heating and quenching process know as MAGNAQUENCH, offers relatively powerful magnets at competitive prices for motors. With higher-energy magnets, motors can be smaller, more efficient, or both for a given output.

C. PERMANENT MAGNET BRUSHLESS DIRECT CURRENT MOTOR

"Brushes require replacement, commutator surfaces wear out and have to be turned, arcing cannot be permitted in certain hazardous locations, and the system imposes severe speed limitations on the motor. With the development of electronic switching devices, it was natural that these would replace the mechanical switching components that are part of the conventional DC motor." Sokira & Jaffe [Ref. 2]. Permanent Magnet Brushless Direct Current (PMBDC) motors are built with a multipole permanent magnet rotor, a wound field stator, electronic switching circuits, and an absolute sensing system that duplicates the torque-speed and torque-current characteristics of a conventional DC motor. The PMBDC motor system consists of a motor, a sensing system, and an electronic commutator and control unit.

The motor consists of a rotor on which permanent magnets are mounted, always arranged in pole pairs. These magnets supply the field flux. The magnetic poles can be thought of as flux gear teeth. The more magnetic pole pairs on the rotor the more teeth on the gear and the higher the torque of the motor. The stator contains the stator winding and is designed in such a way that if the current reaches the right coil or coils at the right time, interaction with the field flux gear teeth occurs, or the gear teeth of the rotor and stator mesh together, and torque is produced. In

rotor and stator mesh together, and torque is produced. In addition there are the usual bearings, end caps, a housing, etc.

In order for the coils to be switched in the correct sequence and at the correct time, the location of the rotor field magnets must be known exactly. Locating magnetic pole pairs requires an absolute sensing system that can be magnetic and consists of Hall sensors, or optical and use encoders, or one of several other arrangements. This function is critical in the operation of the motor.

According to Sokira & Jaffe [Ref. 2] the function of the electronic commutator is to switch the right currents in the right stator coils at the right time and in the right sequence by taking the information supplied by the sensor and processing it with preprogrammed commands to make the motor perform in the way it was intended to perform. This electronic control consists primarily of power devices such as Field Effect Transistors, or FETs, that can handle the motor currents and the control circuits. The control circuits handle very small currents and switch the power transistors. Microprocessors are rapidly becoming a part of these electronic control circuits.

There are different types of PMBDC motors to accommodate different requirements. Frequently the motor length must be short. The most suitable motor for this might be a pancake motor (Figure 3), where the rotor is in disc

form with the conductors arranged radially. Magnetically the armature itself is nothing but an air gap, which also classifies the motor as a moving coil motor. Even though the length of the core is short, the large armature diameter required and the added inertia of the outer connections cause the armature inertia to be somewhat higher than the inertia of a shell armature motor. Another moving-coil motor designed to have very low inertia and low inductance is the shell-type armature motor (Figure 4). The armature is made up of a winding that forms a hollow cylindrical rotor in which the wires are bonded together. Other applications require inside-out motors (Figure 5), where the armature is on the outside, and the stationary member with the magnet forms the inside of the motor. This is a high-inertia motor.

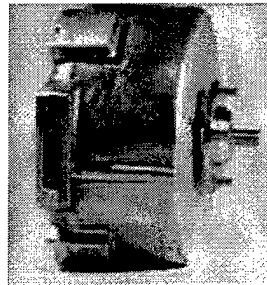


Figure 3 Pancake Motor for Wheel Chair [Ref. 18]

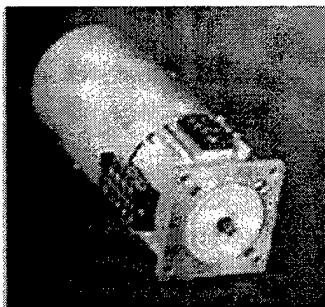


Figure 4 Shell Type Armature Motor for Antenna Adjustment
[Ref. 18]

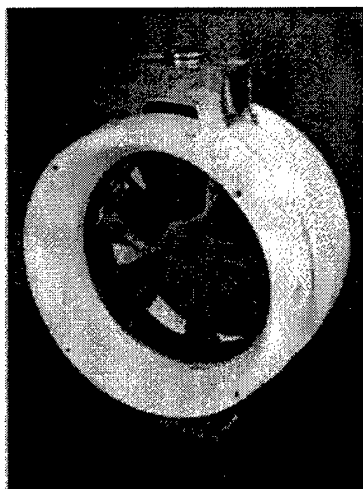


Figure 5 Inside Out Motor [Ref. 18]

V. POWER SOURCE

A. GENERATING CURRENT

Reciprocating engines convert chemical and thermal energy into mechanical energy to perform work. Reciprocating engines are not very energy efficient due to the large thermal losses that occur during this energy conversion. Electrical motors use electric current to perform work. Although electric motors are much more energy efficient than reciprocating engines, the current sources for electric motors are not nearly as efficient for energy storage as the chemical fuels normally used in reciprocating engines.

A current is a moving charge. To make charge carriers flow through a load such as a motor, we have to establish a potential difference between its ends. One way to do this is to connect each end of the motor to a separate conducting electrode, with one charged negatively and the other positively. The problem is that the flow of charge acts to discharge the electrodes, bringing them to the same potential. When this happens the flow of charge stops. To maintain a steady flow of charge in between the electrodes we need a charge PUMP, a device that by doing work on the charge carriers maintains a potential difference between the terminals of the pump. This device is known as an Electromotive Force or EMF device. The device is said to provide an EMF which means it does work on the charge

carriers. Typical EMF devices are batteries, generators, and fuel cells. Although these devices differ widely in their modes of operation, they all perform the same basic function; they do work on charge carriers and thus maintain a potential energy difference between their terminals.

B. BATTERIES

The basic building block of a battery is the cell. A cell is an electrochemical device that converts chemical energy to electricity via oxidation-reduction (redox) reactions. Redox reactions involve a transfer of electrons. The cell separates these reactions in space, half the reactions occurring at the positive electrode, the other half at the negative electrode. By definition, the anode or negative plate is the site of the oxidation reaction and the cathode, or positive plate, the site of the reduction reaction. When the anode and the cathode are connected externally through a load, the cathode gives up electrons to the external circuit, the anode accepts them from the circuit, and ions flow through the electrolyte conducting charge from one plate to the other. A battery is said to discharge as it changes its chemical energy to electrical energy. Only oxidation-reduction reactions can be used to generate electricity. Different types of batteries use different chemical combinations in their electrolyte to do this.

The cell is usually constructed with multiple positive plates connected in parallel interleaved with multiple negative plates also in parallel. This design provides a compact geometric form and minimizes internal electrical resistance to maximize power capability at good ampere hour (A-hr) yields. The battery consists of cells usually connected in series, so that the voltages of the cells add together to give the desired battery voltage. The cell voltage depends on the chemical nature of the anode and cathode materials. The battery capacity depends on the cell voltage and the amounts of anode and cathode materials in the cell. The cell voltage or energy is computed as follows, Bogner, Chorneau, Pickett [Ref. 4].

$$\text{CELL VOLTAGE, } E = -\Delta G/nF$$

where

G = FREE ENERGY

n = NO. OF ELECTRONS

F = FARADAY'S CONSTANT,

26.8 A-hr PER EQUIVALENT

CAPACITY OR A-hr yield = (26.8 X GRAMS OF ACTIVE MATERIAL)/EQUIVALENT WEIGHT OF ACTIVE MATERIAL

TOTAL CELL ENERGY = E X A-hr

Battery inefficiencies are caused by the internal voltage losses due to internal electrical resistance or electrochemical polarization; and, less than 100% use of the positive and negative active materials. Both have a variety of causes. Battery power, (P), is the rate of delivery of energy to the outside circuit.

$$P = EI$$

As the current demand (I) increases, battery voltage (E) decreases due to internal resistance and the polarization phenomena. "Maximum power is delivered at about one half theoretical voltage. As power demand is increased, delivered energy decreases." Bogner, Chorneau, and Pickett, [Ref. 4].

C. FUEL CELL

In principle, a fuel cell operates like a battery. Unlike a battery, a fuel cell does not run down or require recharging. It will produce energy in the form of electricity and heat as long as fuel is supplied. A fuel cell consists of two electrodes sandwiched around an electrolyte. Oxygen passes over one electrode and hydrogen over the other, generating electricity, water, and heat.

Hydrogen fuel is fed into the anode of the fuel cell. Oxygen or air enters the fuel cell through the cathode. Encouraged by a catalyst, the hydrogen atom splits into a proton and an electron, which take different paths to the cathode. The proton passes through the electrolyte. The electrons create a separate current that can be utilized before they return to the cathode, to be reunited with the hydrogen and oxygen in a molecule of water. A fuel cell system which includes a fuel Reformer can utilize the hydrogen from any hydrocarbon fuel-from natural gas to methanol, and even gasoline.

Many types of fuel cells are currently under investigation. Of most interest to this thesis is the Proton Exchange Membrane (PEM) fuel cell. This fuel cell operates at relatively low temperatures, about 200 degrees F, has high power density, can vary its output quickly to meet shifts in power demand, and is suited for applications such as automobiles where quick startup is required. According to the U.S. Department of Energy, they are the primary candidates for light-duty vehicles, for buildings, and potentially for much smaller applications such as replacements for rechargeable batteries in video cameras. Other types of fuel cells are described in Appendix (E).

D. GENERATORS

Generators operate similarly to electric motors, only backwards. For a generator we need to use some type of

mechanical energy to turn the armature. The magnets on the armature generate a rotating magnetic field which induces a current in the windings of the stator. The mechanical energy to turn the armature of the generator is typically supplied by an internal combustion engine. As stated earlier, an internal combustion engine is not very efficient; but, the hydrocarbon fuel it uses is very energy dense. There are relatively lightweight commercially available generators that could be used to power the electric motors for the hang glider. The generator power would typically be alternating current, or AC; however, we could use power rectifiers and filters to convert the AC to DC.

VI. OPTIMAL DESIGN

A. OPTIMIZING THE SYSTEM

We cannot optimize a system by simply optimizing its parts. For system optimization we must look at each of the major component's advantages and disadvantages with respect to the entire system; and then, using these as tradeoffs design the platform to meet the mission requirements in the most efficient manner possible. For our system the major components are the hang glider, the motor, controller, propeller, and the power source. In considering the tradeoffs in optimizing the system, we must consider the type of hang glider, motor, controller, propeller placement on the glider, propeller diameter, thrust required to climb and cruise, motor HP to obtain the thrust, energy density of the power source, and how all this will effect the stability of the hang glider and the weight of the total system.

B. FOOT LAUNCHED MICRO LIGHTS (FLML)

1. Major Types

For our purposes there are three main types of commercial hang gliders. Beginner gliders (Figure 6) have more wing surface area and a smaller aspect ratio. This means they have low stall, or low takeoff and landing speeds, and are easy for the pilot to control or steer. They are usually single surfaced with one layer of sail material

on the top of the glider, which makes them lighter but gives them more parasite drag. Novice gliders (Figure 7) have somewhat less surface area, a larger aspect ratio, and are usually double surfaced with a second layer of material on the bottom of the glider. While they are somewhat more difficult to control and have a slightly higher takeoff and landing speed, they are still relatively forgiving to fly and due to the higher aspect ratio, and smaller surface area and double skin; they have better L/D since there is less parasite drag. The expert gliders (Figure 8) have significantly less surface area, larger aspect ratio and are also double skinned. They are significantly more difficult to control, heavier, and have a much higher takeoff and landing speed.

Foot launched micro lights (FLML) are just that, foot launched. A takeoff speed that can be attained by someone running while holding up the glider is obviously important. This will be somewhat more difficult after we add the weight of motors, propellers, and power source to our glider. The people who will be flying our glider will be military personnel so a glider that is easier to control is also of importance. The double surface will significantly reduce the parasite drag of our glider so this is of concern. The best choice seems to be the novice glider, which will give us a reasonable takeoff and landing speed that can be attained while foot launching the glider, a double surface to

minimize the parasite drag and a higher aspect ratio to minimize induced drag and so reduce the thrust required, while still being a FORGIVING glider concerning ease of control.

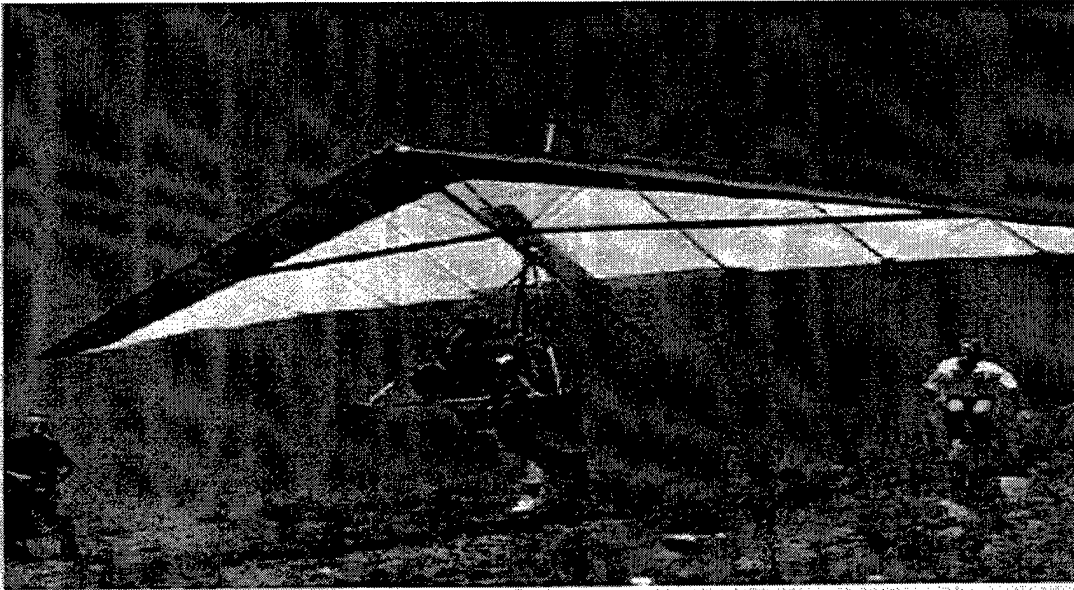


Figure 6 Beginner Hang Glider, Single Surface, Low Aspect Ratio Pagen [Ref. 19]

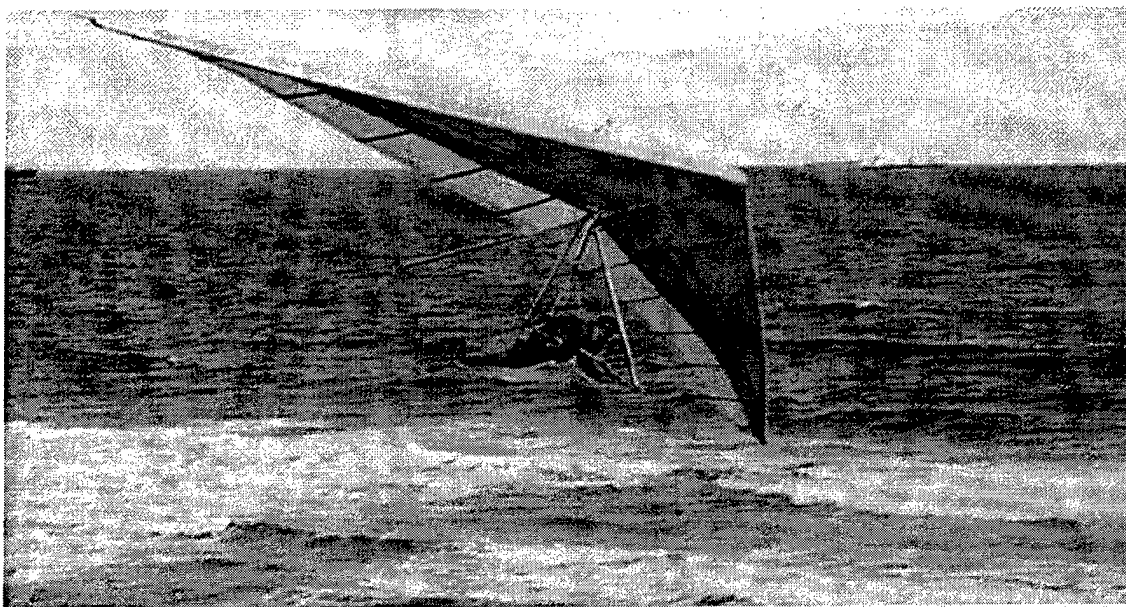


Figure 7 Novice Hang Glider, Double Surface, Higher Aspect Ratio Pagen [Ref. 24]

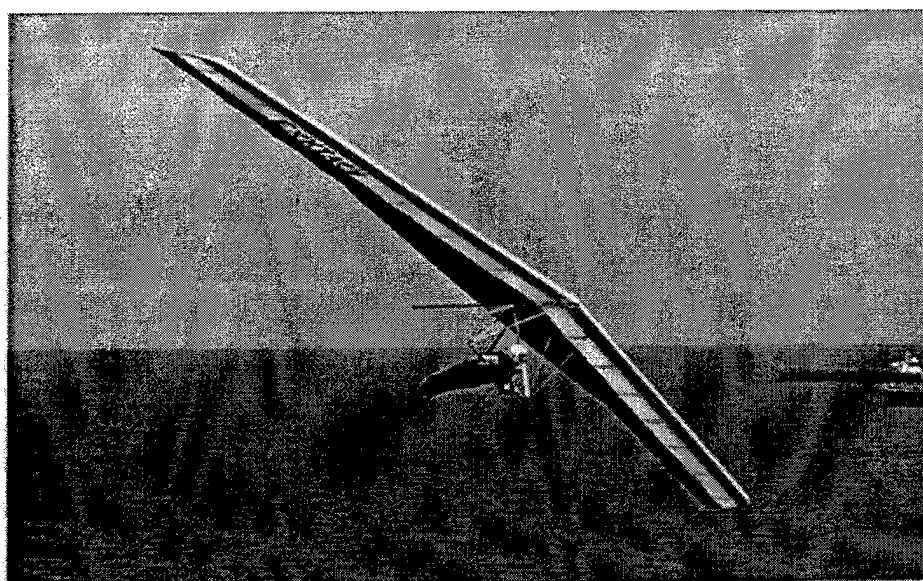


Figure 8 Expert Hang Glider, Double Surfaced, Very High Aspect Ratio Pagen [Ref. 24]

The only disadvantage in not using the expert hang glider is

that we will not get the best L/D, which means we will require more thrust for our glider to fly. More thrust translates into bigger motors, larger propellers, and a larger and heavier power source.

2. Placement of Motor and Propeller

There are several FLML's commercially available today, but; they all fall into one of four major design categories. The categories are based on motor and propeller placement and on how this placement affects the performance of the FLML.

The first design has the propeller and motor on the front of the glider (Figure 9 and 9a). The motor, being the heaviest piece, is mounted above the pilot near the center of gravity, so as not to make the glider nose heavy. The propeller is mounted near the nose of the glider and connected to the motor by a shaft. The advantage of this design is that the propeller diameter can be large since it is mounted high off the ground. The disadvantages are that thrust efficiency is lost due to the long shaft that connects the propeller to the motor, the propeller wash is in the pilots face, and if the glider is nosed into the ground during landing, a not unusual occurrence, the propeller may be broken.

The second design mounts the motor and propeller on the keel of the glider (Figure 10). Advantages are that the

pilot's field of view is unobstructed and the propeller is placed in a more protected position during bad landings. The disadvantages are that the weight of the motor is placed in a position that will make the glider tail heavy which could cause an inadvertent stall and will make takeoffs more difficult.

The third design mounts the motor and propeller in the rear of the glider but this time on the POD that the pilot puts his legs and lower body into while he is flying (Figure 11 and 11a). This position is the same as on the second design except that the motor and propeller assembly are closer to the ground, and will effectively push the pilot who will drag the glider through the air versus pushing the glider which then pulls the pilot through the air. The advantage of this design is that it places the motor weight nearer to the center of gravity. The disadvantages are that the propeller will now have a smaller diameter, and so will be less efficient, which means we will now require a larger motor and a larger and heavier power supply. The placement of the motor and propeller assembly is almost as bad as in design method two and requires FEET in order to keep the propeller from dragging the ground during takeoff and landing. The pilot now has to be careful not to twist his body during flight since this changes the thrust vector as the motor propeller assembly can be shifted if the pilot

twists his lower body instead of shifting his entire body while steering the aircraft.

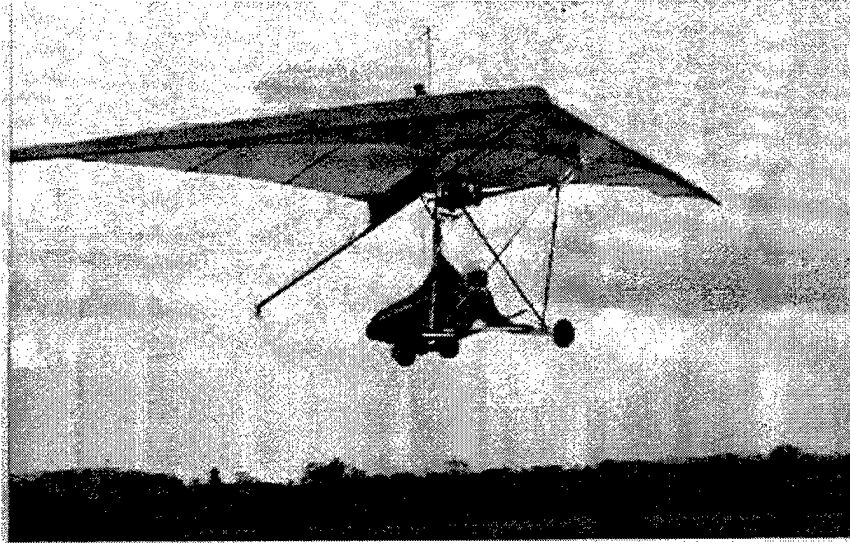


Figure 9 Front Mounted Motor [Ref. 20]

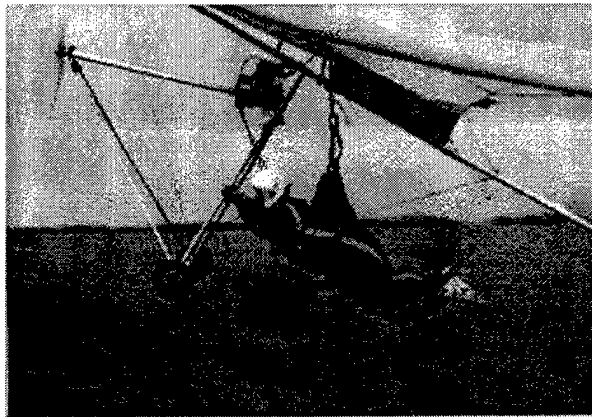


Figure 9a Take Off With Front Mounted Motor [Ref. 20]

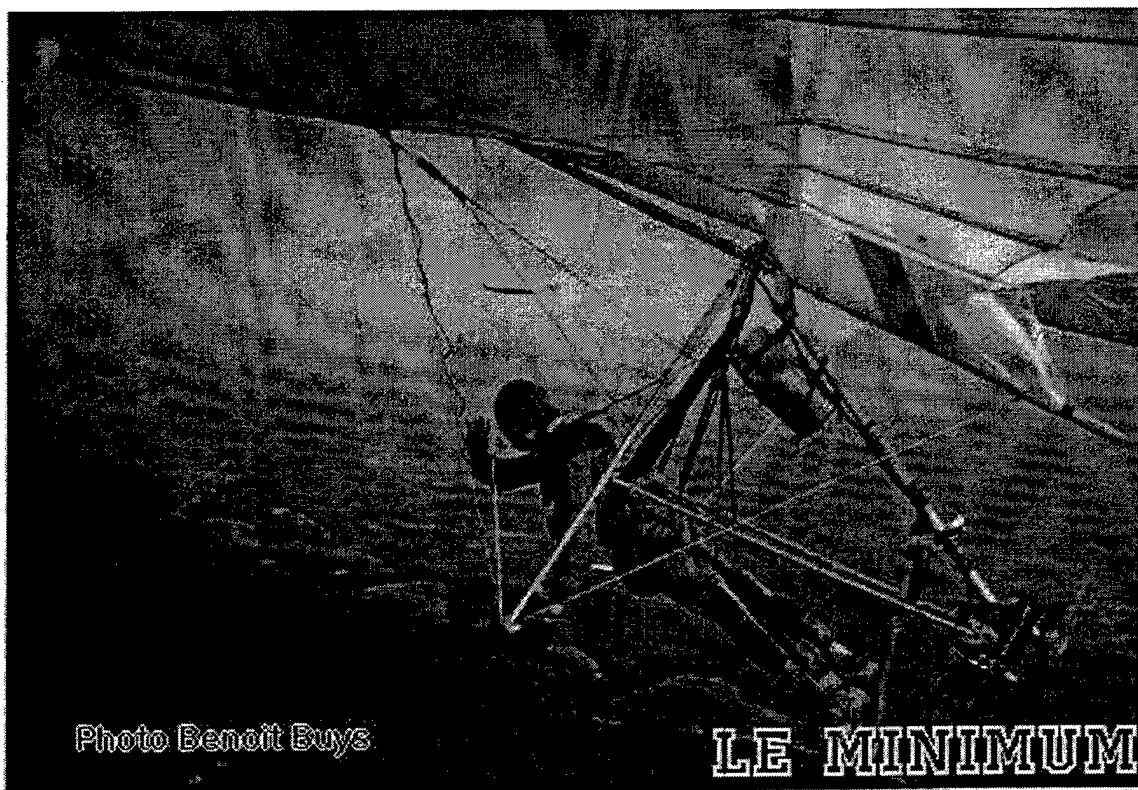


Figure 10 Rear Mounted Motor on Keel [Ref. 21]



Figure 11 Rear Mounted Motor on Pod [Ref. 22]



Figure 11a Take Off With Rear Mounted Motor on Pod [Ref. 22]

A problem discovered during interviews with pilots concerning the first three methods not yet discussed is the gyroscopic precession caused by the turning motor and propeller assembly. As the pilot prepares to takeoff he picks the FLML up, starts the motor, and begins running to create the airflow to generate lift. As soon as the pilot has some airflow creating lift over the wing the effective weight of the glider becomes less allowing him to run faster and generate more lift until there is enough lift to cancel the weight and begin flying. The problem is that the gyroscopic precession created by the motor and propeller assembly tries to push the glider 90 degrees away from the direction that the pilot is running. This problem is aggravated by increasing power to the motor and propeller assembly. This is shown by the following equations from Halliday and Resnick [Ref. 3].

$$K = mr^2\omega^2/2$$

where

$m = \text{mass}$

$r = \text{radius}$

$\omega = d\theta/dt$

With the first three methods described above the pilot is able to use only about 50% of his available power to takeoff and cannot increase power until he has some altitude.

The fourth design method avoids the problem of gyroscopic precession by using two motors and propellers which are counter rotating (Figure 12). The motors are mounted on the down tubes on either side of the pilot with the backs of the motors connected to wires that terminate on the keel of the glider. The advantages of this design are that the gyroscopic precession problem is avoided; the weight of the motors is kept near the center of gravity making takeoffs easier, and the pilots field of view is not obstructed. The disadvantages are the propellers are in the front making them more vulnerable to damage on landing, the placement of the propellers also means that the diameter will be smaller and so the propellers would be less efficient. If one engine is lost, glider controllability will be a problem; and since we are now using two motors,

controllers and propellers the cost of components will be greater.



Figure 12 Motor Mounted on Down Tubes [Ref. 23]

C. MOTOR AND PROPELLER

1. FLML Flight Parameters

As discussed earlier for a hang glider to achieve straight and level flight:

LIFT = WEIGHT

THRUST = DRAG

For a foot launched micro light to takeoff, climb, and maintain altitude; we require that lift exceed weight and thrust exceed drag by some margin. The rate of climb is given in Anderson [Ref. 10].

$R/C = TV-DV/W = \text{RATE OF CLIMB}$

where

T = THRUST

V = AIRSPEED

D = DRAG

W = WEIGHT

The FLML designs discussed above all had three flight parameters in common.

- Capable of climbing at a rate of 300 to 400 feet per minute.

- A gasoline powered reciprocating engine capable of producing approximately 15 HP.

- A propeller along with the motor and gear reduction capable of producing approximately 100 foot pounds of thrust.

2. Motor and Propeller Tradeoffs

Permanent Magnet Brushless Direct Current (PMBDC) motors have many advantages over conventional DC motors:

- More efficient energy utilization due to higher RPMS operation.
- Mechanically more reliable due to fewer mechanical parts.
- Smoother motor operation thus less thermal loss and longer motor life.
- More power output per pound.

The only disadvantages are that PMBDC motors are more expensive than conventional DC motors and it is difficult to effectively use the higher RPMS of the motor to turn a large diameter propeller efficiently.

The higher RPMS that the PMBDC motor utilizes, allows for a lightweight motor that generates high horsepower. The equation is given by Halliday and Resnick [Ref. 3].

$$\text{TORQUE, } T = \omega V^2 / 2$$

where

$$\omega = 2\pi \text{RPMS}$$

$$V = \text{VOLTAGE}$$

The propeller we must use will operate at much lower RPMS than the motor, to be efficient. This is true for any of the motor and propeller designs that we have looked at. Regardless of the design chosen, gear reduction will be required to run the motor at high RPMS while turning the propeller at lower RPMS. This is a big problem since using gear reduction to lower the RPMS of the propeller adds weight and wastes large amounts of energy. A gearbox will weigh approximately 5 to 10 pounds and will decrease efficiency by about 20%. We will have to look at the trade offs to decide if gear reduction is worth the cost in weight and efficiency.

A propeller is basically a wing that has been twisted. The turning motion creates an airflow over the surface which generates the lift force or thrust. This is computed with the following equations according to McCormick [Ref. 12].

$$\text{THRUST, } T = C_T \rho n^2 D^4$$

where

$$\rho = \text{AIR PRESSURE}$$

$$n = \text{REVOLUTION PER SECOND}$$

$$D = \text{PROPELLER DIAMETER}$$

C_T = THRUST COEFFICIENT (FUNCTION OF PROPELLER GEOMETRY)

As the equation demonstrates, the larger the propeller diameter and the faster it turns, the higher the thrust. This is true up to a point. Since each segment of the blade has a different angle of attack due to the twist, and each segment has a different free stream velocity due to its position relative to the hub, with the higher velocity near the tip, each segment would ordinarily have a different lift coefficient. To keep the lift coefficient approximately the same for each segment, the twist or beta and the cord length for each segment or c/R , is varied accordingly. This is what is meant by the geometry of the blade. As the propeller tip speed approaches the speed of sound, a shock wave is created which can destroy the propeller and so the diameter of the blade has to be matched to the RPMS of the motor. The efficiency of the entire blade tends to be highest when the tip speed is about one half the speed of sound. The smaller the propeller diameter, the higher the RPMS that can be used. Also, the higher the air pressure the more thrust is generated. This air pressure is not simply the atmospheric pressure for most aircraft. As the aircraft moves forward through the air, it causes the air striking the propeller, to become compressed. This has the effect of increasing the

air pressure with increasing aircraft speed which effectively increases thrust. This will not work in our case using free tip propellers as a hang glider will not fly safely at airspeeds much greater than 50 mph due to the harmonic oscillations, or vibrations, caused by the flexible wing design. For these reasons the most efficient propeller we can use will have a large diameter and turn at low RPMS.

The diameter of the propeller helps determine how much thrust it can generate. This propeller diameter also helps determine how much power is required from the motor. The power required is computed by McCormick [Ref. 12].

$$\text{POWER, } P = C_p \rho n^3 D^5$$

where

ρ = AIR PRESSURE

n = REVOLUTIONS PER SECOND

D = PROPELLER DIAMETER

C_p = POWER COEFFICIENT (FUNCTION OF
PROPELLER GEOMETRY)

This equation demonstrates that the motor power required is also a function of the thrust required based on the propeller diameter, RPMS, and the free stream velocity.

The tradeoffs we now have are to use a PMBDC motor turning at high RPMS, with a large diameter propeller turning at low RPMS which will require gear reduction. This will limit where we can mount the motor and propeller system. Conversely, we can use a smaller diameter propeller turning at higher RPMS with no gear reduction, but; this will require us to use a more powerful motor and power source which means more weight or less endurance. We can use a ducted fan type of propeller which will effectively increase the velocity of the air flowing into our propeller and so increase its efficiency, but; it will add some weight. The following tables demonstrate these trade offs. The tables were derived using Dr. Mark Drela's propeller software called XROTOR [Ref. 6]. The motors for each example are turning at 10000 RPMS. Table (1) shows the results for a 52 inch diameter propeller powered by a 16 HP motor at a hub speed of 3000 RPMS. The propeller generates over 122 foot pounds of thrust and is 45.3% efficient.

Table (1)

Free Tip Potential Formulation Solution:

	Wake adv. ratio: 0.09914
no. blades : 2	radius(m) : 0.6500 adv. ratio: 0.04897
thrust(N) : 543.604	torque(N-m): 38.1972 power(W) : 12000.003
Efficiency : 0.4530	speed(m/s): 10.000 RPMS : 3000.000
Eff induced: 0.4939	Eff ideal : 0.5303 Tcoef : 6.6811
Tnacel(N) : 0.0001	hub rad.(m): 0.0500 disp. rad.: 0.0500
rho(kg/m3) : 1.22600	Vsound(m/s): 340.000 mu(kg/m-s): 0.1780E-04

Ct: 0.06210 Cp: 0.02109 J: 0.15385

i	r/R	c/R	beta(deg)	CL	Cd	Re	Mach	effi	effp	na.u/U
1	0.085	0.6244	55.516	0.670	0.0089	527700	0.056	0.494	0.973	0.0000
4	0.198	0.3745	32.724	0.670	0.0081	679500	0.119	0.494	0.971	0.0000
7	0.342	0.2483	22.170	0.670	0.0078	775400	0.205	0.494	0.958	0.0000
10	0.482	0.1838	17.480	0.670	0.0078	809400	0.289	0.494	0.944	0.0000
13	0.612	0.1459	14.893	0.670	0.0080	815500	0.367	0.494	0.929	0.0000
16	0.727	0.1199	13.264	0.670	0.0084	796700	0.437	0.494	0.914	0.0000
19	0.825	0.0980	12.162	0.670	0.0089	739400	0.495	0.494	0.899	0.0000
22	0.903	0.0758	11.402	0.670	0.0099	625800	0.542	0.494	0.880	0.0000
25	0.959	0.0514	10.902	0.670	0.0116	450100	0.576	0.494	0.855	0.0000
28	0.991	0.0253	10.624	0.670	0.0154	229500	0.595	0.494	0.811	0.0000

New rotor geometry created

B 2 number of blades
 RT 0.6500 tip radius
 RH 0.0500 hub radius
 RW 0.0500 hub wake displacement body radius
 V 10.0000 airspeed
 A --- advance ratio
 R 3000.0000 RPMS
 T --- thrust
 P 12000.0000 power
 CC 0.6700 lift coefficient (constant)
 CL linear lift coefficient (root,tip)
 CX lift coefficient (cursor input)
 CR read CL(r/R) from file
 CW write CL(r/R) to file

Table (2) shows the results for a propeller of 2 feet in diameter powered by an 8 HP motor with a hub speed of 10000 RPMS and no gear reduction. The propeller generates 47.12 foot pounds of thrust and is 35% efficient. This is a two motor and propeller combination, but it does not quite generate the 100 foot-pounds of thrust we need. Table (3) shows the results for the same two motor and propeller combination with gear reduction to generate a hub speed of

4000 RPMS. This propeller generates 148 foot pounds of thrust and is 55% efficient. Table (4) shows the results for the same two motor and propeller combination with a ducted propeller and no gear reduction. The duct captures more air and accelerates it into the propeller effectively making the propeller diameter larger. This propeller generates over 135 foot-pounds of thrust and is 56% efficient.

Table (2)

Free Tip Potential Formulation Solution:

Wake adv. ratio: 0.07619
 no. blades : 2 radius(m) : 0.3048 adv. ratio: 0.03133
 thrust(N) : 209.585 torque(N-m): 5.7296 power(W) : 6000.000
 Efficiency : 0.3493 speed(m/s): 10.000 RPMS : 10000.000
 Eff induced: 0.4112 Eff ideal : 0.4380 Tcoef : 11.7144
 Tnacel(N) : -0.0002 hub rad.(m): 0.0500 disp. rad.: 0.0500
 rho(kg/m3) : 1.22600 Vsound(m/s): 340.000 mu(kg/m-s): 0.1780E-04

Ct: 0.04456 Cp: 0.01256 J: 0.09843

i	r/R	c/R	beta(deg)	CL	Cd	Re	Mach	effi	effp	na.u/U
1	0.168	0.2410	32.955	0.950	0.0124	267900	0.156	0.411	0.966	0.0000
4	0.244	0.1710	25.787	0.950	0.0124	277400	0.227	0.411	0.956	0.0000
7	0.368	0.1178	19.837	0.950	0.0127	289500	0.344	0.411	0.937	0.0000
10	0.498	0.0886	16.357	0.950	0.0134	295100	0.467	0.411	0.914	0.0000
13	0.622	0.0712	14.019	0.950	0.0145	296500	0.583	0.411	0.887	0.0000
16	0.734	0.0596	12.215	0.950	0.0163	292900	0.688	0.411	0.856	0.0000
19	0.829	0.0501	10.699	0.950	0.0193	278300	0.778	0.411	0.818	0.0000
22	0.905	0.0400	9.390	0.950	0.0242	242500	0.849	0.411	0.766	0.0000
25	0.960	0.0278	8.317	0.950	0.0331	178700	0.900	0.411	0.693	0.0000
28	0.991	0.0138	8.173	0.950	0.0432	91900	0.930	0.411	0.626	0.0000

New rotor geometry created

B 2 number of blades
 RT 0.3048 tip radius
 RH 0.0500 hub radius

RW 0.0500 hub wake displacement body radius
 V 10.0000 airspeed
 A --- advance ratio
 R 10000.0000 RPMS
 T --- thrust
 P 6000.0000 power
 CC 0.9500 lift coefficient (constant)
 CL linear lift coefficient (root,tip)
 CX lift coefficient (cursor input)
 CR read CL(r/R) from file
 CW write CL(r/R) to file

Table (3)

Ducted Potential Formulation Solution:

Vdisk/Vslip: 1.00000 Wake adv. ratio: 0.20019
 no. blades : 2 radius(m) : 0.3048 adv. ratio: 0.07832
 thrust(N) : 331.619 torque(N-m): 14.3240 power(W) : 6000.003
 Efficiency : 0.5527 speed(m/s): 10.000 RPMS : 4000.000
 Eff induced: 0.5711 Eff ideal : 0.3690 Tcoef : 18.5353
 Tnacel(N) : 104.6351 hub rad.(m): 0.0500 disp. rad.: 0.0500
 rho(kg/m3) : 1.22600 Vsound(m/s): 340.000 mu(kg/m-s): 0.1780E-04

Ct: 0.44071 Cp: 0.19620 J: 0.24606

i	r/R	c/R	beta(deg)	CL	Cd	Re	Mach	effi	effp	na.u/U
1	0.168	1.3091	63.556	0.950	0.0090	591600	0.063	0.571	0.980	0.0000
4	0.244	0.9852	50.399	0.950	0.0088	629600	0.090	0.571	0.982	0.0000
7	0.368	0.7198	37.822	0.950	0.0085	695800	0.135	0.571	0.979	0.0000
10	0.498	0.5629	30.530	0.950	0.0083	741800	0.185	0.571	0.975	0.0000
13	0.622	0.4654	26.208	0.950	0.0083	769000	0.231	0.571	0.971	0.0000
16	0.734	0.4017	23.474	0.950	0.0083	784500	0.274	0.571	0.966	0.0000
19	0.829	0.3589	21.672	0.950	0.0084	793000	0.310	0.571	0.962	0.0000
22	0.905	0.3302	20.477	0.950	0.0084	797200	0.338	0.571	0.959	0.0000
25	0.960	0.3120	19.719	0.950	0.0085	798900	0.359	0.571	0.957	0.0000
28	0.991	0.3021	19.311	0.950	0.0085	799300	0.371	0.571	0.955	0.0000

New rotor geometry created

B 2 number of blades
 RT 0.3048 tip radius
 RH 0.0500 hub radius

RW 0.0500 hub wake displacement body radius
 V 10.0000 airspeed
 A --- advance ratio
 R 4000.0000 RPMS
 T --- thrust
 P 6000.0000 power
 CC 0.9500 lift coefficient (constant)
 CL linear lift coefficient (root,tip)
 CX lift coefficient (cursor input)
 CR read CL(r/R) from file
 CW write CL(r/R) to file

Table (4)

Ducted Potential Formulation Solution:

Vdisk/Vslip: 1.00000 Wake adv. ratio: 0.07362
 no. blades : 2 radius(m) : 0.3048 adv. ratio: 0.03133
 thrust(N) : 300.838 torque(N-m): 5.7296 power(W) : 5999.996
 Efficiency : 0.5014 speed(m/s) : 10.000 RPMS : 10000.000
 Eff induced: 0.5983 Eff ideal : 0.3831 Tcoef : 16.8148
 Tnacel(N) : 87.0160 hub rad.(m): 0.0500 disp. rad.: 0.0500
 rho(kg/m3) : 1.22600 Vsound(m/s): 340.000 mu(kg/m-s): 0.1780E-04

Ct: 0.06397 Cp: 0.01256 J: 0.09843

i	r/R	c/R	beta(deg)	CL	Cd	Re	Mach	effi	effp	na.u/U
1	0.168	0.2261	32.798	0.950	0.0127	252200	0.156	0.598	0.965	0.0000
4	0.244	0.1591	25.417	0.950	0.0128	258500	0.228	0.598	0.954	0.0000
7	0.368	0.1083	19.489	0.950	0.0131	266300	0.344	0.598	0.933	0.0000
10	0.498	0.0810	16.070	0.950	0.0139	270000	0.467	0.598	0.908	0.0000
13	0.622	0.0652	13.779	0.950	0.0150	271600	0.584	0.598	0.880	0.0000
16	0.734	0.0554	12.006	0.950	0.0168	272400	0.688	0.598	0.848	0.0000
19	0.829	0.0491	10.512	0.950	0.0194	272900	0.778	0.598	0.811	0.0000
22	0.905	0.0451	9.218	0.950	0.0231	273100	0.849	0.598	0.768	0.0000
25	0.960	0.0425	8.156	0.950	0.0280	273200	0.900	0.598	0.721	0.0000
28	0.991	0.0412	8.016	0.950	0.0280	273300	0.930	0.598	0.714	0.0000

New rotor geometry created

B 2 number of blades
 RT 0.3048 tip radius
 RH 0.0500 hub radius
 RW 0.0500 hub wake displacement body radius

V 10.0000 airspeed
 A --- advance ratio
 R 10000.0000 RPMS
 T --- thrust
 P 6000.0000 power
 CC 0.9500 lift coefficient (constant)
 CL linear lift coefficient (root,tip)
 CX lift coefficient (cursor input)
 CR read CL(r/R) from file
 CW write CL(r/R) to file

If we use a 20% inefficiency factor for the gear reduction we see that the propeller in Table (3) generates about 118 foot pounds of thrust while the one in Table (2) generates about 94 foot pounds, not a tremendous difference when we take into account the additional weight of the gear box required. The ducting used in Table (4) increases our efficiency by 20% and seems to be the best choice compared to the other two. Summarizing from the tables:

TABLE (2) PROPELLER = $47 \times 2 = 94$ FT/LBS

TABLE (3) PROPELLER = $148 - (148 \times 0.2) = 118$ FT/LBS

TABLE (4) PROPELLER = $67.5 \times 2 = 135$ FT/LBS

More detailed information and the equations to obtain propeller geometry is given in Appendix (A).

D. POWER SOURCE CONSIDERATIONS

1. Battery

Batteries come in a variety of sizes, shapes, weights, and designed capabilities. Batteries are generally designed for specific applications. Some batteries are designed to provide steady power for long periods of time. Others provide a relatively high power output for shorter periods of time. Certain applications require a capability for a high power output or surge, for a short period of time and then provide a lower steady power output for the rest of the time. Some batteries are rechargeable, others are not. Some can be recharged many times, others only a few times. Higher shelf life, or a battery that doesn't discharge itself when no load is placed on it, is important in certain applications, while other applications do not require this.

The main advantages of batteries with respect to our requirements are that they can be tailored to our specific application, they can be recharged, and they are relatively inexpensive. The main disadvantages are that as an energy storage device, batteries are inefficient (when comparing watts per kilogram), and; batteries generally don't respond well to surge, or power on demand requirements.

Battery technology is improving every year. A comparison of the tradeoffs available with different types

of batteries is displayed on the following chart (Figure 13).

Generic battery technology comparison

Page under development. Surprised? These numbers are gathered from multiple sources under different conditions. So comparisons are difficult at best and any actual comparison should use proven data for a particular model of battery. Batteries perform differently due to different processes used by different manufacturers and different models from the same manufacturer will perform differently depending on what they are optimized for. The actual application will dramatically affect a battery's performance and the choice of battery.

Technology	Density				Cycle life to 80% DOD	self discharge %/month	maturity	cost			Range* +/-50% km	unique features
	energy Wh/kg	power W/kg	energy Wh/l	power W/l				current \$/kWh	future \$/kWh	environmental		
Flooded lead acid					600	20	mature	100	100	low with recycling	96	modest performance lead
Advanced lead acid	35	71	412	955	500	5	production	150	100?	low with recycling	160	high performance lead
Nickel Cadmium	50	150			2000?	100	mature			high cadmium		
Nickel Metal Hydride	80	200	220	600	600+		production	2000	600	low	320	
Lithium Ion	100	300			1200		laboratory			low		
Lithium Polymer (3M)	155	220	315	445	600+	1000	prototype			low		can pack in body panels saving space!
Lithium Polymer Potential	400	500	1000		600+		laboratory			low		can pack in body panels saving space!
Sodium Nickel Chloride	90	150	100	200		400	prototype		300			Recharged by Zn electrode replacement
Zinc Air	200	200	100	30			prototype	300	100	low		Mechanical!
Flywheel							laboratory			low		
Ultra Capacitor		5		10**3 10**8			laboratory			low		
Vanadium Redox							laboratory					Electrical or mechanical recharge by replacing electrolyte

* - Range values are HIGHLY dependent on aerodynamics, battery mass, vehicle mass, drive train efficiency, weather, tires and other factors. Consequently, a highly optimized state of the art vehicle can easily get 2 to 3 times the range of a vehicle not optimized for range for a given battery technology. The range numbers are included to give a relative feel for the battery technology without having to derive it from energy density. The range assumes an efficient vehicle with good aerodynamics in the 1000 kg without batteries sedan range driven on dry pavement using some energy conserving driving habits.

Conversion factors: 1km = 0.62 miles, 1 mile = 1.6 km

Data are optimized, independent values. For example, when testing for peak power (power density) energy is removed from the battery so fast that it may only have 10-50% of it's capacity. When testing for capacity (energy density), the power levels are lower to get a higher capacity.

Data extracted from hear say, manufacturers, and EE Times.

Some of the data is from small cells like AA batteries. Data for EV batteries is used where available.

Data is selected to reflect higher density battery implementations without going into astronomical cost premiums.

Data reflects the electric vehicle market. I.e. NiMh batteries are in production for portable electronics but are in a prototype stage for electric vehicle size batteries.

Depending on the technology, state of development, production volumes and size of battery cell these numbers can easily vary by +/-50%. Cost in some cases may be off by a factor of 10 or more as laboratory or prototype batteries move into high volume production.

[home]

m.t.thompson@iecc.org

Figure 13 Battery Comparison [Ref. 15]

2. Fuel Cell

Fuel cells offer some advantages over batteries. They are much more energy efficient storage devices compared to batteries (as measured by watts per kilogram). Certain types such as Proton Exchange Membrane (PEM) fuel cells are much better at providing power on demand. The technology is advancing every year and since the major automobile manufacturers are investing heavily in the research, large advances are expected to be made. The main disadvantages of today's fuel cells are the cost, the fact that the technology is still maturing, and that they can not be recharged like batteries. The fuel, hydrogen and oxygen for PEM, must be replaced as it is used. This means that one of our requirements, to be able to recharge the power source with a solar panel in the field, can not be met with this technology.

3. Generator

The major advantage of using a generator to provide electrical power for our hang glider is that we could use a hydrocarbon fuel which is very energy dense. The major disadvantages are that we would need to use an internal combustion engine to provide mechanical energy to the generator which is not very energy efficient, we have to add fuel, can not recharge with a solar panel in the field; and generators are also not very energy efficient (comparing

watts per kilogram) due to their heavy weight. Generators are built for specific commercial applications, usually to provide portable or backup power for conventional power sources. A generator of the type we would require would have to be specially built and so, expensive. The only advantage of the generator, that of using a hydrocarbon energy dense fuel, could also be met by using a fuel cell.

4. Analysis of Power Requirement for Electrically Propelled Hang Glider

This is an approximate analysis of the power requirements for an Electrically Powered Hang Glider in climb and cruise mode. All units are in MKS. The equations were computed using MATHCAD.

First we will define all of the input parameters.

1. Rate of Climb.

Rate of climb is usually expressed in feet per minute.

$$\text{Rate}_{\text{climb}} := 300 \frac{\text{ft}}{\text{min}}$$

$$\text{Rate}_{\text{climb}} = 1.524 \cdot \text{m} \cdot \text{s}^{-1}$$

2. Power to Climb.

The power required to climb at the above rate is expressed in HP

$$P_{\text{climb}} := 15 \text{ hp}$$

$$P_{\text{climb}} = 11.185 \cdot \text{kW}$$

3. Height to Climb.

$$h_{\text{climb}} := 1000 \text{ ft}$$

$$h_{\text{climb}} = 304.8 \cdot \text{m}$$

4. Time to Climb.

$$t_{\text{climb}} := \frac{h_{\text{climb}}}{\text{Rate}_{\text{climb}}}$$

$$t_{\text{climb}} = 3.333 \cdot \text{min}$$

5. Energy for Climb.

$$E_{\text{climb}} := P_{\text{climb}} \cdot t_{\text{climb}}$$

$$E_{\text{climb}} = 2.237 \cdot 10^6 \cdot \text{J}$$

Convert to kWh

$$E_{\text{climb_kWh}} := E_{\text{climb}} \cdot 10^{-3} \cdot \frac{1}{3600}$$

$$E_{\text{climb_kWh}} = 0.621 \cdot \text{kg} \cdot \text{m}^2 \cdot \text{s}^{-2}$$

6. Analysis of Silver-Zinc Battery Pack.

$$N_{\text{cells}} := 70$$

$$V_{\text{cell}} := 1.47 \text{ V}$$

7. The Current Required for Climb.

$$V_{\text{bat}} := N_{\text{cells}} \cdot V_{\text{cell}}$$

$$V_{\text{bat}} = 102.9 \cdot \text{V}$$

$$Q_{\text{cell}} := 20 \cdot 3600 \text{ C} \quad \text{for 20 AMPS \& 1 HR}$$

$$\eta_{\text{motor_controller}} := 0.9 \quad \text{OR } 90\%$$

$$I_{\text{climb}} := \frac{P_{\text{climb}}}{V_{\text{bat}} \cdot \eta_{\text{motor_controller}}}$$

$$I_{\text{climb}} = 120.781 \cdot \text{A}$$

8. Percentage of Battery Capacity used to Climb.

$$Q_{\text{climb}} := I_{\text{climb}} \cdot t_{\text{climb}}$$

$$Q_{\text{climb}} = 2.416 \cdot 10^4 \cdot \text{C}$$

$$Q_{\text{climb_percent}} := 100 \cdot \frac{Q_{\text{climb}}}{Q_{\text{cell}}}$$

9. Percentage of Battery Capacity used to Climb 1000 feet in 3 minutes.

$$Q_{\text{climb_percent}} = 33.55$$

10. The Current Required for Cruise.

$$P_{\text{cruise}} := 4 \text{ hp}$$

$$I_{\text{cruise}} := \frac{P_{\text{cruise}}}{V_{\text{bat}} \cdot \eta_{\text{motor_controller}}}$$

$$I_{\text{cruise}} = 32.208 \cdot \text{A}$$

11. Penalty Paid For High Discharge Rate.

The battery delivered capacity is a function of the battery discharge current. The nominal capacity is specified

for the discharge current numerically equal to 1/10 of the nominal capacity in Ah (for a 20 Ah battery the nominal discharge current is 2 A). If a battery is discharged at a current higher than the nominal the battery will deliver less than the nominal capacity. (The higher the discharge current, the higher the penalty).

Since the battery for the glider is discharged at a high current the capacity reduction will be significant. This is approximately modeled by the penalty function with three parameters (maximum penalty, penalty coefficient, and the ratio of the actual discharge current and the nominal discharge current).

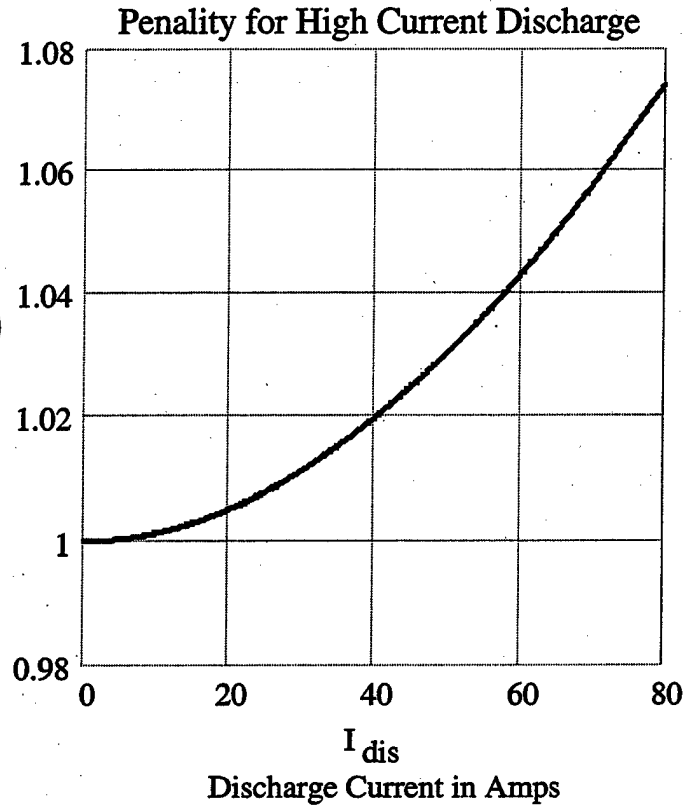
$$P(p_{\max}, p_c, I_{\text{dis}}, I_{\text{nom}}) := \frac{1}{\frac{1}{p_{\max}} + \frac{1 - \frac{1}{p_{\max}}}{1 + p_c \cdot \left(\frac{I_{\text{dis}}}{I_{\text{nom}}}\right)^2}}$$

$$p_{\max} := 2 \quad p_c := 1 \cdot 10^{-4} \quad I_{\text{nom}} := 2 \text{ A}$$

$$I_{\text{dis}} := 0,01 \cdot I_{\text{nom}} \dots 40 \cdot I_{\text{nom}}$$

Battery Capacity Reduction

$$P(p_{\max}, p_c, I_{\text{dis}}, I_{\text{nom}})$$



The charge available at any given time is a function of the history of the battery discharge up to that time. This is quantified by the available charge $Q(t)$.

We will assume one climb to 1000 feet in three minutes and then maintain cruise flight at that altitude.

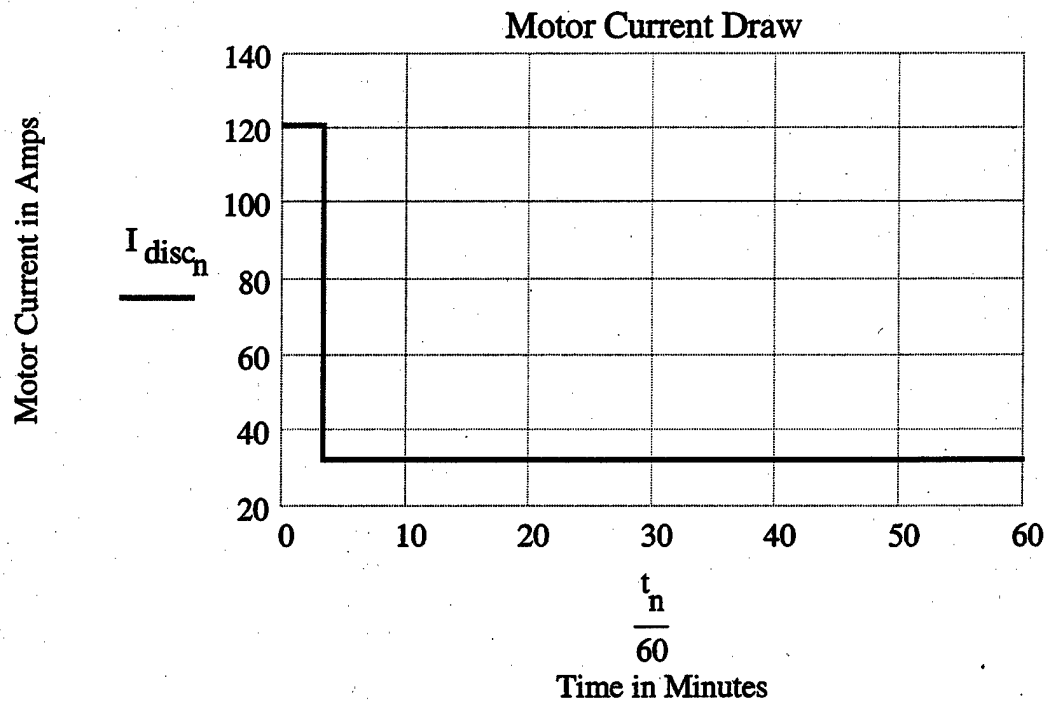
$$N_{\text{sec}} := 3600$$

$$n := 0, 1 \dots N_{\text{sec}}$$

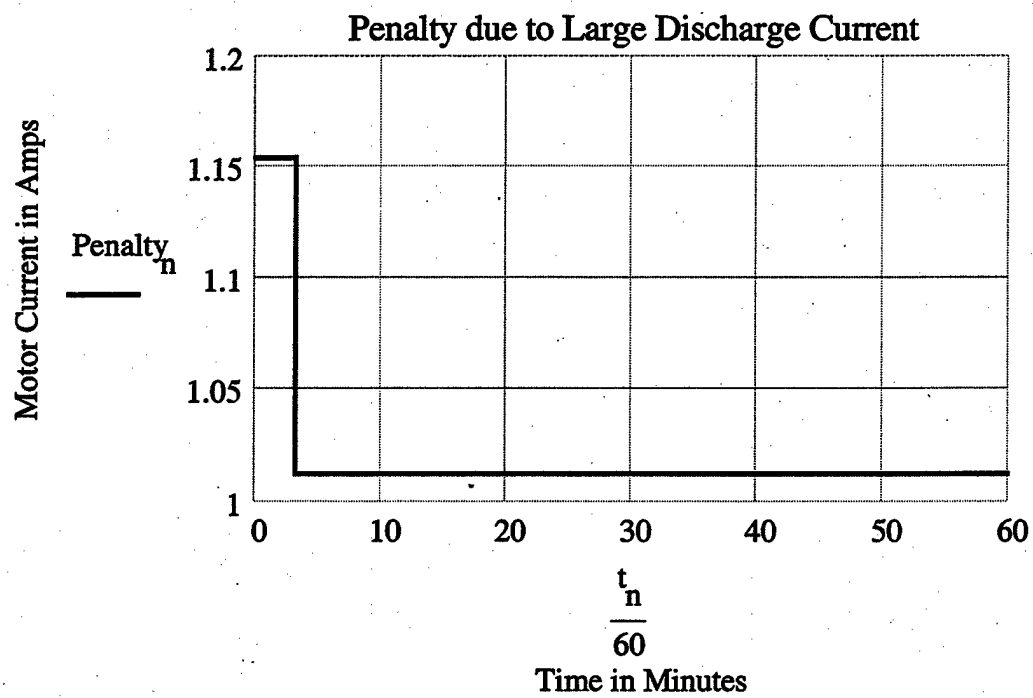
$$\Delta t := 1 \text{ s}$$

$$t_n := n \cdot \Delta t$$

$$I_{\text{disc}_n} := \text{if}(t_n < t_{\text{climb}}, I_{\text{climb}}, I_{\text{cruise}})$$



$$\text{Penalty}_n := P(p_{max}, p_c, I_{disc_n}, I_{nom})$$

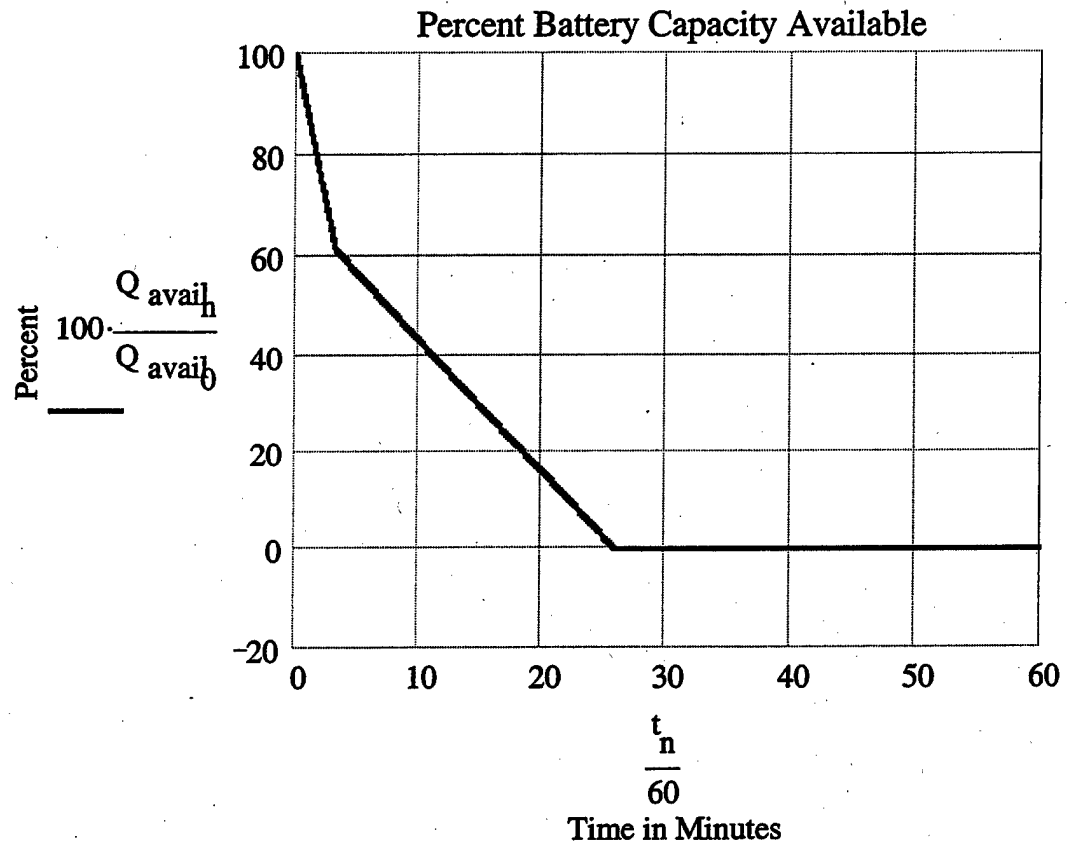


$$Q_{avail_0} := Q_{cell}$$

$$n := 1..N_{sec}$$

$$Q_{avail_n} := \text{if}(Q_{avail_{n-1}} > 0, Q_{avail_{n-1}} - I_{disc_n} \cdot \Delta t \cdot \text{Penalty}_n, 0)$$

$$n := 0..N_{sec}$$



As the graph above demonstrates, with one climb to 1000 feet at maximum power; and, cruising at 4 HP, we can expect a total flight time of approximately 26 minutes.

VII. DESIGN PROPOSAL FOR A RECONNAISSANCE AND INTELLIGENCE DELIVERY EQUIPMENT (RIDE) SYSTEM

In accordance with the mission requirements specified at the beginning of this thesis; the following design proposal is believed to best meet these mission requirements.

A. HANG GLIDER DESIGN

The hang glider selected is a PULSE 2-18 model manufactured by AIRWAYS, Inc. This is a novice glider with a double surface. This hang glider has forgiving handling characteristics, offers a good L/D ratio, and a low drag profile. It has the following dimensions.

ASPECT RATIO,	AR = 5.9
SURFACE AREA,	S = 189 FT²
WING SPAN,	b = 33.5 FT
WEIGHT OF GLIDER	W_G = 60 LBS
WEIGHT GLIDER SUPPORTS	W = 250-280 LBS
CORD AT ROOT,	C_R = 19.47 FT
CORD AT TIP,	C_T = 0.67 FT
MAX CORD THICKNESS	t/c = 0.67-1 FT

SWEEP AT NOSE = 126 DEGREES

WASHOUT = 18 DEGREES

RECOMMENDED NEVER EXCEED SPEED = 50 MPH

STALL SPEED = 10-12 MPH

MINIMUM SINK SPEED = 15-16 MPH

BEST GLIDE (L/D) = 25 MPH

BEST CRUISE SPEED = 30 MPH

Using the U.S. Air Force DatComm method, a parasite drag coefficient, C_{D0} of 0.066 was obtained. This derivation is given in Appendix (B). The following equations are given in "The Fundamentals of Aerodynamics" and the "Introduction to Flight" by John D Anderson, [Ref. 9 & 10].

$$\text{LIFT COEFFICIENT Climb, } C_{L\max} = 2W/S\rho V^2 = 1.55$$

where

W = AIRCRAFT WEIGHT = 300 LBS

S = SURFACE AREA = 189 FT²

$\rho = 0.002378$ SLUGS/FT³

V = 29.4 FEET PER SECOND

(ASSUMING 20 MPH FOR CLIMB)

$$\text{LIFT COEFFICIENT CRUISE} = C_{LCRUISE} = 2W/S\rho V^2 = 0.69$$

where

$$V^2 = \text{VELOCITY AT CRUISE} = 44 \text{ FEET PER SECOND} = 30 \text{ MPH}$$

$$\text{DRAG COEFFICIENT CLIMB, } C_{DCLIMB} = C_{DO} + C_{DI} = C_{DO} + C_L^2 / \pi \epsilon AR =$$

0.23

where

$$C_{DO} = 0.066$$

$$C_{LCLIMB} = 1.55$$

$$\epsilon = 0.8 \text{ (WING EFFICIENCY)}$$

$$AR = 5.9$$

$$\text{DRAG COEFFICIENT CRUISE, } C_{DCRUISE} = C_{DO} + C_L^2 / \pi \epsilon AR = 0.09$$

where

$$C_{LCRUISE} = 0.69$$

$$\text{DRAG CLIMB, } D_{CLIMB} = q C_{DCLIMB} S = 48.2 \text{ LBS}$$

where

$$q = 1/2 \rho V^2$$

$$\text{DRAG CRUISE, } D_{CRUISE} = q C_{DCRUISE} S = 39.14 \text{ LBS}$$

$$\text{LIFT, } L = q C_L S = 300 \text{ LBS}$$

FOR CLIMB AT 300 FEET PER MINUTE

THRUST FOR CLIMB, $T_{CLIMB} = (R/C)W/V_{CLIMB} + D_{CLIMB} = 99.4 \text{ FT LBS}$

where

RATE OF CLIMB = $R/C = 300 \text{ FT/MIN} = 5 \text{ FT/S}$

WEIGHT OF AIRCRAFT = $W = 300 \text{ POUNDS}$

VELOCITY OF CLIMB = $V_{CLIMB} = 29.4 \text{ FT/S}$

DRAG OF CLIMB = $D_{CLIMB} = 48.2 \text{ POUNDS}$

POWER FOR CLIMB, $P_{CLIMB} = T_{CLIMB}V_{CLIMB}/550 = (99.4\text{LBS} \times 29.4 \text{ FT/S})/550 = 5.32 \text{ HP}$ (BEFORE CALCULATING PROPELLER AND MOTOR INEFFICIENCIES)

THRUST OF CRUISE, $T_{CRUISE} = W/L/D_{CRUISE} = 300/300/39.14 = 39.14 \text{ LBS}$

POWER OF CRUISE, $P_{CRUISE} = \text{SQRT}(2W^3C_{DCRUISE}^2/\rho SC_{LCRUISE}^3) = 3.13 \text{ HP}$

(ESTIMATED AT CRUISE BEFORE INEFFICIENCIES)

B. METHOD OF MOUNTING THE MOTOR AND PROPELLER

Method 4 of mounting the motor and propeller system will allow us to use 100% of available power during takeoff. We will mount two counter rotating motor and propeller systems, one on each side of the down tubes. We will be

constrained somewhat on the propeller diameter we can use; but, it will allow us to keep the weight of the motors near the center of gravity located approximately one foot above the pilots chest, which will make for better controllability during takeoff and cruise flight. The propellers, while located somewhat forward are not in a catastrophically bad position concerning the possibility of NOSING the hang glider in during landing and possibly breaking a propeller.

Since we will be using two motors and controllers instead of one, the motors can be approximately half as powerful or about 7.5 horsepower each. This design is also the only one feasible since a light-weight PMBDC 15 HP motor does not seem to exist at present. Although the propellers will have a somewhat smaller diameter because of their placement, about 2 feet in diameter maximum, they only need to generate approximately 50 foot pounds of thrust each.

C. MOTOR, CONTROLLER AND PROPELLER

The motor selected weighs 6 pounds. It is a PMBDC motor from FISHER ELECTRIC INDUSTRIES (Figure 11). It will generate 8HP at 12000 RPMS. The controller is a high current, transistor switched, Hall effect sensor model designed by MAGNA POWER, INC. using MOTOROLA components. The motor and controller combination will require a power source of 100 volts and 60 amps for each motor, in order to generate a total of 12 kilowatts of power required for

climbing. When the hang glider is in cruise mode it will require less power, approximately 4 HP or 3 kilowatts. Using a propeller with a diameter of 2 feet with these motors and controllers will generate approximately 50 foot-pounds of thrust. The most efficient speed for a propeller of this diameter is approximately 4000 RPMS, but; as demonstrated in tables (2) and (3) we get better results without gear reduction. The motors will have to turn at approximately 10000 RPMS under the 50 foot pounds of load to generate the full 8 HP each, required for climb. The motor and propeller systems will be shipped to MAGNA POWER, for integration with the controllers. A variometer to control power into the motor will be used as a throttle to increase motor power on demand. This variometer will use Pulse Width Modulation to control power to the motor. The controller will run the motor at a constant RPMS.



Figure 14 Fisher 8 HP Motor [Ref. 18]

The load on the motor is a function of the angle of attack of the aircraft, which puts varying loads, or requirements for thrust, on the propeller. The load, and so thrust requirements, will be greater during climb than during cruise, since the angle of attack is greater during climb. Schematics of the motor and controller are given in Appendix (D). What we see is that our propeller is only about 35% efficient. The power requirement is given below.

POWER REQUIRED TO FLY, $P_F = 5.3 \text{ 1HP}$

PROPELLER EFFICIENCY, $\eta_P = 0.35$

MOTOR EFFICIENCY, $\eta_M = 0.9$

POWER TO CLIMB, $P_C = 5.31 + (5.31 \times 0.75) = 9.3 \text{ HP}$

This 9.3 HP is the total estimated power required from both motors. As was previously mentioned, for most of the design methods researched, a 15 HP engine was used. Our calculations show that we could use less motor power, $P_c = 9.3 \text{ HP}$; but, the propeller code showed that at 16 HP without gear reduction we would not quite generate 100 foot-pounds of thrust. We can climb with this motor and propeller combination, but; probably not quite at 300 feet per minute. If we use a ducted fan design (table 4), we can generate 135 foot-pounds of thrust or use less power. Using 5.75 HP from each motor or 11.5 HP total, we can generate 100 foot pounds

of thrust with the ducted propeller design. This is close to the 9.3 HP we computed using Anderson's [Ref. 9 & 10] equations.

D. POWER SOURCE SELECTED

1. Tradeoffs for Different Power Sources

Although a fuel cell would have been the first choice for a power source because of its excellent power on demand capability; a lightweight PEM fuel cell that meets our power requirements has not yet been developed commercially. One was found (Figure 15) that was lightweight, but it did not deliver the required power. While it might be possible to have one built that could deliver 12 kW for approximately 3-4 hours at a weight of about 50 pounds, the cost is prohibitive. A conversation with Mr. Henry Derouk, International Fuel Cell, the company that builds fuel cells for NASA, stated that the research and development could cost well over a million dollars. The same could be said for the generator. A special one-of-a-kind generator would have to be built and it would still suffer from some of the same problems mentioned earlier according to a conversation with Mr. Johnny Baldwin, U.S. Army Space and Missile Defense Command. Batteries, although not very efficient power storage devices are still the best devices available today at a reasonable cost. One battery from the 3M Company was very good; but, at present it is still in pre-production and

cost prohibitive, over \$40,000. Silver-Zinc batteries, although older technology, still appear to be best suited for this application. Additional information on the battery from 3M and the Silver-Zinc batteries used are listed in Appendix (C) and the fuel cell in Appendix (E).

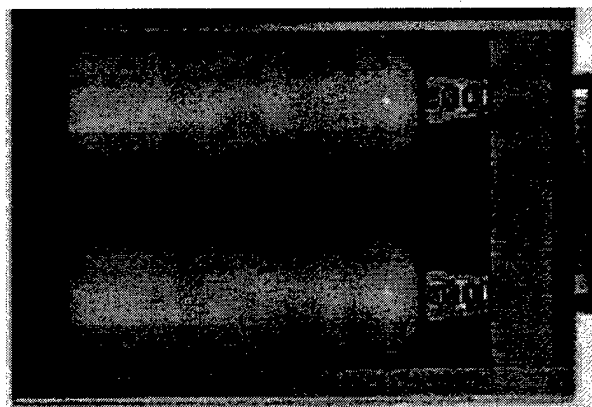
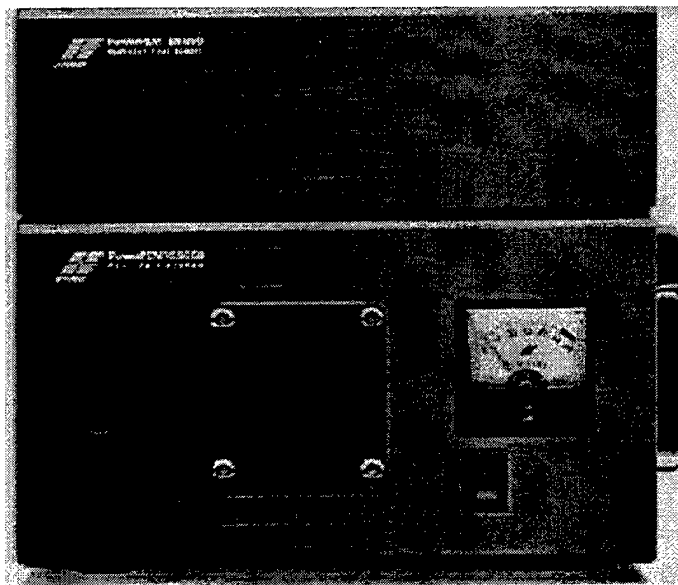


Figure 15 H-Power Fuel Cell [Ref. 17]

VIII. CONCLUSIONS AND FOLLOW ON RESEARCH

A. CONCLUSIONS

As can be seen from the power analysis, a Silver-Zinc battery weighing approximately 60 pounds, shown in the YARDLEY Inc. chart in Appendix (C), (70 cells at 13.5 ounces, 1.47 volts ea., 120 Max amps, 20 Ahr capacity); will give the glider approximately a 3 minute climb at maximum power, and about 23 minutes of cruise flight at the estimated 4 HP required.

CELL WEIGHT, $W_C = 13.5$ OUNCES

BATTERY WEIGHT 70 CELLS, $W_B = 13.5 \times 70 = 59$ LBS

NOMINAL VOLTAGE $= 1.47 \times 70 = V_N = 102.9$ VOLTS

MINIMUM VOLTAGE $= 1.33 \times 70 = V_M = 93.1$ VOLTS

MAXIMUM CURRENT $= 120$ AMPS, AT 17.5 AMP HR

NOMINAL AMP HOURS $= 20$

POWER $=$ VOLTAGE \times CURRENT $= V \times I$

TIME TO CLIMB 1000 ft at 300 ft per min $= 1000/300 = 3.34$ min

ENERGY MAX $= E_M = 93.1V \times 17.5A\text{-hr} = 1629$ W-hr

ENERGY CLIMB $= 16HP \times 746W/HP \times 3.34/60$ hr $= 664.44$ W-hr

ENERGY CRUISE $=$ ENERGY MAX - ENERGY CLIMB $= 964.81$ W-hr

TIME CRUISE $= 964.81$ W-hr $/ (4HP \times 746W/HP \times 60$ min/hr) $= 19.39$ min

TOTAL FLIGHT TIME = TIME CRUISE + TIME CLIMB = 22.74 min

The total weight of the aircraft now comes to:

GLIDER = 60

x2 MOTORS = 12

x2 PROPS = 2

x2 DUCTS = 4

x2 CONTROLLERS = 4

x2 MOUNTING ARMS = 2

BATTERY = 60

***AIRCRAFT WEIGHT = 144 POUNDS**

Add a 200 pound pilot and we are now close to our maximum allowable weight of 350 pounds.

Our aircraft will climb at the rate of 300 to 400 feet per minute and cruise at 30 to 50 mph. It will lift a 200 pound load. Using commercial-off-the-shelf (COTS) components that are not too expensive will work; but, it does not meet all of our stated mission requirements. The system just described would cost approximately \$40,000 to build. The problems with the aircraft include:

- Aircraft is too heavy, 144 versus 130 pounds.

- Not enough endurance, 23 versus 120 minutes of flight.

- Glider will not break down to a man portable load for ground movement, 12 versus 6 feet long.

Using inexpensive components that were not designed to work together for optimizing our aircraft has not been totally successful.

B. FOLLOW ON RESEARCH

There are several improvements that would allow us to meet or exceed our stated mission requirements. If we use components such as those described in this thesis, but; design each so that the total SYSTEM is optimized rather than using commercial-off-the-shelf components, we can truly optimize the aircraft.

There are several problem areas to be studied and each would offer component improvement that would increase the overall aircraft performance. First would be to reduce the thrust required to fly, second would be to increase the motor and propeller combination efficiency, and third would be to reduce the weight of the power source while increasing its energy density.

To reduce the thrust required to fly, the hang glider will need to generate more lift, have a better L/D, and have less total drag. While modern hang gliders are marvels of aeronautical engineering; there have been no major

improvements in design since the early 1980's. By using composite materials it should be possible to build a lighter and aerodynamically CLEANER hang glider with a larger aspect ratio. Since a composite glider would be lighter the pilot's weight would be effectively increased for purposes of controlling the glider, i.e., weight shift to climb, descend, and turn; so we could increase the aspect ratio giving us more lift while still maintaining pilot controllability. Wing spars which maintain wing rigidity without using king posts and wires are being used on newer expert hang gliders today. This greatly reduces the drag of the glider, but; they also increase the weight. By using composite materials it should be possible to use the wing spars and keep the weight down. Concerning the portability of the glider on the ground, there is one hang glider called the Target by Aeros Inc, that will break down to a tube of 6 feet in length and approximately 6 inches in diameter. It was not used for this design because it is single surfaced and thus has more parasite drag than the Pulse 2-18. It should be possible to further reduce the length of the ground transportable tube by removing the sail, not a lightly undertaken job at present. Ideally, the whole assembly could be broken down and stored in the pilot's POD for easy ground movement.

The optimization of the motor and propeller assembly could reduce the power required by increasing efficiency so

that the same thrust can be obtained with less motor power. One way to do this would be to use a pancake designed PMBDC motor with a very large diameter armature. Making the motor this large in diameter will reduce the effectiveness of the propeller somewhat since a large diameter hub reduces efficiency, but; it will dramatically increase the torque, and so the power of the motor at lower RPMS, possibly to the point that gear reduction would not be required to achieve a high propeller efficiency. The propeller geometry and diameter can then be matched to the motor and a duct could be used to further increase the efficiency. This could increase the thrust using less motor power since we have increased our motor and propeller combination efficiency by designing the motor for low RPMS and high torque and designing our propeller and duct specifically for our high torque at lower RPMS motor. Another method would be to build a multiple blade ducted fan propeller. This ducted fan along with the motor would be more like a fan jet engine, but; optimized for low free stream velocity and an extremely high RPMS motor. If enough slip stream velocity and air volume could be generated inside the duct behind the fan, a stator could be used to further increase the total thrust of the blades. This design would maximize the PMBDC motor's main design advantage, the use of high RPMS, and turn this energy into thrust.

Finally, we have to find a better battery than the Silver-Zinc's used in this design. As stated earlier, a battery in pre-production by the 3M Company would give our aircraft a flight endurance of 90 minutes at a battery weight of 43 pounds. Battery technology will continue to improve, possibly to the point that we could get our 2-4 hours of endurance at a power consumption rate of 12 kW. Batteries would enable us to re-charge the power source in the field by using a solar panel, thus eliminating a fuel re-supply requirement. The biggest improvements in energy density for electrical storage devices may come from fuel cells. Although this technology is not yet mature to the point that a lightweight fuel cell is available for our use, it is probably only a matter of time. Progress is being rapidly made by fuel cell companies doing research with the major automobile manufacturers for the next generation of electric cars. This also means there will be more models, better designs, lighter, more efficient, more powerful PMBDC motors available in the near future. A combination of the above mentioned component improvements would allow for the development of an electrically powered hang glider, that would more than meet the stated mission requirements listed at the beginning of this thesis.

LIST OF APPENDICES

A. PROPELLER THEORY [REF. 6]

XROTOR User Guide
August 1996
Mark Drela

last update 10

General Description

=====

XROTOR is an interactive program for the design and analysis of ducted and free-tip propellers and windmills. It consists of a collection of menu-driven routines which perform various useful functions such as:

- Design of minimum induced loss rotor (propeller or windmill)
- Prompted input of an arbitrary rotor geometry
- Interactive modification of a rotor geometry
- Twist optimization of an arbitrary rotor for minimum induced loss
- Analysis of a rotor with a wealth of choices of operating parameters
- Incoming slipstream effects (from an upstream propeller, viscous wake...)
- Multi-point parameter display
- Structural analysis and corrections for twist under load
- Acoustic analysis with dB noise footprint predictions
- Interpolation of geometry to radii of interest
- Plotting of geometry, aerodynamic parameters, and performance maps
- ...

Program Execution

=====

It is recommended that the X-window graphics generated by XROTOR be in reverse video for better visibility. This is selected by setting the following shell variable:

```
% setenv XPLOT11_BACKGROUND black
```

XROTOR is simply run from the terminal, with up to two arguments:

```

% XROTOR
or % XROTOR save_file
or % XROTOR save_file case_file

```

In any case, the following TOP LEVEL menu and prompt pop up:

```

QUIT      Exit program
.AERO      Display or change airfoil characteristics
NAME s     Set or change case name

ATMO r     Set fluid properties from standard atmosphere
VSOU r     Set/change fluid speed of sound
DENS r     Set/change fluid density
VISC r     Set/change fluid viscosity

NACE f     Specify nacelle geometry file
DUCT r     Duct/free-tip option toggle
VRAT r     Change duct velocity ratio

ARBI       Input arbitrary rotor geometry
.DESI      Design rotor geometry
.MODI      Modify rotor geometry
.OPER      Calculate off-design operating points
.BEND      Calculate structural loads and deflections
.NOIS      Calculate and plot acoustic signature
JMAP       Calculate Cp vs J operating map

INTE       Interpolate geometry to specified radii
SAVE f     Write rotor to restart file
LOAD f     Read rotor from restart file
WDEF f     Write current settings to xrotor.def file.

VPUT f     Save slipstream velocity profiles
VGET f     Read slipstream velocity profiles
VCLR       Clear slipstream velocity profiles

HARD       Hardcopy current plot
WIND       Windmill/propeller plotting mode toggle
PLOP       Plotting options

```

```

XROTOR     c>

```

Specifying the save_file argument will automatically cause the LOAD command to be executed, which reads a previously-saved rotor. Specifying the case_file argument will also cause the case file to be read, which is equivalent to executing CGET from the .OPER menu.

In general, the commands preceded by a period place the user in another lower-level menu. Simply typing <Return> will cause an exit back up to the higher-level menu:

```
XROTOR  c>  desi
```

```
.DESI  c>  <Return>
```

```
XROTOR  c>
```

This convention is used throughout XROTOR.

All commands which are not preceded by a period are executed immediately, and the user is prompted for another command. The lowercase letters i,r,f,s following some commands indicate the type of argument(s) expected by the command:

```
i  integer
r  real
f  filename
s  character string
```

For example, to set Standard US Atmosphere fluid properties corresponding to 10 km flight altitude, one can issue the command

```
XROTOR  c>  atmo 10
```

Omitting the argument always results in a prompt. For example:

```
XROTOR  c>  atmo
```

```
flight altitude (km)  r>  10
```

Specifying an altitude of -1 sets the properties for water (special case).

```
Rotor Design
=====
```

The DESI command, which transfers to the design menu, produces the command prompt

```
.DESI  c>
```

Typing a " ? " will print out the DESI menu:

```
INPU      Input  design parameters... design rotor
.EDIT     Change design parameters... design rotor

FORM      Toggle between Graded Mom. and Potential Form.
```

WAKE Toggle between rigid and self-deforming wake

DISP Display current design point

TERS Toggle between terse and verbose output

NAME s Set or change case name

PLOT i Plot various rotor parameters

ANNO Annotate current plot

HARD Hardcopy current plot

SIZE r Change plot-object size

The design procedure allows calculation of a rotor chord and blade angle (c/R, beta) distributions to achieve a Minimum Induced Loss (MIL) circulation distribution. This can be either the

i) Betz-Prandtl distribution (Graded-Momentum Formulation),
or ii) Goldstein distribution (Potential Formulation),
depending on the state of the FORM toggle.

Design process

The design of a new rotor is typically begun with the INPU command, which prompts the user for all required design-parameter inputs, and then follows by displaying the input-modification menu.

B	2	number of blades
RT	1.5000	tip radius
RH	0.1000	hub radius
RW	0.0500	hub wake displacement body radius
V	10.0000	airspeed
A	---	advance ratio
R	200.0000	RPMS
T	---	thrust
P	800.0000	power
CC	0.5000	lift coefficient (constant)
C		lift coefficient (arbitrary)

..EDIT Parameter, Value (or <Return>) c>

This echoes the user's inputs and allows any of them to be changed by specifying the parameter keywords and new values. For example

..EDIT Parameter, Value (or <Return>) c> B 3
..EDIT Parameter, Value (or <Return>) c> V 8
..EDIT Parameter, Value (or <Return>) c> <Return>

will change the blade number to 3, the airspeed to 8.0, and then redesign the rotor. This input-modification menu can

be invoked repeatedly with the EDIT command. The intent here is to allow rapid modification of design parameters with immediate feedback on the resulting design.

The design parameters contain two redundant pairs:

advance ratio
RPMS

thrust
power

Only one parameter in each pair can be prescribed. The remaining parameter is then a result of the design calculation.

All the design parameters will retain their values for the length of the XROTOR session. Hence the designed rotor can be analyzed in the other menus, and can then be further redesigned in DESI just by invoking EDIT again.

Rotor Modification =====

The MODI command, which transfers to the modification menu, produces the command prompt

.MODI c>

Typing a " ? " will print out the MODI menu:

```
BLAD i  Set new number of blades
MODC    Modify chord distribution
MODB    Modify blade twist angle distribution
SCAL rr Scale current chords
TLIN r  Add linear blade twist (proportional to r/R)
RTIP r  Change tip radius
RHUB r  Change hub radius
RWAK r  Change hub wake displacement body radius
XPAX r  Change pitch-axis x/c

OPTI    Optimize blade twist angles for current planform

PLOT i  Plot various rotor parameters
ANNO    Annotate current plot
HARD    Hardcopy current plot
SIZE r  Change plot-object size
```

The MODC and MODB commands allow modification of the existing c/R and beta distributions via cursor input. These

can also be changed in more simple ways with the SCAL and TLIN commands.

The RTIP, RHUB, RWAK commands are used to change their corresponding radii. The c/r and beta distributions are preserved as closely as possible. The XPAX command changes the chordwise x/c location of the pitch axis. Currently this only has an effect on the plotted blade geometry.

The OPTI command is a hybrid between the Design and Modification operations. It will re-twist the rotor (the beta distribution) to achieve a MIL circulation while holding the current chord distribution fixed --- i.e. it "optimizes" the twist. This command must be used cautiously, since the MIL circulation will not be achievable if the blade stalls somewhere. Also, the "optimum" MIL distribution is not necessarily the best in an overall sense, since the rotor may be made worse at other operating points. This is the same situation as when a rectangular wing is "optimized" by twisting it to achieve an elliptical loading at one flight condition -- it becomes worse at most other lift coefficients. When the OPTI command is issued, it will list the changes to the current blade angle distribution, followed by a prompt for an underrelaxation factor.

Blade angle changes

i	r/R	d(beta)
1	0.106	-1.232
2	0.129	-1.359
3	0.165	-1.543
.		
.		
28	0.991	-3.163
29	0.997	-3.168
30	0.999	-3.171

Enter relaxation factor for blade angle changes: 1.000

The actual blade angle changes applied to the blade will be scaled by the specified relaxation factor. Usually, a value smaller than the default of 1.000 works best, since off-design operation is then less likely to be adversely affected.

Arbitrary-rotor input

=====

An arbitrary rotor geometry is input via the ARBI command at TOP LEVEL. This prompts the user for a number of operating and geometric parameters, and then prompts for the radial distribution of r/R , chord/ R , blade angle. The chord and angle distributions are splined radially and interpolated to the internal computational stations. All other XROTOR operations can then proceed as usual.

Rotor analysis

=====

The OPER command, which transfers to the operating menu, produces the command prompt

.OPER c>

Typing a " ? " will result in the rather extensive OPER menu:

ADVA r	Prescribe advance ratio
RPMS r	Prescribe RPMS
THRU r	Prescribe thrust
TORQ r	Prescribe torque
POWE r	Prescribe power
MOTO rr	Prescribe torque(RPMS) motor characteristic
ASEQ rrr	Calculate case sequence of advance ratios
RSEQ rrr	Calculate case sequence of RPMS
VSEQ rrr	Calculate case sequence of flight speeds
BSEQ rrr	Calculate case sequence of blade angles
CLRC	Clear case accumulator
ADDC	Add current point point to case accumulator
CPUT f	Write current case accumulator to file
CGET f	Read cases from file
CASE i	Select case
ATMO r	Set fluid properties from standard atmosphere
VELO r	Set or change flight speed
ANGL r	Change collective blade angle
FORM	Toggle between Graded Mom. and Potential Form.
WAKE	Toggle between rigid and self-deforming wake
NAME s	Set or change case name
WRIT f	Write current operating point to disk file
DISP	Display current operating state
TERS	Toggle between terse and verbose output
PLOT i	Plot various rotor parameters

ANNO	Annotate plot
HARD	Hardcopy current plot
SIZE r	Change plot-object size

Hopefully, most of these commands are self-explanatory. An operating state can be specified by any one of the ADVA, RPMS, THRU, TORQ, POWE, or MOTO commands. Care must be taken when using the latter four commands, since the specified thrust, torque, or power may not be achievable by the current rotor, especially in the windmill mode.

The MOTO command can be used to automatically determine the RPMS which matches the torque of the propeller and motor.

This requires specification of the torque(RPMS) function for the motor. Currently, a linear relation is assumed, and is specified by the torque and RPMS intercepts. This is an accurate model of a DC electric motor, with the intercepts being the stall torque and the no-load RPMS. Some other torque(RPMS) function can be implemented in SUBROUTINE APITER (in xoper.f).

A number of operating-point cases can be stored in the "case accumulator", which can be filled up on-by-one with the ADDC command, or with the ASEQ,RSEQ,VSEQ,BSEQ commands. These automatically sweep through one of the four corresponding parameters, appending to the case accumulator in the process. A case can then be quickly recomputed by specifying its index via the CASE command.

A few OPER and TOP LEVEL commands must be explained in more detail ...

... FORM command (mentioned earlier)

This allows the user to switch between two different methods of calculating induced velocities and induced losses. Both methods treat the rotor blades as lifting lines, and both assume that the disk loading is relatively low and hence the wake contraction and the wake self-deformation are small.

Graded Momentum Formulation.

This is the classical theory of propellers revived recently by E.E. Larrabee. It relies on the Betz-Prandtl tip loss fudge factor which assumes that the rotor has a low advance ratio and/or many blades. As a result, this formulation is not suitable for advance ratios greater than about 0.5. Its chief advantage is extreme computational economy.

Potential Formulation.

This is a more modern approach which solves for the helically-symmetric potential flow about a rigid helicoidal wake and hence is valid for all blade numbers and advance ratios. It is an extension of Goldstein's 2 and 4 blade solution to all blade numbers and arbitrary radial load distributions. On the negative side, this approach is computationally more expensive than Graded Momentum, but still requires a fraction of a second per operating point on a RISC workstation. This method also treats finite radius rotor hubs and nacelle installations, which the Betz-Prandtl fudge factor cannot deal with properly. The method also readily accepts a tip casing boundary condition, which is enabled/disabled with the DUCT command at TOP LEVEL.

... JMAP command

This produces data for a two-dimensional plot of C_p versus J , with contours of equal efficiency and blade angle. This is a compact way of summarizing propeller performance and is used by Hamilton Standard. The routine can run for some time, especially if the Potential Formulation is used. A crude plot with "ragged" contours can be generated fairly quickly, but much more runtime will be needed if a very high-quality plot is to result. The data produced by JMAP is written to an unformatted file specified by the user, and plotted later with the separate JPLOT program.

Acoustic Calculations

=====

Executing the NOIS command enters the .NOIS menu:

```
P   rrr Calculate acoustic p(t) at observer x,y,z
FOOT rr Calculate dB ground noise footprint
NTIM i Change number of time samples
UNIT   Toggle coordinate unit  m,ft

AOC  r Set constant blade cross-sectional area/c**2
AFIL f Set blade cross-sectional area/c**2 from file

PLOT i Plot various acoustic parameters
HARD   Hardcopy current plot
ANNO   Annotate plot
SIZE r Change plot-object size
```

The P command calculates a pressure signature $p(t)$ at any point in space, over one blade-passing period. The position can be specified in either feet or meters, which is toggled

with the UNIT command. The calculation method used is taken from the following two References.

G.Succi,
"Design of Quiet Efficient Propellers", SAE Paper 790584, 1979.

Note: Equation (16) in this Reference is mistyped.

G.Succi, D.Munro, J.Zimmer,
"Experimental Verification of Propeller Noise Prediction", AIAA-80-0994.

Note: equations (8) and (9) in this Reference are mistyped.

The method uses the retarded-time concept. A sphere collapsing towards the observer at the speed of sound "collects" acoustic signals from the blade thickness and the blade loading where and when it intersects the blades during its inward travel. The sum of all these signals then results in an instantaneous acoustic pressure p seen by the observer when the sphere collapses on him at some later time. The method requires that the blade speed along the observer's line of sight be subsonic, because the blade must not run past the inward-collapsing sphere from behind. This invalidates the method.

If the relative blade-tip Mach is close to unity, then the resulting pressure signal will be very "spiky". The number of time samples per blade period may need to be increased with the NTIM command to maintain good resolution of the $p(t)$ signal.

One contribution to the acoustic pressure is due to the blade airfoil's cross-sectional area, which is set with the AOC command, and is specified as A/c^2 . For most airfoils, this is roughly related to the thickness/chord ratio:

$$A/c^2 \sim 0.7 t/c.$$

The AOC command sets a radially-constant value of A/c^2 , which should correspond to its value near the tip, since that's where most of the noise generation occurs. For more accuracy, an arbitrary A/c^2 distribution can be read in from a file via the AFIL command. This file has the format

```
r/R  A/c^2
r/R  A/c^2
```

```
:
:
```

where r/R increases outward along the blade.

Immediately after the $p(t)$ signal is generated, it is Fourier-decomposed, and the dB values of the individual harmonic components are displayed. These can also be plotted with PLOT 2. The Fourier decomposition is defined as follows.

$$p(t) = \text{Real} \left[\sum_{k=1}^{\infty} C_k \exp(-ikwt) \right]$$

$w = \text{blade-passing radian frequency}$

$k = 1$
 $k = \text{number of blades} \times \text{prop shaft speed}$

The individual dB value for each component is defined relative to 20 microPascals:

$$\text{dB}(k) = 20 \log_{10} \left(\sqrt{1/2} |C_k| / 20e-6 \right)$$

The total dB level uses the r.m.s. pressure:

$$\text{total dB} = 20 \log_{10} \left(p_{\text{rms}} / 20e-6 \right)$$

where

$$p_{\text{rms}}^2 = \frac{1}{2\pi} \int_0^{2\pi} p^2 d(wt) = \frac{1}{2} \sum_{k=1}^{\infty} |C_k|^2$$

The FOOT command calculates the total dB level at each point of a rectangular grid at a specified distance under the aircraft, thus forming ground noise-level contours.

Higher-Order Corrections

=====

The light-loading assumption states that a trailing vortex sheet remains in the path of the rotor blade which created it. In XROTOR, the inviscid efficiency of the rotor η_{ai} is used to estimate the self-induced motion of the vortex sheets to yield a "wake advance ratio" L_w which differs from the rotor advance ratio (this is the core of Theodorsen's theory).

$$L_w = (V/WR) / \eta_{ai}$$

This "wake advance ratio" is then used to define the vortex sheet geometry which is an important parameter in the

calculation of induced velocities. The net result is more realistic behavior at high disk loadings. A similar technique was employed by David Munroe in his propeller noise PhD work at MIT around 1980. In XROTOR, the correction is an option which can be enabled/disabled with the WAKE command from the OPER or the DESI menus, and is employed by both the Graded Momentum and Potential Formulations. Note that this is not a true "free wake" model since the wake will deform itself in pitch, but not in contraction or in roll-up (which for sanity's sake is thoroughly neglected here). Incidentally, the wake self-deformation makes the overall calculation method perfectly consistent with the actuator disk model for arbitrarily large disk loading in the limit of zero advance ratio (and zero blade profile drag, of course). The fixed-wake model does not have this property.

Incoming Slipstream Effects

=====

XROTOR has the capability to approximately model the effects of an upstream or downstream propeller. In a counter-rotating configuration, for example, the downstream prop will effectively see a freestream with additional axial and rotational velocity components. The upstream propeller will only see an additional axial component, and only if the two props are sufficiently close (within a few radii). The two propellers need not have the same radius.

To analyze a typical counter-rotating configuration, for example, one might begin by designing or analyzing the front propeller assuming it is unaffected by the rear one. The VPUT command will then write out the circumferential averages of its far-downstream slipstream velocity components to a named file. The format for a slipstream file is

```
R(1)  VAXIAL(1)  VTANG(1)
R(2)  VAXIAL(2)  VTANG(2)
.      .      .
.      .      .
R(N)  VAXIAL(N)  VTANG(N)
```

with R in meters, and V in m/s. VAXIAL is positive for downstream velocities, and VTANG is positive in the prop rotation direction. This file can be subsequently read in with the VGET command before the rear propeller is designed or analyzed. What velocities the rear propeller actually "sees" depends on its axial location and rotation direction relative to the front propeller, and whether or not the

propellers are inside a duct. The user will be asked to specify the weights to apply to the input axial and tangential velocity components. Appropriate weights are:

Vaxial Vtang.

For calculating front prop which is far ahead of rear

prop: 0.0 0.0

For calculating front prop which is just ahead of rear

prop: 0.5 0.0

For calculating rear prop which is just behind front

prop: 0.5 +/-1.0

For calculating rear prop which is far behind front

prop: 1.0 +/-1.0

The tangential velocity weight is +1.0 for co-rotating propellers, and -1.0 for counter-rotating propellers. If both propellers are in a duct, then all the Vaxial weights should be 0.5. This incidentally will also account for the additional induction velocity set up by the props inside the duct.

After the aft propeller is designed, its slipstream velocity components can be written out with VPUT to another named file, and this can be read in with VGET for a subsequent re-design of the front propeller, with the appropriate velocity weights chosen from the table above (typically

Vaxial = 0.5, Vtang = 0.0)

If desired, the rear propeller can be subsequently redesigned with the slipstream from the new front prop, ad infinitum. Fortunately, if each propeller is designed for a specific thrust or power, this iteration will converge fairly quickly. For preliminary design, only redesigning the front propeller once will typically suffice.

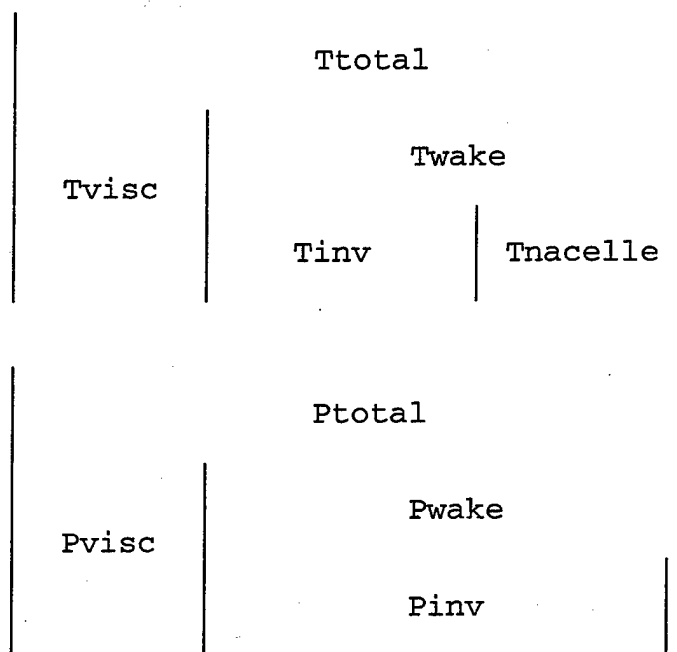
If a rotor is designed and/or analyzed with a non-zero slipstream velocity profiles and then saved with the SAVE command from TOP LEVEL, the slipstream profiles are saved with it. When the rotor is read back in later using LOAD, the original slipstream information is read in as well, and will overwrite any slipstream information already present (appropriate messages are printed). Hence, it is not necessary to load in the original slipstream file before the loaded rotor is analyzed.

It should be pointed out that a slipstream profile file can be generated by any means available to the user. It does not necessarily have to be generated with VPUT. The V distributions are splined to the radial stations of the prop being analyzed.

Nacelle Corrections

=====

If the rotor hub is embedded in a nacelle or fuselage, or even if the rotor is operating in the vicinity of a nacelle, the thrust, power absorbed, and overall efficiency can be substantially different than if the presence of the nacelle is ignored. Also, the optimum (minimum induced loss) radial circulation distribution can be significantly altered by the presence of the nacelle. The calculation of the thrust is further complicated by the nacelle's perturbation flowfield changing the thrust on the rotor, and the rotor's pressure field causing a thrust force on the nacelle. What really counts is the sum of the rotor and nacelle thrust (or drag). In XROTOR, the inviscid thrust, power, and ideal efficiency are calculated for both the rotor alone and for the rotor/nacelle combination. To summarize...



In the actual calculations, the total thrust and power are computed by

$$\begin{aligned} T_{total} &= T_{visc} + T_{wake} \\ P_{total} &= P_{visc} + P_{wake} \end{aligned}$$

with T_{wake} and P_{wake} being calculated on an inviscid "equivalent rotor", which has no nacelle and which has the same far vortex wake as the real rotor. T_{visc} and P_{visc} are calculated by direct integration of the blade profile drag on the real rotor.

The nacelle thrust (or drag) is calculated indirectly by

$$\begin{aligned} T_{nacelle} &= T_{wake} - T_{inv} \\ P_{nacelle} &= P_{wake} - P_{inv} = 0 \text{ always} \end{aligned}$$

with T_{inv} and P_{inv} being calculated by direct integration of the blade profile lift forces on the real rotor. It is reassuring that $P_{nacelle}$ always turns out to vanish, since a fixed axisymmetric nacelle cannot possibly deliver power to or from the flow.

The radial circulation distribution of the "equivalent rotor", which is needed to calculate its thrust and power, is determined using mass conservation and Kelvin's circulation theorems. Just behind a rotor, the circumferential circulation around a streamtube of some radius is simply the total bound circulation on the rotor blades at that radius, and this circulation cannot change downstream (Kelvin's theorem). The streamtube's radius, on the other hand, will change downstream as the average velocity in the streamtube changes and/or the cross-sectional area of any nacelle in the center changes. The contraction and velocity are related by mass continuity requirements. Specifically, if we define

$$\begin{aligned} r &= \text{real rotor radial coordinate} \\ U(r) &= \text{real rotor freestream + average induced axial velocity} \\ u(r) &= \text{perturbation velocity induced by nacelle at rotor} \\ r' &= \text{equivalent rotor radial coordinate} \\ U'(r') &= \text{equivalent rotor freestream + average induced axial velocity} \end{aligned}$$

then the radial location of the streamtube at the real rotor (r) and its location at the equivalent rotor (r') are related by the differential mass continuity equation:

$$(U+u) r dr = U' r' dr'$$

If this relation is satisfied, the real-rotor and equivalent-rotor streamtubes from r and r' will coincide in the far wake and have the same axial velocity since their mass flow will be the same. If they also have the same circulation, their tangential velocity will be the same, and thus the far wakes from the real and equivalent rotors will be the same.

The "correspondence" function $r'(r)$ is obtained by numerically integrating the ODE above. To do this requires that the initial value of $r'(r)$ corresponding to the blade root at $r = r_0$ be specified, say $r'(r_0) = r_0'$. The best

value for this equivalent rotor (and far wake) "core radius" r_0' is the radius of the displacement body of the nacelle far downstream. The displacement body cross-sectional area far downstream A_{inf} is just the drag area of the nacelle, and is related to the viscous drag D on the nacelle and the freestream dynamic pressure q by

$$D = q A_{inf} \quad \text{and} \quad A_{inf} = \pi (r_0')^2$$

Once the function $r'(r)$ and thus $r(r')$ is determined, the bound circulation distribution on the equivalent rotor is then simply $G'(r') = G[r(r')]$, where $G[r]$ is the bound circulation on the real rotor at radius r .

A minor simplification is made in the integration of the ODE above. Instead of using the average axial induced velocity, the local induced velocity at the propeller is used instead. This is a reasonable approximation, especially at the inner radii where the streamtubes have the greatest relative radius changes.

The nacelle perturbation velocity $u(r)$ which appears in the ODE can in principle be determined by any potential flow calculation method. In XROTOR, it is determined by a simple model where the nacelle (assumed axisymmetric) is replaced by a distribution of sources and sinks along its centerline. The source strength m is then related to the nacelle cross-sectional area distribution $A(z)$ (more precisely, $A(z)$ should be the cross-sectional area of the viscous displacement body of the nacelle, since this is what the outer potential flow really "sees").

$$m(z) = U \frac{dA}{dz}$$

where z is the axial coordinate increasing downstream. The perturbation velocity is then calculated by integrating over this source distribution:

$$u(r) = \frac{1}{4\pi} \int \frac{m(z) [\bar{z} - z]}{[(\bar{z} - z)^2 + r^2]^{3/2}} dz$$

where the rotor is located at the axial location $z = \bar{z}$. The nacelle area distribution $A(z)$ can be loaded from a file into XROTOR via the NACE command at TOP LEVEL. The file

must have one of two forms, specifying the area $A(z)$ directly, or indirectly via the radius $r(z)$

\bar{z}	A_{inf}		\bar{z}	$-r_0'$
z_1	A_1		z_1	$-r_1$
z_2	A_2		z_2	$-r_2$
z_3	A_3	OR	z_3	$-r_3$
\vdots	\vdots		\vdots	\vdots
\vdots	\vdots		\vdots	\vdots
\vdots	\vdots		\vdots	\vdots
z_n	A_n		z_n	$-r_n$

where the axial coordinates $z_1, z_2, z_3 \dots$ (in meters) must be monotonically increasing downstream. A negative number is assumed to be a body radius, and is then immediately used to determine the corresponding area:

$$A = \pi r^2$$

A_{inf} is the nacelle profile-drag area D/q , and the corresponding radius r_0' is then the far wake displacement radius described earlier.

It must be pointed out that even if the nacelle perturbation velocities are negligible, the difference between the displacement body radii at the rotor and far downstream can still give a non-zero nacelle thrust and also change the optimum circulation distribution. Therefore, XROTOR allows the user to set these radii independent of the nacelle geometry. These radii are input as design parameters for the DESI minimum induced loss design routine. The far wake displacement body radius can also be changed independently at any time with the RWAK command from the .MODI menu.

If a rotor is designed and/or analyzed after loading a nacelle area distribution file and then saved with the SAVE command from TOP LEVEL, the perturbation velocities and far wake displacement body radius are saved with it. When the rotor is read back in later using LOAD, this information is read in as well. It is not necessary to load in the original nacelle area file or to set the displacement body radius before the loaded rotor is analyzed.

If a counter-rotating configuration on a nacelle is analyzed, the nacelle effects are simply superimposed on the incoming-slipstream effects described in the previous section.

Structural Loads and Deflections

=====

The BEND command from TOP LEVEL gives the structural-routine prompt:

```
.BEND c>
```

Typing a " ? " will result in the BEND menu being displayed:

```
READ f Read in blade structural properties
EVAL  Evaluate structural loads and deflections
CLR   Clear all structural deflections

DEFL  Set new twist = static + structural twist
REST  Set new twist = static twist
SETS  Set static twist = current - structural twist

WRIT f Write structural solution to disk file

PLOT i Plot structural parameters
ANNO  Annotate plot
HARD  Hardcopy current plot
SIZE r Change plot-object size
```

A 3-axis nonlinear slender beam model is used to model the structural behavior of the blade. Before any structural calculations can be performed, it is necessary to define the blade's structural properties via the READ command, which reads a file of the following format:

```
Name-label
Case-label
Variable-label
R(1) EIXX(1) EIYY(1) EA(1) GJ(1) EK(1) M(1) MXX(1) XOCG(1)
XOSC(1) RST(1)
R(2) EIXX(2) EIYY(2) EA(2) GJ(2) EK(2) M(2) MXX(2) XOCG(2)
XOSC(2) RST(2)
.
.
.
R(N) EIXX(N) EIYY(N) EA(N) GJ(N) EK(N) M(N) MXX(N) XOCG(N)
XOSC(N) RST(N)
```

The first three lines are arbitrary alphanumeric labels which are ignored. The following lines give the structural properties along the radius, (dimensioned in SI units!):

```
R      radius (must monotonically increase)
EIXX   in-plane stiffness
```

EIYY out-of-plane stiffness
 EA extensional stiffness
 GJ torsional stiffness
 EK extensional/torsional stiffness (torsion per extension-strain)
 M mass density / length
 MXX pitch axis inertia / length
 XOCG x/c of section CG
 XOSC x/c of section shear center (structural axis)
 RST structural radius for strain evaluation

These variables are splined to the computational stations.

The EVAL command will then calculate and display the structural solution for the current operating point. The display has the following format.

i	r/R	u/R	w/R	t	Mz	Mx	T
P				(deg)	(N-m)	(N-m)	(N-m)
(N)							
1	0.041	0.000	0.000	0.00	127.79	182.19	-103.77
25684.4							
4	0.184	0.000	0.000	-0.22	94.93	108.46	-103.34
24878.7							
7	0.335	-0.001	0.001	-0.32	65.59	54.51	-91.82
22061.5							

i	r/R	Ex	Ez	Ey	E _{max}	g
		/1e3	/1e3	/1e3	/1e3	/1e3
1	0.041	0.243	-0.367	0.695	1.135	-0.505
4	0.184	0.103	-0.261	0.748	1.028	-0.179
7	0.335	0.108	-0.200	0.853	1.080	-0.103

The axis definitions are:

X aft along prop rotation axis
 Y radial along blade
 Z perpendicular to blade: $X \times Y = Z$

u/R and w/R are the deflections in the X and Z directions, and t is the torsional twist (positive in the increasing incidence direction). Mz and Mx are the bending moments about the Z and X axes, while T is the moment about the radial Y axis (i.e. torsion). P is the tensile load.

The strains E_x and E_z are those due to bending in the X and Z directions, while E_y is the strain due to extension in the Y direction. E_{max} is the maximum strain calculated by $E_{max} = \sqrt{E_x^2 + E_z^2} + E_y$. g is the shear strain due to twist t . E_x , E_z , and g are evaluated at the local radius input via the RST array described above.

The structural twist t can be added to the static blade geometry angles by issuing the DEFL command (with the lifting line model, only the twist is significant). One can subsequently go to OPER to recalculate the aero solution, and then back to BEND to recalculate the structural solution and add the new twist, etc. Normally, this iteration is not necessary unless the twists are very severe.

The DEFL command can always be reversed with REST command, which resets the blade twists back to the static values. The SETS command subtracts the twists from the static blade angles themselves, and is not reversible as such. It is used to set that static twist which under load will give the current twist.

The structural twist t can be added to the static blade geometry angles by issuing the DEFL command (with the lifting line model, only the twist is significant). One can subsequently go to OPER to recalculate the aero solution, and then back to BEND to recalculate the structural solution and add the new twist, etc. Normally, this iteration is not necessary unless the twists are very severe.

The DEFL command can always be reversed with REST command, which resets the blade twists back to the static values. The SETS command subtracts the twists from the static blade angles themselves, and is not reversible as such. It is used to set that static twist which under load will give the current twist.

Output =====

All output goes directly to the terminal screen. In addition, the same output can be also written to a disk file by the WRIT command. The first time WRIT is issued, the user will be prompted for a file name, which will then be used for the disk output. If that file already exists on disk, the output can be appended to it.

In addition to the primary output file, a save file with all the attributes of the current rotor (including the airfoil characteristics and operating parameters) can be created at any time with the SAVE command. The user is asked for a file name each time. The LOAD command is used to read the save file later.

XROTOR uses the Xplot11 (modified Versaplot) plot package, which drives X-terminals and can generate a PostScript file of the current window plot at any time. The hardcopy is not affected by the reverse-video selection described earlier.

The default PostScript output is black & white, but color PostScript can be selected by setting the IDEVRP variable appropriately in SUBROUTINE INIT (in xrotor.f). Color PostScript can also be selected at runtime from the PLOP menu at TOP LEVEL.

Start-up default file =====

XROTOR tries to read most of its control parameters from the xrotor.def file at startup. If this file is not found, then hardwired defaults set in SUBROUTINE SETDEF are used instead.

Many of the control parameters can be altered during runtime. A new xrotor.def file containing them can be written with the WDEF command, so that they will be automatically restored when XROTOR is started again.

Units and Non-dimensionalization =====

XROTOR uses SI units for all dimensioned input and output. However, all internal calculations are performed with variables normalized with the following quantities:

R	tip radius
V	freestream speed
rho	freestream density

Some of the output uses conventional normalization definitions:

$$T_c = T / (0.5 \rho V^2 \pi R^2)$$

105

$$P_c = P / (0.5 \rho V^3 \pi R^2)$$

$$C_t = T / (\rho D^4 n^4) \quad ; \quad D = 2R$$

$$C_p = T / (\rho D^5 n^5) \quad ; \quad n = \text{revs. per second}$$

$$J = V / (n D) = \pi V / (W R) \quad ; \quad W = 2 \pi n \text{ rad/s}$$

$$\eta = T_c / P_c = J C_t / C_p \quad (\text{total efficiency})$$

The circulation "Gamma" is displayed on some of the plots in the Betz-Prandtl canonical form:

$$G = B (\text{Gamma}/VR) / (2 \pi L_w)$$

where L_w is the wake advance ratio, related to the geometric advance ratio V/wR and the inviscid efficiency η_i by

$$\eta_i L_w = V/(WR)$$

In the actuator disk limit η_i is the ideal (Froude) efficiency, and G approaches unity. Hence, G shows how close the real prop disk loading is to this ideal limit.

Since all internal calculations are done in non-dimensional variables, if all input is in some other consistent set of units, all output will be in the same set of units. Only the SI unit labels on the formatted output will be wrong. A modification to SUBROUTINE ATMO will also be necessary to convert its SI output to whatever units are desired.

Blade Section Properties =====

The $CL(\alpha)$ function is defined in five analytic regions bounded by four alpha values: ALF1 --> ALF4 .

Region 1) Negative stall:	$\alpha < \text{ALF1}$
Region 2) Incipient negative stall:	$\text{ALF1} < \alpha < \text{ALF2}$
Region 3) Linear unstalled:	$\text{ALF2} < \alpha < \text{ALF3}$
Region 4) Incipient positive stall:	$\text{ALF3} < \alpha < \text{ALF4}$

Region 5) Positive stall: $ALF4 < \alpha$

In Region 1) $CL = CL_{min}$

In Region 2) $CL = \text{quadratic } f(\alpha)$

In Region 3) $CL = m_{2D} (a - a_o)$

In Region 4) $CL = \text{quadratic } f(\alpha)$

In Region 5) $CL = CL_{max}$

The user only needs to specify the following parameters.

a_o = zero-lift angle of attack ; Fortran
name: (A0)
 o

m_{2D} = incompressible 2D lift curve slope dCL/da
(DCLDA)
 $2D$

CL_{min}, CL_{max} = stall limits (CL_{min}, CL_{max})

CL_{inc} = CL increment from stall onset to complete stall
(CLCON)
 inc

The program calculates $ALF1 \rightarrow ALF4$ in SUBROUTINE ALFINI from these parameters. SUBROUTINE CLFUNC implements the piecewise $CL(\alpha)$ function.

A Prandtl-Glauert compressibility correction is employed by multiplying the incompressible CL values above by the factor $1/\sqrt{1 - M^2}$, where M is the local Mach number. The $ALF1 \dots ALF4$ values are adjusted so as to leave CL_{max} and CL_{min} unaffected. It should be kept in mind that the P-G correction tends to overpredict loading near the tip, since it doesn't entirely account for the significant radial Mach number gradient and associated tip relief. A 3-D full-potential or Euler method is needed to properly model these effects.

Like CL, profile CD is defined piecewise in alpha such that in the unstalled region, CD has a quadratic dependence on CL and a power-law dependence on Reynolds number as follows.

$$CD = \left| CD_o + b (CL_o - CL)^2 \right| \left(\frac{Re}{Re_{Ref}} \right)^f$$

where

CD_o = minimum drag coefficient ; Fortran name:
(CDMIN)

CL_o = CL at which CD = CD_o
(CLDMIN)

b = CL weighting coefficient d(CD)/d(CL**2)
(DCDCL2)

Re_{Ref.} = Reynolds Number at which CD formula applies
(REREF.)

f = Reynolds Number scaling exponent.
(REXP)

Typically:

f = -0.1 to -0.2 for high-Re turbulent flow
Re > 2M
f = -0.5 to -1.5 for "low-Re" regime Re ~ 200K..800K
f = -0.3 to -0.5 for mostly-laminar airfoils at Re < 100K

Obviously, the particular choice of f is strongly case-dependent, especially in the intermediate "low-Re" regime.

Only the above parameters are supplied by the user, and the program figures out the CD(alpha) function in SUBROUTINE CDCALC.

A crude stall model is used to smoothly merge the unstalled and fully stalled lift curve portions. A crude treatment is justified on the grounds that a stalled rotor blade airfoil will have properties vastly different than those of a stalled a 2-D section due to the presence of powerful centrifugal and Coriolis forces on the separating boundary layer fluid.

The Prandtl-Glauert scaling is also applied to the CD value calculated above. This is a smoother rise in drag than the very sudden drag-divergence behavior seen in typical transonic airfoils, but is deemed adequate given the approximate nature of the overall profile-property model.

The PLOT command in the .AERO menu displays the profile properties for $Re = REREF$, and several Mach numbers. The $CL(\alpha)$ parameters can be altered with the LIFT command, which queries the user with the current value of each parameter as the default response:

```
.AERO  c> lift
```

```
Zero-lift alpha (deg)  : -3.0000
d(Cl)/d(alpha) (/rad) : 6.00000
Maximum Cl              : 1.2000
Minimum Cl              : -0.6000
Cm                      : -0.10000
```

A new value can be given at each prompt, or just hitting <Return> will retain the current value.

NOTE:

The CL_{max} and CL_{min} stall limits can sometimes give convergence difficulties in analysis cases if the Newton solver enters an artificial stall-hysteresis loop. For general use, it is generally advisable to set these stall limits arbitrarily large, e.g.

```
CLmax = +10
CLmin = -10
```

This will give reliable convergence, but the solutions should then be monitored for unreasonably large local CL values.

Windmills
=====

Although XROTOR input and output is biased towards propellers, windmill design and analysis can be performed with nearly equal facility. The main thing to remember is that a windmill is a propeller with NEGATIVE blade CL's, thrust, torque, power, and also a reciprocated efficiency. About the only complication comes into the section properties CL(alpha) and CD(alpha). Since the section CL values are negative in the propeller sense, the blade airfoils are always "upside down" in a windmill. The curves must be Ref.lected about the origin. Specifically, the following changes must be made:

a	---->	- a
o		o
CL	---->	- CL
o		o
CL	---->	- CL
min		max
CL	---->	- CL
max		min

The REF.L command from the AERO menu will perform these Ref.lections at runtime. Of course, these can be made the default by altering the XROTOR.DEF start-up file appropriately. When a windmill is being designed, negative CL values must still be specified along with the negative thrust or power.

Caveat
=====

The code is written with many safeguards against unintended crashes. However, it is always easy to input data which will result in a non-unique or even impossible analysis or design problem. For instance, specifying power for a given windmill will in general have two solutions, one on each side of the power peak. Specifying a power above or near the peak will cause convergence failure or maybe even a program crash. Specifying thrust (tower load) instead, may help in such a situation. Specifying a thrust, torque, or power which will stall all or part of the blades sometimes leads to trouble, while specifying an advance ratio is generally safe whether or not the blades stall.

The self-deforming wake algorithm can be touchy if a high windmill disk loading is combined with very low advance ratios. In such a case, some pathological non-physical situation such as reverse far-slipstream velocity might

occur. The mathematical model is incapable of handling such flows, especially if they don't exist in the real world. One can always disable the self-deforming wake algorithm to get a more robust code, although accuracy might suffer as a result.

B. PARASITE DRAG COEFFICIENT DERIVATION [REF. 13]

The following derivation is in accordance with the United States Air Force DatComm for estimating parasite drag. The following dimensions are for the Pulse 2-18.

ASPECT RATIO,	AR = 5.9
SURFACE AREA,	S = 189 FT ²
WING SPAN,	b = 33.5 FT
WEIGHT OF GLIDER	W _G = 60 LBS
WEIGHT GLIDER SUPPORTS	W = 250-280 LBS
CORD AT ROOT,	C _R = 19.47 FT
CORD AT TIP,	C _T = 0.67 FT
MAX CORD THICKNESS	t/c = 0.67-1 FT

SWEEP AT NOSE = 126 DEGREES
WASHOUT = 18 DEGREES

RECOMMENDED NEVER EXCEED SPEED = 50 MPH
STALL SPEED = 10-12 MPH
MINIMUM SINK SPEED = 15-16 MPH
BEST GLIDE (L/D) = 25 MPH
BEST CRUISE SPEED = 30 MPM

For a wing:

$$C_{DO} = 2 C_f [1 + 2 (t/c) + 100(t/c)^4]$$

where

C_f = AVERAGE TURBULENT SKIN FRICTION COEFFICIENT
BASED ON Re_c FOR ONE SIDE OF A FLAT PLATE. IT IS ASSUMED THAT
B.L. TRANSITION TAKES PLACE AT OR NEAR THE LEADING EDGE.

$$Re_c = \rho Vc/\mu = Vc/\nu$$

where

V = THE FREE STREAM VELOCITY
c = THE MEAN AERODYNAMIC CORD = C_A
 μ = THE VISCOSITY OF AIR

$$C_f = 0.455(\text{LOG}_{10} \text{Re}_c)^{-2.58}$$

THE MEAN AERODYNAMIC CORD IS OBTAINED FROM:

$$c_A = 2/3C_R(1 + \lambda + \lambda^2/1 + \lambda)$$

where

$$\lambda = C_T/C_R = 0.67/19.47 = 0.03424$$

C_T = CORD AT THE WING TIP = 0.67 FEET

C_R = CORD AT THE WING ROOT = 19.47 FEET

$$c_A = 2/3(19.47)[1 + 0.03424 + 0.03424^2/1.03424] = 1.001$$

$$\text{Re}_c = 22 \cdot 1.001 / 3.7373 \times 10^{-7} = 58932757$$

$$C_f = 0.455(\text{LOG}_{10} 58932757)^{-2.58} = 0.0022944$$

$$C_{DO} = 2(0.0022944) \cdot (1 + 2(0.03) + 100(0.03)^4) = 0.004864 \text{ TAKE OFF}$$

FOR THE PILOT:

The subsonic zero lift body drag is assumed to be composed of skin friction drag and base drag, with normal pressure drag being negligibly small. For a more conservative estimate the boundary layer is assumed to be entirely turbulent.

$$C_{DO(B)} = C_{DO(F)} + C_{DO(b)}$$

where

$$C_{do(B)} = 1.02C_f[1 + 1.5/(L_B/d)^{3/2} + 7/(L_B/d)^2]S_W/S_B + C_{DO(b)}$$

where

$$\text{Re} = VL_B/\mu$$

L_B = PILOT LENGTH = 6 FEET

d = MAXIMUM BODY DIAMETER = 3 FEET

L_B/d = FINENESS RATIO = 2

$$S_W = \text{WETTED SURFACE AREA EXCLUDING BASE} = 2\pi r^2 = 1.5$$

$$S_B = \text{BODY FRONTAL AREA} = 2\pi r h = 12 \text{ FT}$$

$$R_e = 22 \times 6 / 3.3737 \times 10^{-7} = 353196158$$

$$C_f = 0.455(\text{LOG}_{10} 353196158)^{-2.58} = 0.0017939$$

$$C_{DO(B)} = 1.02(0.0017939)[1 + 1.5/2^{1.5} + 7/2^3]1.5/12 + C_{DOB}$$

$$C_{DO(B)} = 3.54 \times 10^{-4} + C_{DO(b)}$$

where

$$C_{DO(b)} = 0.29[(d_b/d)^3/\text{SQRT}(C_{DO(F)})]$$

$$d_b = 1.82$$

$$C_{DO(b)} = 0.29[1.82/3]^3/\text{SQRT}(3.54 \times 10^{-4})] = 0.3442$$

$$C_{DObody \text{ isolated}} = C_{DO(b)} \times b/S = 0.3442 \times 33.5/189 = .061$$

$$C_{DOtotal} = C_{DOWing} + C_{DObody} = 0.004864 + 0.061 = 0.066$$

C. BATTERY TECHNOLOGY [REF. 15 & 16]

Electric Vehicle Battery Performance Goals

To ensure an acceptable driving range between charges, the EV industry is seeking better batteries. The U.S. Advanced Battery Consortium (USABC) set specific battery performance goals for electric vehicle batteries. Meeting the mid-term goals would allow the expansion of the market, while achieving the long-term goals would allow electric vehicles to be competitive with current gasoline-powered vehicles.

USABC Battery Performance Goals		
Parameter	Mid-Term Target	Long-Term Target
Life (cycles)	600	1000
Life (years)	5	10
Piece cost (\$/kWh)	150	100
Mass (kg)	500	200
Volume (litres)	296	133
Recharge time (hrs from 80% DOD)	6	3
Self-discharge	15 (%/48hrs)	15 (%/Month)
Peak power (W/kg)	150	400
Power density (W/litre)	135	600
Energy density (Wh/litre)	135	300
Specific energy (Wh/kg)	80	200

To meet consumer driving range demands, automobile manufacturers and their supplier organizations are working on all aspects of EV design. The biggest influence on driving range is ultimately the capacity of the battery.

Battery Type	Driving Range	Horsepower	Speed/MPH
Lead Acid	40-90 miles	90+	70-80
Advanced Lead Acid	60 miles	100	80
Nickel-Metal-Hydride	60-80 miles	66	80+
Lithium Ion	120 miles	80	74
Lithium Polymer	150-200 miles	*tbd	*tbd

The Lithium Polymer Battery Concept

The lithium polymer battery is considered to be the best long-term solution for powering electric vehicles.

Sample Module Specifications	
Nominal Voltage (V)	20

Capacity at C/3 Rate (Ah)	119
Maximum Current (A)	365
Specific Energy (Wh/kg)	155
Energy Density (Wh/dm ³)	220
Power Density (W/dm ³)	445
Specific Power (W/kg)	315
Cycle Life at 80% DoD	600 cycles, targeted at 1000 cycles
Typical Weight (kg)	15.7
Volume (dm ³)	11
Dimensions	Application specific

Cell Chemistry

The concept involves an all-solid-state electrochemical cell made of two reversible lithium ion electrodes, one acting as a source of lithium ions during discharge and the other as a corresponding sink for the lithium ions.

- The two electrodes are separated by a thin, ionically conductive polymer membrane acting both as an electrolyte and as a separator between the electrodes.
- The anode electrode is made of an ultra-thin lithium foil that serves both as a lithium source and a current collector.
- The positive electrode is a material based on a reversible intercalation compound of vanadium oxides, which is blended with polymer electrolyte and carbon to form a plastic composite that is backed by a metal foil current collector.
- The operating temperature is normally maintained at 60-80°C (140-176°F) to achieve the fast lithium-ion transport power necessary for electric vehicle acceleration.

The Laminate

A lithium polymer cell is made by laminating together five thin materials--an insulator, a lithium foil anode, a solid polymeric electrolyte, a metallic oxide cathode and a current collector. A finished electric vehicle battery will contain virtually miles of web laminate.

- Once the laminate is formed, it is wound into a cell, completing the basic building block of a unit cell.
- A large number of these unit cells are connected in a series to provide the 300+ volts needed to power today's electric vehicles.
- By adjusting the thickness and length of the materials in the cells and the number and arrangement of the cells, the battery can be designed to suit the power and energy needs of many vehicle designs.

Cell Construction

- 3M mills and compounds the basic materials, prepares the polymer electrolyte, creates a thin film of cathode material and rolls it all into a continuous web polymer half cell.
- 3M sends its polymer half cell rolls to Hydro-Québec, which produces the lithium foil anode with a patented, proprietary metallic lithium process.
- Hydro-Québec laminates the polymer half cell with its lithium anode, rolling up completed cells. It then winds cells, assembles modules and battery packs, and tests the packs to verify performance.
- Once electrochemical testing is completed, all modules and packs are torn down at Hydro-Québec, where post-mortem analysis helps solve problems and Ref.ine the lithium polymer battery technologies.

The Winding Technique

Ultra-thin lithium foil from Hydro-Québec is paired with solid polymer and cathode webs from 3M to form a composite laminate less than 0.004 inches thick. Three different winding techniques were evaluated as part of the lithium polymer battery research:

The flat roll and flat stack designs produce "prismatic" cells.

The "Jelly Roll" produces a cylindrical cell. Cylindrical cells, while easier to produce, waste volume when assembled in a rectangular battery enclosure.

Flat roll, prismatic cells have been selected for electric vehicle applications because they provide the highest energy density, better cycle life performance and improved design flexibility.

Thermal Management

The lithium polymer battery design incorporates an insulated, controlled thermal management system to keep the battery at the optimal operating temperature.

At its current state of research, the battery operates best at temperatures between 60-80°C (140-176°F).

The system uses less than 200W of energy to keep the battery warm.

Insulation surrounds the battery pack to minimize heat loss.

Thermal management ensures that the battery operates efficiently for up to three days without a plug-in.

Voltage Curve

The operating voltage range is between 3.2 and 2.0 volts related to the depth of discharge. Unlike most current battery technologies, the lithium polymer battery system has no secondary reaction during the charging process. The advantage is that during normal charging, the cell coulombic efficiency is 100 percent and energy efficiency is 95 percent.

Cycle Life

Lithium polymer batteries will have a life expectancy of about 10 years, based on the following equation:

150 miles/charge X 600 cycles = close to 100,000 miles useful life.

Product Information

***Just Imagine What These Silvercel Advantages
Can Do For Your Application***

LIGHTWEIGHT

RUGGED

Yardney Technical Products Inc.(YTPI) rechargeable Silvercels weigh anywhere from one-third to one-fifth that of nickel-cadmium and lead-acid cells of a comparable energy output.

COMPACT

Depending on size and conditions of use, to do the same job, our silver-zinc cells will only require one-half to one-fourth the space of the other widely used rechargeable cells.

POWERFUL

YTPI Silvercels can be discharged at tremendously high rates. This, combined with their high energy output, makes them ideal for such high-rate applications as missiles, space launch vehicles, torpedoes and torpedo targets.

STABLE VOLTAGE

Because of the resistance of silver monoxide, electrodes vary little with the state of charge, a stable operating voltage is provided until nearly all the capacity is withdrawn.

SAFE

We are very proud of the fact that our silver-zinc cells have not ever caused or contributed to an accident in which personnel were seriously injured.

RELIABLE

Our Silvercels can be used on applications with very demanding dynamic exposures as evidenced by their wide spread end use on so many missile and space launch vehicle applications.

RECHARGEABLE

Yardney Technical Products Inc. silver-zinc cells can provide hundreds of charge/discharge cycles under ideal operating conditions.

WIDE SELECTION OF SIZES

Silvercels are available in an almost endless variety of ampere-hour sizes and prismatic shapes. Many other cells(0.1 to 20,000 ampere hours) are available in addition to the "standard models" listed on this web site.

VARIETY OF CELL TYPES

YTPI Silvercels come in three distinct classes of cells: **Error! Bookmark not defined.** for maximum cycle and wet life, **Error! Bookmark not defined.** for greater high rate capability, and **Error! Bookmark not defined.** to optimize rate capability for applications not requiring many cycles or an extensive activated life.

PACKAGING ADAPTABILITY

With the variety of sizes, shapes and types, the individual cell concept allows you to arrange series strings of cells to provide any voltage desired.

CUSTOMIZED CELL DESIGNS

***Characteristics of Yardney Silvercels ®
"LR", "HR" & "PM" Series Silver-Zinc Cells***

LR: Long Life, Low Rate
HR: Medium Life, High Rate
PM: Limited Life, Optimum Performance

Energy Output:

40-90 watt-hours per pound and 2.5-8.0 watt-hours per cubic inch, depending on cell type, model and conditions of use; as much as 120 watt-hours per pound and 11.0 watt-hours per cubic inch for certain special models and applications.

Power Output:

From 50-150 watts per pound and 4-10 watts per cubic inch (continuously) for "LR" Type Cells, to 150-500 watts per pound and 10-35 watts per cubic inch (continuously) for "PM" Type Cells. On an intermittent basis, values two times the indicated power output are possible (i.e., 1000 watts per pound and 70 watts per cubic inch).

Open-Circuit Cell Voltage:

1.82-1.86 volts when fully charged, 1.61-1.63 volts when partially charged.

Nominal Voltage Under Load:

1.5 volts.

Plateau Voltage Regulation:

$\pm 2\%$ at a fixed load and temperature limits within $\pm 10^\circ\text{F}$.

Silver-Zinc Systems

In the late 1940's Yardney Technical Products (then Yardney Electric Corporation) first developed a useful silver-zinc cell after its founder, Michel Yardney, collaborated with Henry Andre, a French Professor who published a meticulous study on the silver oxide-zinc couple. The inherent weight and size advantages of the couple allowed us to develop a marketable product that today provides power for torpedoes, submarines, aircraft, missiles, space vehicles and other weight/size sensitive applications. The wide and continued acceptance of this couple over the last fifty years can be attributed to an energy density/specific energy advantage of approximately 4 to 1 over the commonly used systems (lead-acid and nickel-cadmium). The system also provides a moderate cycle life/wet life, a good high rate capability, and a fairly flat discharge voltage and a low self discharge rate.

Although it is a secondary (rechargeable) system, it can be optionally designed for primary (one shot) applications such as space launch vehicles. An outstanding charge retention has allowed us to design a special class of long life "reserve" or remotely activated batteries for missiles in which electrolyte is not introduced to the cell until just at the time of use.

High Energy Density Silver-Zinc Cells

**Portable Industrial
Equipment
Photographic Equipment**

**Military Applications
Aircraft Applications**

**Portable
Electronics
Medical
Electronics
Space Exploration
Undersea
Propulsion**

Silver-Cadmium Systems

Shortly after the acceptance of the Ag-Zn System, Yardney developed the silver-cadmium system. Comparatively, it provides a much improved cycle and shelf life while providing an energy output more than twice that possible with commonly used systems of the same weight and volume.

Although not use as widely as the silver-zinc system, through the years, batteries with Yardney Silcads have been used on many applications where the cycle life requirement is greater than that possible with silver-zinc and, yet, a somewhat lower energy density/specific energy is acceptable. In addition, the fact that Yardney can, and does, provide these cells in the sealed condition for some applications has made them especially useful for intermediate life satellites and other special space missions.

Silver Chloride-Magnesium Systems

Yardney became heavily involved in AgCl-Mg Systems in the early 1960's. This high power, high energy system uses seawater as the electrolyte and is ideally suited for propulsion and ignition of torpedoes and other seawater deployed naval devices such as flares, buoys, etc.

The extent of our capabilities in this area is evidenced by the fact that we were the only manufacturer ever to build the large MK67 MOD 1 Propulsion Battery for the MK45 Torpedo and continue to manufacture the MK61 MOD O for the MK44 Torpedo. We also manufacture numerous small special units varying in size from a few watt hours to several hundred watt hours.

D. SCHEMATICS OF MOTOR AND CONTROLLER [REF. 8 & 18]

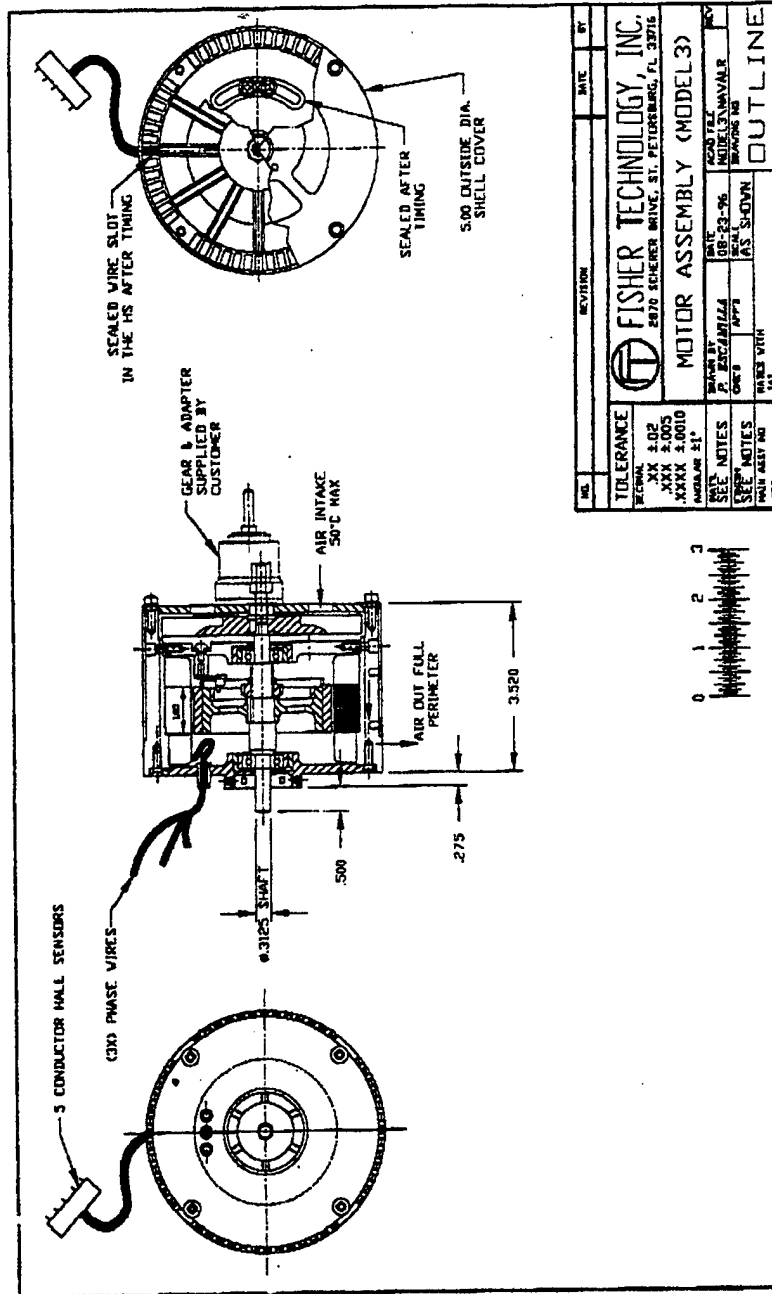
05-12-99 11:40AM FROM FISHER TECHNOLOGY

P02

Naval Post Graduate School
Fisher Model M3/10AFS brushless DC Motor

Ref: Quote 604

Specifications	
Output Power:	8 kW
Voltage:	100 Volts 0-peak, line-to-line
Current:	70 amps per phase
Speed:	12,000 RPM
Lamination dia:	Model 3
Steel thickness:	.009 laminations
Number of slots:	30 slots
Lamination length:	1.00 inch
Wire Gauge:	24 AWG, Class H
Number of conductors:	10
Number of turns:	5 turns, 1 coil per pole
Magnet Length:	1.00 inch (axial)
Magnet Thickness:	.200 inch (radial)
Number of poles:	10 poles
Magnet Material:	27 MGO Samarium Cobalt





MOTOROLA

CONTROLLER SCHEMATICS

Order this document by MC33035/D

MC33035

Brushless DC Motor Controller

The MC33035 is a high performance second generation monolithic brushless DC motor controller containing all of the active functions required to implement a full featured open loop, three or four phase motor control system. This device consists of a rotor position decoder for proper commutation sequencing, temperature compensated reference capable of supplying sensor power, frequency programmable sawtooth oscillator, three open collector top drivers, and three high current totem pole bottom drivers ideally suited for driving power MOSFETs.

Also included are protective features consisting of undervoltage lockout, cycle-by-cycle current limiting with a selectable time delayed latched shutdown mode, internal thermal shutdown, and a unique fault output that can be interfaced into microprocessor controlled systems.

Typical motor control functions include open loop speed, forward or reverse direction, run enable, and dynamic braking. The MC33035 is designed to operate with electrical sensor phasings of 60°/300° or 120°/240°, and can also efficiently control brush DC motors.

- 10 to 30 V Operation
- Undervoltage Lockout
- 6.25 V Reference Capable of Supplying Sensor Power
- Fully Accessible Error Amplifier for Closed Loop Servo Applications
- High Current Drivers Can Control External 3-Phase MOSFET Bridge
- Cycle-By-Cycle Current Limiting
- Pinned-Out Current Sense Reference
- Internal Thermal Shutdown
- Selectable 60°/300° or 120°/240° Sensor Phasings
- Can Efficiently Control Brush DC Motors with External MOSFET H-Bridge

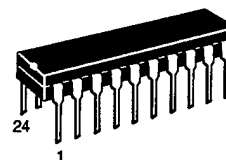
ORDERING INFORMATION

Device	Operating Temperature Range	Package
MC33035DW	$T_A = -40^\circ \text{ to } +85^\circ \text{C}$	SO-24L
MC33035P		Plastic DIP

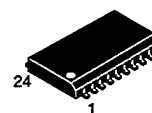
BRUSHLESS DC MOTOR CONTROLLER

SEMICONDUCTOR TECHNICAL DATA

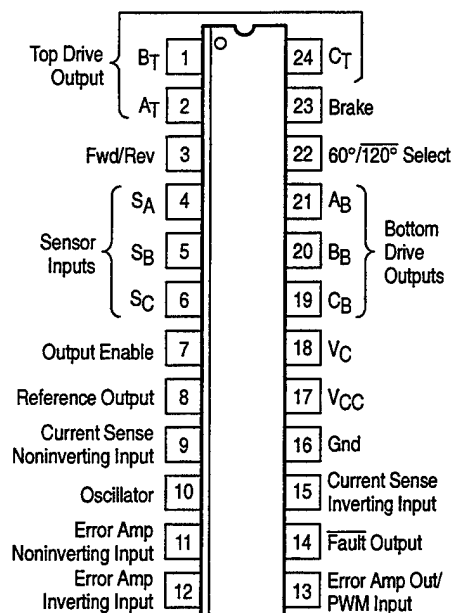
P SUFFIX
PLASTIC PACKAGE
CASE 724



DW SUFFIX
PLASTIC PACKAGE
CASE 751E
(SO-24L)



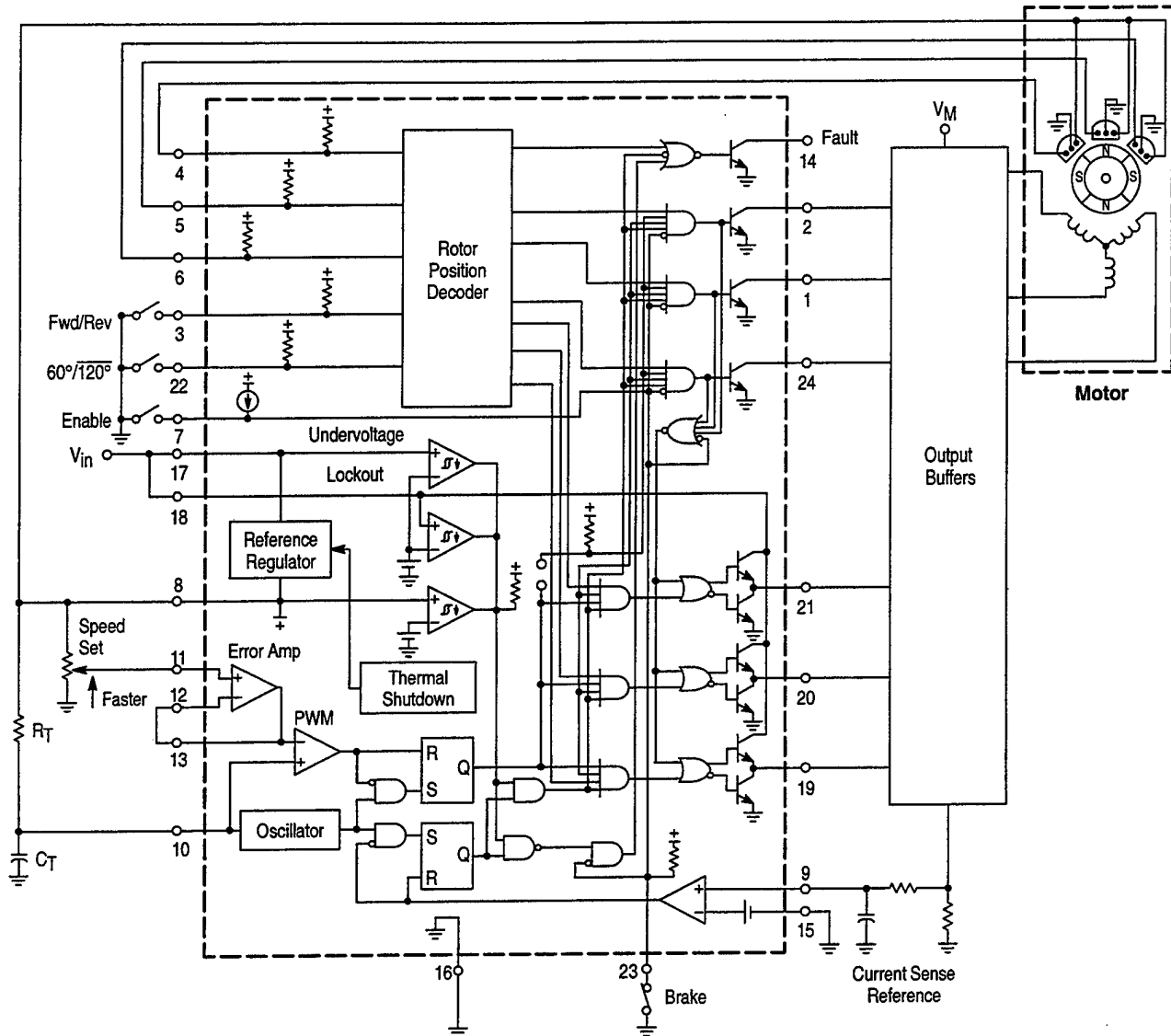
PIN CONNECTIONS



(Top View)

MC33035

Representative Schematic Diagram



This device contains 285 active transistors.

MAXIMUM RATINGS

Rating	Symbol	Value	Unit
Power Supply Voltage	V_{CC}	40	V
Digital Inputs (Pins 3, 4, 5, 6, 22, 23)	—	V_{ref}	V
Oscillator Input Current (Source or Sink)	I_{OSC}	30	mA
Error Amp Input Voltage Range (Pins 11, 12, Note 1)	V_{IR}	−0.3 to V_{ref}	V
Error Amp Output Current (Source or Sink, Note 2)	I_{Out}	10	mA
Current Sense Input Voltage Range (Pins 9, 15)	V_{Sense}	−0.3 to 5.0	V
Fault Output Voltage	$V_{CE(Fault)}$	20	V
Fault Output Sink Current	$I_{Sink(Fault)}$	20	mA
Top Drive Voltage (Pins 1, 2, 24)	$V_{CE(top)}$	40	V
Top Drive Sink Current (Pins 1, 2, 24)	$I_{Sink(top)}$	50	mA
Bottom Drive Supply Voltage (Pin 18)	V_C	30	V
Bottom Drive Output Current (Source or Sink, Pins 19, 20, 21)	I_{DRV}	100	mA
Power Dissipation and Thermal Characteristics P Suffix, Dual In Line, Case 724 Maximum Power Dissipation @ $T_A = 85^\circ\text{C}$ Thermal Resistance, Junction-to-Air	P_D $R_{\theta JA}$	867 75	mW $^\circ\text{C/W}$
DW Suffix, Surface Mount, Case 751E Maximum Power Dissipation @ $T_A = 85^\circ\text{C}$ Thermal Resistance, Junction-to-Air	P_D $R_{\theta JA}$	650 100	mW $^\circ\text{C/W}$
Operating Junction Temperature	T_J	150	$^\circ\text{C}$
Operating Ambient Temperature Range	T_A	−40 to +85	$^\circ\text{C}$
Storage Temperature Range	T_{stg}	−65 to +150	$^\circ\text{C}$

ELECTRICAL CHARACTERISTICS ($V_{CC} = V_C = 20\text{ V}$, $R_T = 4.7\text{ k}$, $C_T = 10\text{ nF}$, $T_A = 25^\circ\text{C}$, unless otherwise noted.)

Characteristic	Symbol	Min	Typ	Max	Unit
----------------	--------	-----	-----	-----	------

REFERENCE SECTION

Reference Output Voltage ($I_{ref} = 1.0\text{ mA}$) $T_A = 25^\circ\text{C}$ $T_A = -40^\circ\text{ to } +85^\circ\text{C}$	V_{ref}	5.9 5.82	6.24 —	6.5 6.57	V
Line Regulation ($V_{CC} = 10\text{ to } 30\text{ V}$, $I_{ref} = 1.0\text{ mA}$)	Reg_{line}	—	1.5	30	mV
Load Regulation ($I_{ref} = 1.0\text{ to } 20\text{ mA}$)	Reg_{load}	—	16	30	mV
Output Short Circuit Current (Note 3)	I_{SC}	40	75	—	mA
Reference Under Voltage Lockout Threshold	V_{th}	4.0	4.5	5.0	V

ERROR AMPLIFIER

Input Offset Voltage ($T_A = -40^\circ\text{ to } +85^\circ\text{C}$)	V_{IO}	—	0.4	10	mV
Input Offset Current ($T_A = -40^\circ\text{ to } +85^\circ\text{C}$)	I_{IO}	—	8.0	500	nA
Input Bias Current ($T_A = -40^\circ\text{ to } +85^\circ\text{C}$)	I_{IB}	—	−46	−1000	nA
Input Common Mode Voltage Range	V_{ICR}	(0 V to V_{ref})			V
Open Loop Voltage Gain ($V_O = 3.0\text{ V}$, $R_L = 15\text{ k}$)	A_{VOL}	70	80	—	dB
Input Common Mode Rejection Ratio	$CMRR$	55	86	—	dB
Power Supply Rejection Ratio ($V_{CC} = V_C = 10\text{ to } 30\text{ V}$)	$PSRR$	65	105	—	dB

- NOTES: 1. The input common mode voltage or input signal voltage should not be allowed to go negative by more than 0.3 V.
2. The compliance voltage must not exceed the range of −0.3 to V_{ref} .
3. Maximum package power dissipation limits must be observed.

ELECTRICAL CHARACTERISTICS (continued) ($V_{CC} = V_C = 20$ V, $R_T = 4.7$ k, $C_T = 10$ nF, $T_A = 25^\circ\text{C}$, unless otherwise noted.)

Characteristic	Symbol	Min	Typ	Max	Unit
ERROR AMPLIFIER					
Output Voltage Swing					V
High State ($R_L = 15$ k to Gnd)	V_{OH}	4.6	5.3	—	
Low State ($R_L = 15$ k to V_{ref})	V_{OL}	—	0.5	1.0	
OSCILLATOR SECTION					
Oscillator Frequency	f_{OSC}	22	25	28	kHz
Frequency Change with Voltage ($V_{CC} = 10$ to 30 V)	$\Delta f_{OSC}/\Delta V$	—	0.01	5.0	%
Sawtooth Peak Voltage	$V_{OSC(P)}$	—	4.1	4.5	V
Sawtooth Valley Voltage	$V_{OSC(V)}$	1.2	1.5	—	V
LOGIC INPUTS					
Input Threshold Voltage (Pins 3, 4, 5, 6, 7, 22, 23)					V
High State	V_{IH}	3.0	2.2	—	
Low State	V_{IL}	—	1.7	0.8	
Sensor Inputs (Pins 4, 5, 6)					μA
High State Input Current ($V_{IH} = 5.0$ V)	I_{IH}	—150	—70	—20	
Low State Input Current ($V_{IL} = 0$ V)	I_{IL}	—600	—337	—150	
Forward/Reverse, $60^\circ/120^\circ$ Select (Pins 3, 22, 23)					μA
High State Input Current ($V_{IH} = 5.0$ V)	I_{IH}	—75	—36	—10	
Low State Input Current ($V_{IL} = 0$ V)	I_{IL}	—300	—175	—75	
Output Enable					μA
High State Input Current ($V_{IH} = 5.0$ V)	I_{IH}	—60	—29	—10	
Low State Input Current ($V_{IL} = 0$ V)	I_{IL}	—60	—29	—10	
CURRENT-LIMIT COMPARATOR					
Threshold Voltage	V_{th}	85	101	115	mV
Input Common Mode Voltage Range	V_{ICR}	—	3.0	—	V
Input Bias Current	I_{IB}	—	—0.9	—5.0	μA
OUTPUTS AND POWER SECTIONS					
Top Drive Output Sink Saturation ($I_{sink} = 25$ mA)	$V_{CE(sat)}$	—	0.5	1.5	V
Top Drive Output Off-State Leakage ($V_{CE} = 30$ V)	$I_{DRV(leak)}$	—	0.06	100	μA
Top Drive Output Switching Time ($C_L = 47$ pF, $R_L = 1.0$ k)					ns
Rise Time	t_r	—	107	300	
Fall Time	t_f	—	26	300	
Bottom Drive Output Voltage					V
High State ($V_{CC} = 20$ V, $V_C = 30$ V, $I_{source} = 50$ mA)	V_{OH}	($V_{CC} - 2.0$)	($V_{CC} - 1.1$)	—	
Low State ($V_{CC} = 20$ V, $V_C = 30$ V, $I_{sink} = 50$ mA)	V_{OL}	—	1.5	2.0	
Bottom Drive Output Switching Time ($C_L = 1000$ pF)					ns
Rise Time	t_r	—	38	200	
Fall Time	t_f	—	30	200	
Fault Output Sink Saturation ($I_{sink} = 16$ mA)	$V_{CE(sat)}$	—	225	500	mV
Fault Output Off-State Leakage ($V_{CE} = 20$ V)	$I_{FLT(leak)}$	—	1.0	100	μA
Under Voltage Lockout					V
Drive Output Enabled (V_{CC} or V_C Increasing)	$V_{th(on)}$	8.2	8.9	10	
Hysteresis	V_H	0.1	0.2	0.3	
Power Supply Current					mA
Pin 17 ($V_{CC} = V_C = 20$ V)	I_{CC}	—	12	16	
Pin 17 ($V_{CC} = 20$ V, $V_C = 30$ V)		—	14	20	
Pin 18 ($V_{CC} = V_C = 20$ V)	I_C	—	3.5	6.0	
Pin 18 ($V_{CC} = 20$ V, $V_C = 30$ V)		—	5.0	10	

Figure 1. Oscillator Frequency versus Timing Resistor

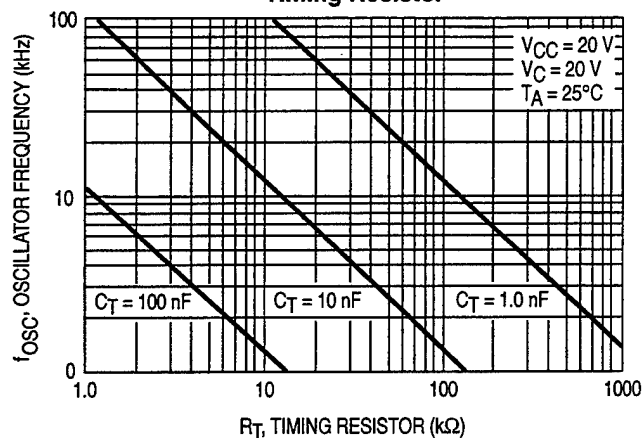


Figure 2. Oscillator Frequency Change versus Temperature

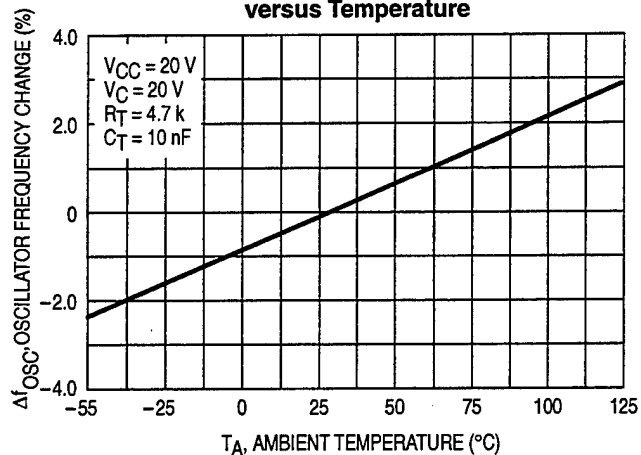


Figure 3. Error Amp Open Loop Gain and Phase versus Frequency

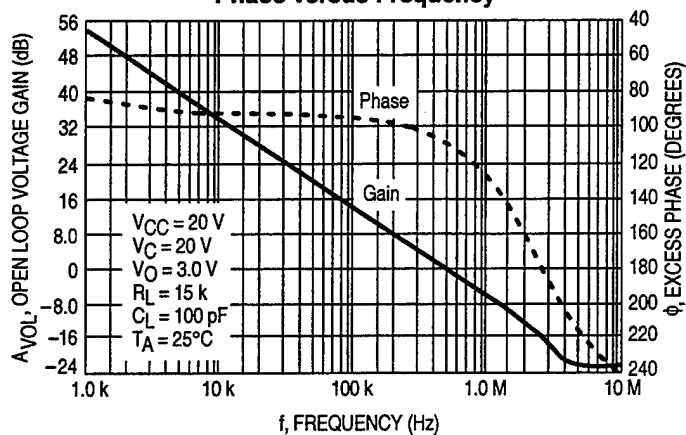


Figure 4. Error Amp Output Saturation Voltage versus Load Current

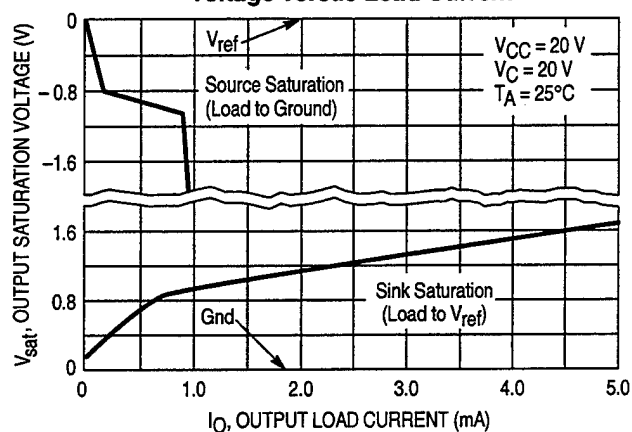


Figure 5. Error Amp Small-Signal Transient Response

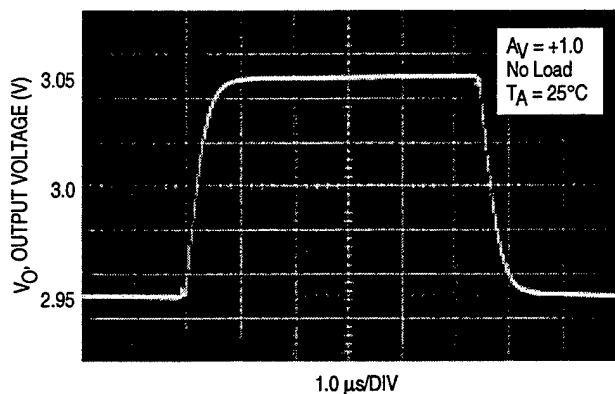


Figure 6. Error Amp Large-Signal Transient Response

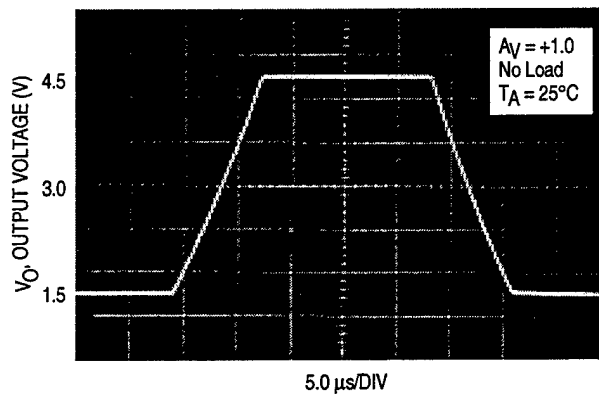


Figure 7. Reference Output Voltage Change versus Output Source Current

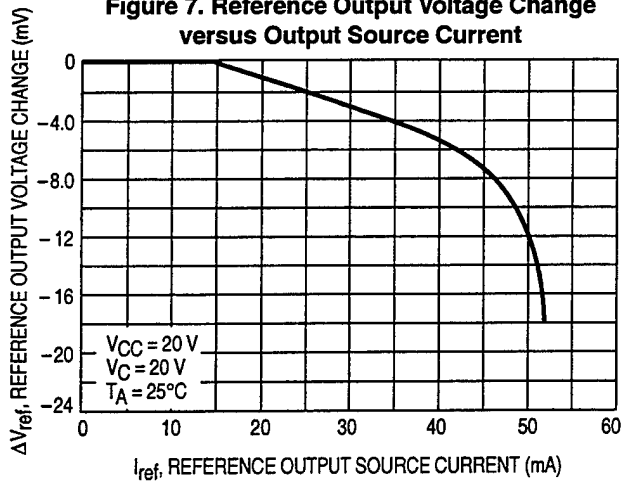


Figure 8. Reference Output Voltage versus Supply Voltage

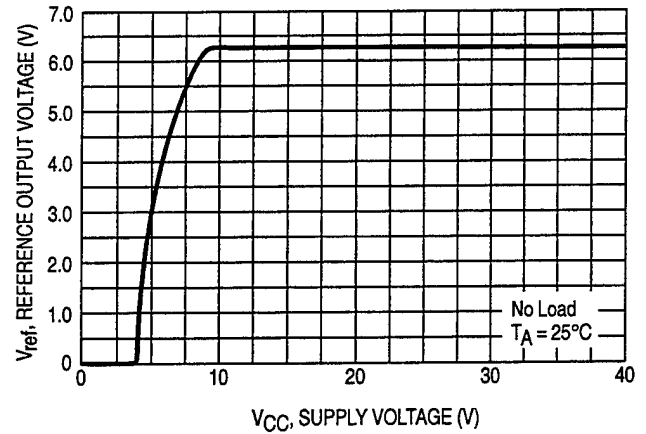


Figure 9. Reference Output Voltage versus Temperature

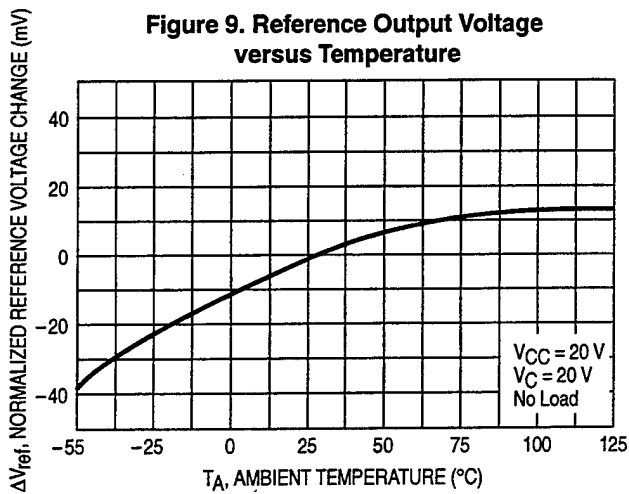


Figure 10. Output Duty Cycle versus PWM Input Voltage

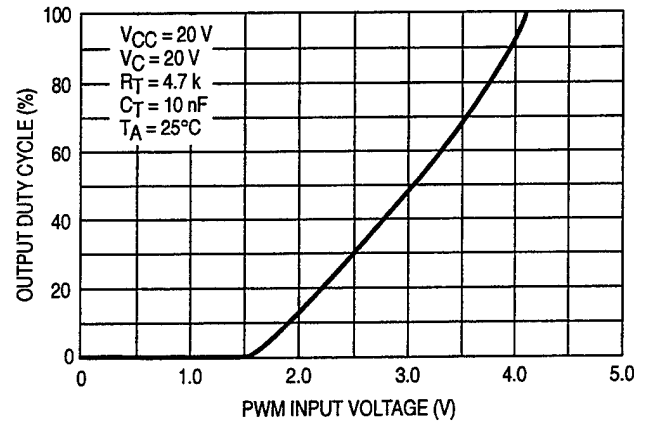


Figure 11. Bottom Drive Response Time versus Current Sense Input Voltage

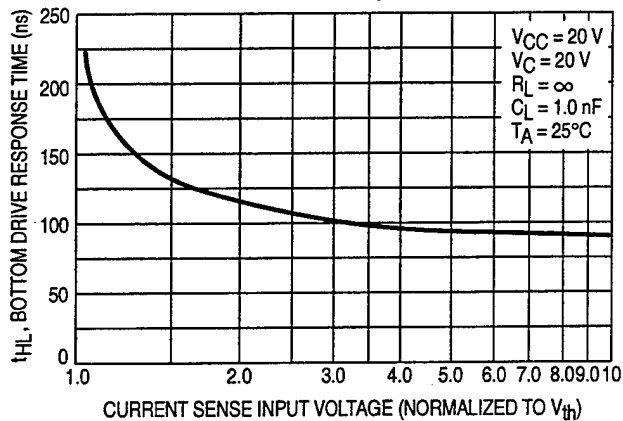


Figure 12. Fault Output Saturation versus Sink Current

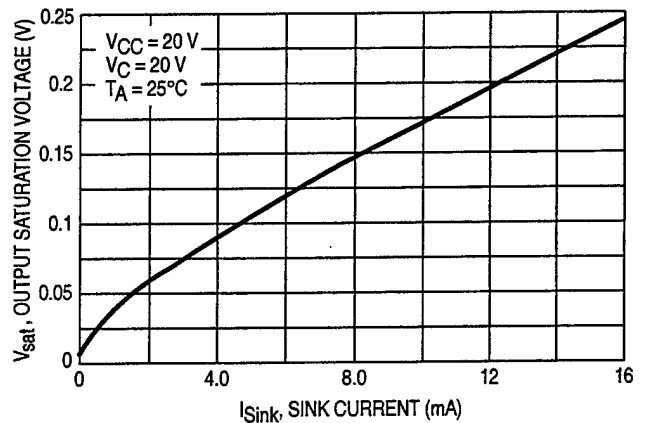


Figure 13. Top Drive Output Saturation Voltage versus Sink Current

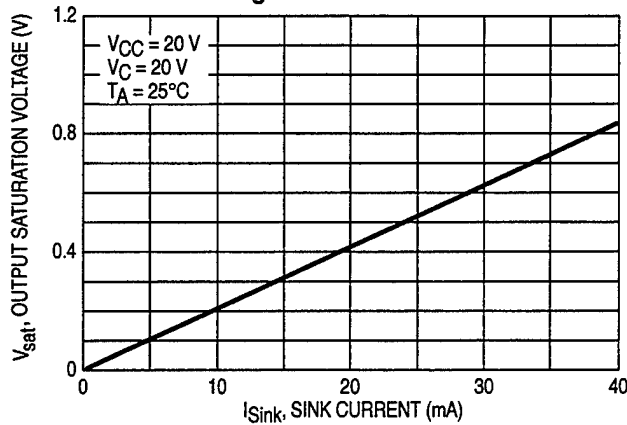


Figure 14. Top Drive Output Waveform

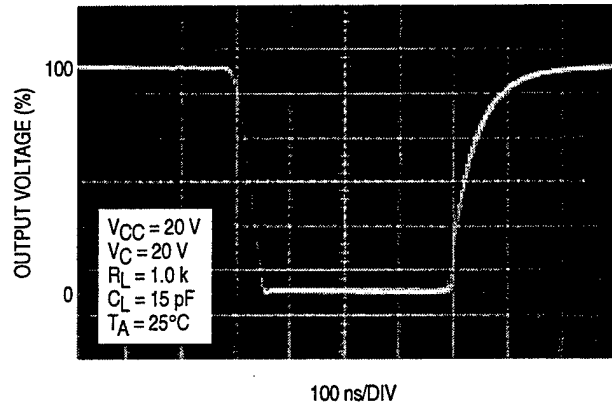


Figure 15. Bottom Drive Output Waveform

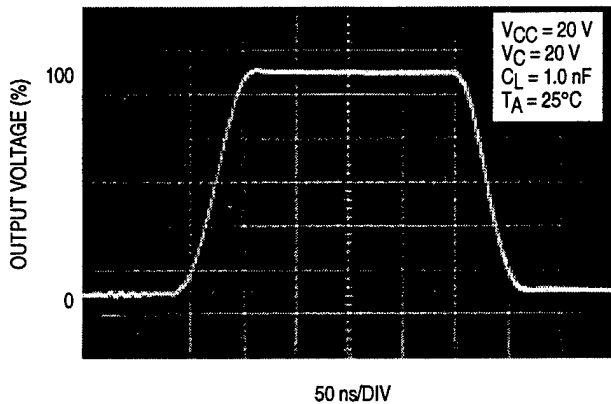


Figure 16. Bottom Drive Output Waveform

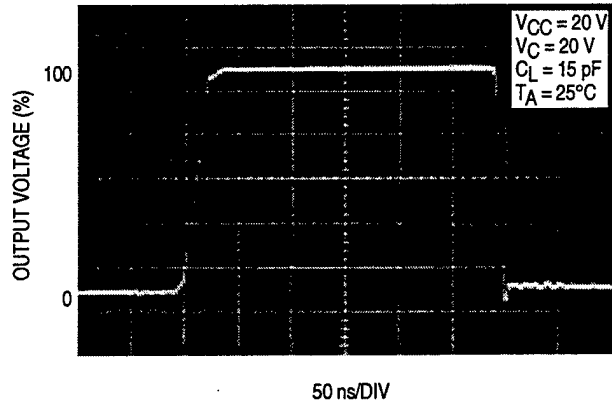


Figure 17. Bottom Drive Output Saturation Voltage versus Load Current

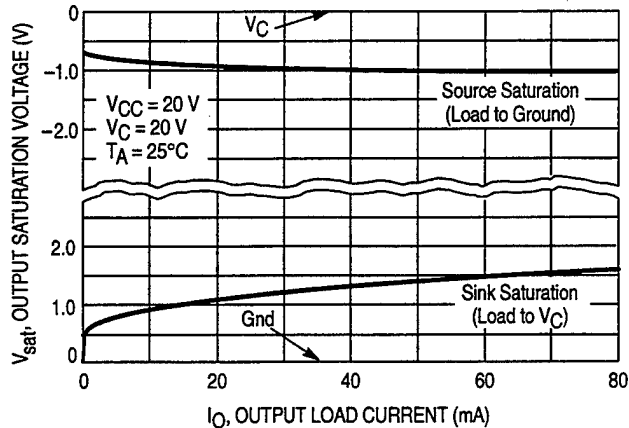
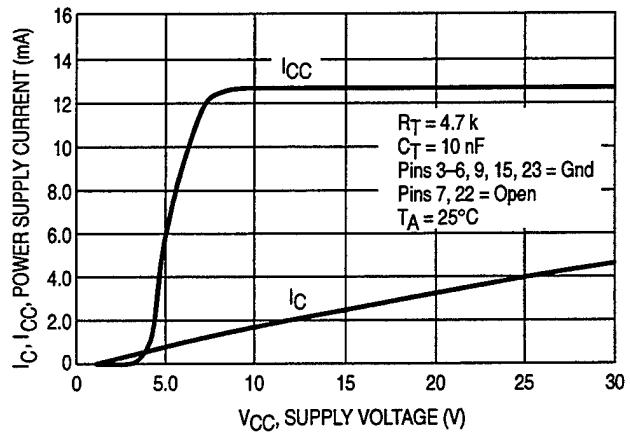


Figure 18. Power and Bottom Drive Supply Current versus Supply Voltage



PIN FUNCTION DESCRIPTION

Pin	Symbol	Description
1, 2, 24	B _T , A _T , C _T	These three open collector Top Drive outputs are designed to drive the external upper power switch transistors.
3	Fwd/Rev	The Forward/Reverse Input is used to change the direction of motor rotation.
4, 5, 6	S _A , S _B , S _C	These three Sensor Inputs control the commutation sequence.
7	Output Enable	A logic high at this input causes the motor to run, while a low causes it to coast.
8	Reference Output	This output provides charging current for the oscillator timing capacitor C _T and a reference for the error amplifier. It may also serve to furnish sensor power.
9	Current Sense Noninverting Input	A 100 mV signal, with respect to Pin 15, at this input terminates output switch conduction during a given oscillator cycle. This pin normally connects to the top side of the current sense resistor.
10	Oscillator	The Oscillator frequency is programmed by the values selected for the timing components, R _T and C _T .
11	Error Amp Noninverting Input	This input is normally connected to the speed set potentiometer.
12	Error Amp Inverting Input	This input is normally connected to the Error Amp Output in open loop applications.
13	Error Amp Out/PWM Input	This pin is available for compensation in closed loop applications.
14	Fault Output	This open collector output is active low during one or more of the following conditions: Invalid Sensor Input code, Enable Input at logic 0, Current Sense Input greater than 100 mV (Pin 9 with respect to Pin 15), Undervoltage Lockout activation, and Thermal Shutdown.
15	Current Sense Inverting Input	Reference pin for internal 100 mV threshold. This pin is normally connected to the bottom side of the current sense resistor.
16	Gnd	This pin supplies a ground for the control circuit and should be referenced back to the power source ground.
17	V _{CC}	This pin is the positive supply of the control IC. The controller is functional over a minimum V _{CC} range of 10 to 30 V.
18	V _C	The high state (V _{OH}) of the Bottom Drive Outputs is set by the voltage applied to this pin. The controller is operational over a minimum V _C range of 10 to 30 V.
19, 20, 21	C _B , B _B , A _B	These three totem pole Bottom Drive Outputs are designed for direct drive of the external bottom power switch transistors.
22	60°/120° Select	The electrical state of this pin configures the control circuit operation for either 60° (high state) or 120° (low state) sensor electrical phasing inputs.
23	Brake	A logic low state at this input allows the motor to run, while a high state does not allow motor operation and if operating causes rapid deceleration.

INTRODUCTION

The MC33035 is one of a series of high performance monolithic DC brushless motor controllers produced by Motorola. It contains all of the functions required to implement a full-featured, open loop, three or four phase motor control system. In addition, the controller can be made to operate DC brush motors. Constructed with Bipolar Analog technology, it offers a high degree of performance and ruggedness in hostile industrial environments. The MC33035 contains a rotor position decoder for proper commutation sequencing, a temperature compensated reference capable of supplying a sensor power, a frequency programmable sawtooth oscillator, a fully accessible error amplifier, a pulse width modulator comparator, three open collector top drive outputs, and three high current totem pole bottom driver outputs ideally suited for driving power MOSFETs.

Included in the MC33035 are protective features consisting of undervoltage lockout, cycle-by-cycle current limiting with a selectable time delayed latched shutdown mode, internal thermal shutdown, and a unique fault output that can easily be interfaced to a microprocessor controller.

Typical motor control functions include open loop speed control, forward or reverse rotation, run enable, and dynamic braking. In addition, the MC33035 has a 60°/120° select pin which configures the rotor position decoder for either 60° or 120° sensor electrical phasing inputs.

FUNCTIONAL DESCRIPTION

A representative internal block diagram is shown in Figure 19 with various applications shown in Figures 36, 38, 39, 43, 45, and 46. A discussion of the features and function of each of the internal blocks given below is referenced to Figures 19 and 36.

Rotor Position Decoder

An internal rotor position decoder monitors the three sensor inputs (Pins 4, 5, 6) to provide the proper sequencing of the top and bottom drive outputs. The sensor inputs are designed to interface directly with open collector type Hall Effect switches or opto slotted couplers. Internal pull-up resistors are included to minimize the required number of external components. The inputs are TTL compatible, with their thresholds typically at 2.2 V. The MC33035 series is designed to control three phase motors and operate with four of the most common conventions of sensor phasing. A 60°/120° Select (Pin 22) is conveniently provided and affords the MC33035 to configure itself to control motors having either 60°, 120°, 240° or 300° electrical sensor phasing. With three sensor inputs there are eight possible input code combinations, six of which are valid rotor positions. The remaining two codes are invalid and are usually caused by an open or shorted sensor line. With six valid input codes, the

decoder can resolve the motor rotor position to within a window of 60 electrical degrees.

The Forward/Reverse input (Pin 3) is used to change the direction of motor rotation by reversing the voltage across the stator winding. When the input changes state, from high to low with a given sensor input code (for example 100), the enabled top and bottom drive outputs with the same alpha designation are exchanged (A_T to A_B , B_T to B_B , C_T to C_B). In effect, the commutation sequence is reversed and the motor changes directional rotation.

Motor on/off control is accomplished by the Output Enable (Pin 7). When left disconnected, an internal 25 μA current source enables sequencing of the top and bottom drive outputs. When grounded, the top drive outputs turn off and the bottom drives are forced low, causing the motor to coast and the $\overline{\text{Fault}}$ output to activate.

Dynamic motor braking allows an additional margin of safety to be designed into the final product. Braking is accomplished by placing the Brake Input (Pin 23) in a high state. This causes the top drive outputs to turn off and the bottom drives to turn on, shorting the motor-generated back EMF. The brake input has unconditional priority over all other inputs. The internal 40 k Ω pull-up resistor simplifies interfacing with the system safety-switch by insuring brake activation if opened or disconnected. The commutation logic truth table is shown in Figure 20. A four input NOR gate is used to monitor the brake input and the inputs to the three top drive output transistors. Its purpose is to disable braking until the top drive outputs attain a high state. This helps to

prevent simultaneous conduction of the the top and bottom power switches. In half wave motor drive applications, the top drive outputs are not required and are normally left disconnected. Under these conditions braking will still be accomplished since the NOR gate senses the base voltage to the top drive output transistors.

Error Amplifier

A high performance, fully compensated error amplifier with access to both inputs and output (Pins 11, 12, 13) is provided to facilitate the implementation of closed loop motor speed control. The amplifier features a typical DC voltage gain of 80 dB, 0.6 MHz gain bandwidth, and a wide input common mode voltage range that extends from ground to V_{ref} . In most open loop speed control applications, the amplifier is configured as a unity gain voltage follower with the noninverting input connected to the speed set voltage source. Additional configurations are shown in Figures 31 through 35.

Oscillator

The frequency of the internal ramp oscillator is programmed by the values selected for timing components R_T and C_T . Capacitor C_T is charged from the Reference Output (Pin 8) through resistor R_T and discharged by an internal discharge transistor. The ramp peak and valley voltages are typically 4.1 V and 1.5 V respectively. To provide a good compromise between audible noise and output switching efficiency, an oscillator frequency in the range of 20 to 30 kHz is recommended. Refer to Figure 1 for component selection.

Figure 19. Representative Block Diagram

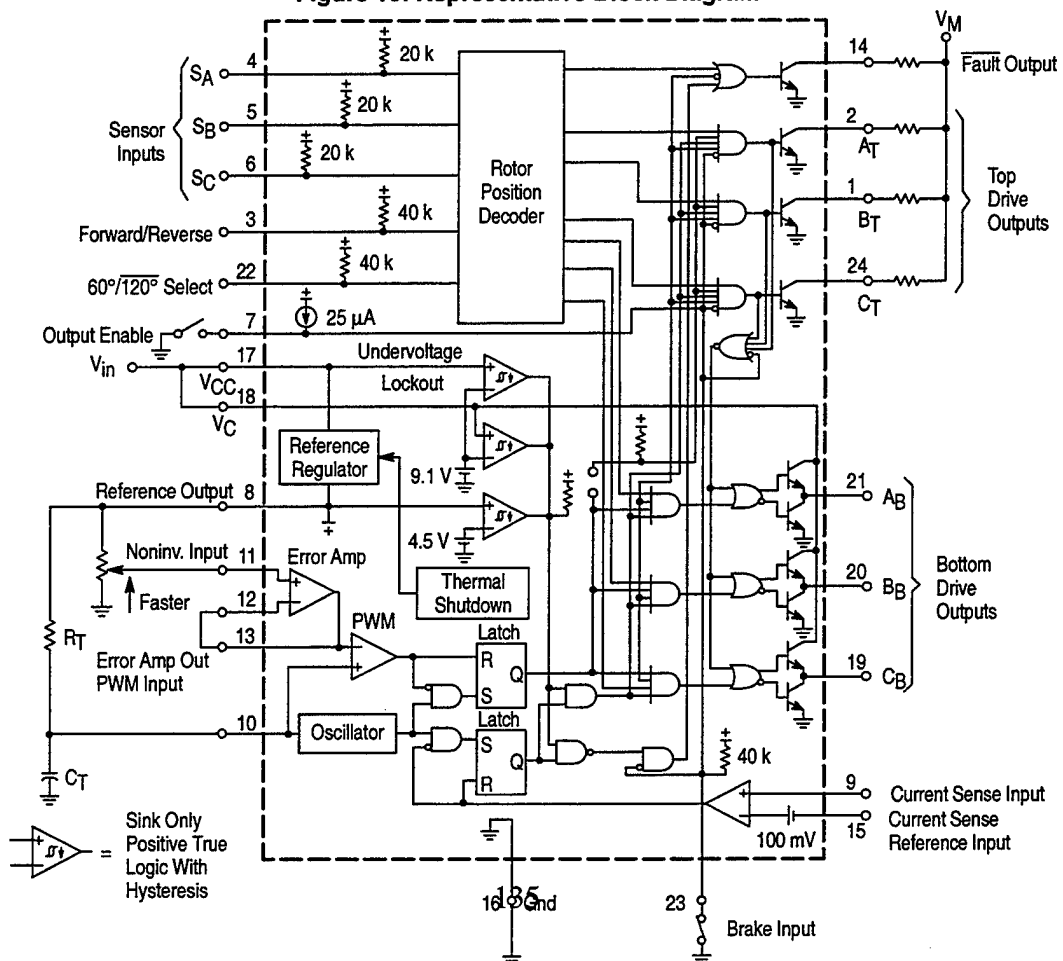


Figure 20. Three Phase, Six Step Commutation Truth Table (Note 1)

Inputs (Note 2)										Outputs (Note 3)								
Sensor Electrical Phasing (Note 4)										Top Drives			Bottom Drives					
S _A	60° S _B	S _C	S _A	120° S _B	S _C					F/R	Enable	Brake	Current Sense	A _T	B _T			C _T
1	0	0	1	0	0	1	1	0	0	0	1	1	1	0	0	1		1
1	1	0	1	1	0	1	1	0	0	1	0	1	0	0	1	1	1	
1	1	1	0	1	0	1	1	0	0	1	0	1	1	0	0	1	1	
0	1	1	0	1	1	1	1	0	0	1	1	0	1	0	0	1	1	
0	0	1	1	0	1	1	1	0	0	1	1	0	0	1	0	1	1	
0	0	0	1	0	1	1	1	0	0	0	1	1	0	1	0	1	1	
1	0	0	1	0	0	0	1	0	0	1	1	0	1	0	0	1	(Note 5) F/R = 0	
1	1	0	1	1	0	0	1	0	0	1	1	0	0	1	0	1		1
1	1	1	0	1	0	0	1	0	0	0	1	1	0	1	0	1		1
0	1	1	0	1	1	0	1	0	0	0	1	1	0	0	1	1		1
0	0	1	1	0	0	0	1	0	0	1	0	1	0	0	1	1		1
0	0	0	1	0	1	0	1	0	0	1	0	1	1	0	0	1		1
1	0	1	1	1	1	X	X	0	X	1	1	1	0	0	0	0	(Note 6) Brake = 0	
0	1	0	0	0	0	X	X	0	X	1	1	1	0	0	0	0		
1	0	1	1	1	1	X	X	1	X	1	1	1	1	1	1	1	0	(Note 7) Brake = 1
0	1	0	0	0	0	X	X	1	X	1	1	1	1	1	1	1	0	
V	V	V	V	V	V	X	1	1	X	1	1	1	1	1	1	1	1	(Note 8)
V	V	V	V	V	V	X	0	1	X	1	1	1	1	1	1	1	0	(Note 9)
V	V	V	V	V	V	X	0	0	X	1	1	1	0	0	0	0	0	(Note 10)
V	V	V	V	V	V	X	1	0	1	1	1	1	0	0	0	0	0	(Note 11)

- NOTES: 1. V = Any one of six valid sensor or drive combinations. X = Don't care.
 2. The digital inputs (Pins 3, 4, 5, 6, 7, 22, 23) are all TTL compatible. The current sense input (Pin 9) has a 100 mV threshold with respect to Pin 15. A logic 0 for this input is defined as < 85 mV, and a logic 1 is > 115 mV.
 3. The fault and top drive outputs are open collector design and active in the low (0) state.
 4. With 60°/120° select (Pin 22) in the high (1) state, configuration is for 60° sensor electrical phasing inputs. With Pin 22 in low (0) state, configuration is for 120° sensor electrical phasing inputs.
 5. Valid 60° or 120° sensor combinations for corresponding valid top and bottom drive outputs.
 6. Invalid sensor inputs with brake = 0; All top and bottom drives off, Fault low.
 7. Invalid sensor inputs with brake = 1; All top drives off, all bottom drives on, Fault low.
 8. Valid 60° or 120° sensor inputs with brake = 1; All top drives off, all bottom drives on, Fault high.
 9. Valid sensor inputs with brake = 1 and enable = 0; All top drives off, all bottom drives on, Fault low.
 10. Valid sensor inputs with brake = 0 and enable = 0; All top and bottom drives off, Fault low.
 11. All bottom drives off, Fault low.

Pulse Width Modulator

The use of pulse width modulation provides an energy efficient method of controlling the motor speed by varying the average voltage applied to each stator winding during the commutation sequence. As C_T discharges, the oscillator sets both latches, allowing conduction of the top and bottom drive outputs. The PWM comparator resets the upper latch, terminating the bottom drive output conduction when the positive-going ramp of C_T becomes greater than the error amplifier output. The pulse width modulator timing diagram is shown in Figure 21. Pulse width modulation for speed control appears only at the bottom drive outputs.

Current Limit

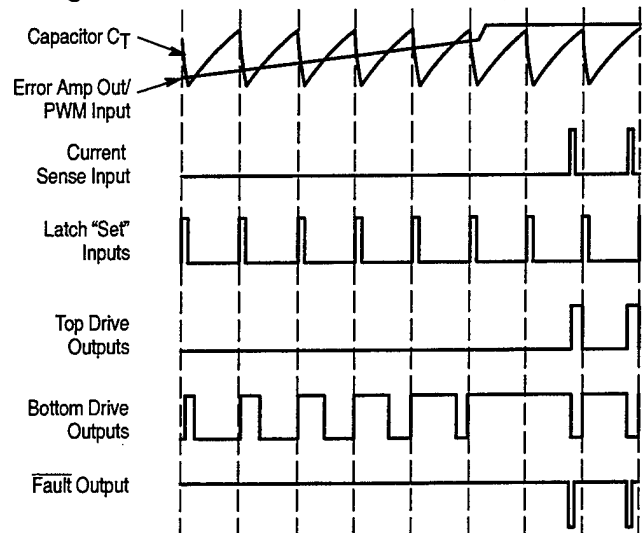
Continuous operation of a motor that is severely over-loaded results in overheating and eventual failure. This destructive condition can best be prevented with the use of cycle-by-cycle current limiting. That is, each on-cycle is treated as a separate event. Cycle-by-cycle current limiting is accomplished by monitoring the stator current build-up each time an output switch conducts, and upon sensing an over current condition, immediately turning off the switch and holding it off for the remaining duration of oscillator ramp-up period. The stator current is converted to a voltage by inserting a ground-referenced sense resistor R_S (Figure 36) in series with the three bottom switch transistors (Q₄, Q₅, Q₆). The voltage developed across the sense resistor is monitored by the Current Sense Input (Pins 9 and 15), and compared to the internal 100 mV reference. The current sense comparator inputs have an input common mode range of approximately 3.0 V. If the 100 mV current sense threshold is exceeded, the comparator resets the

lower sense latch and terminates output switch conduction. The value for the current sense resistor is:

$$R_S = \frac{0.1}{I_{\text{stator(max)}}}$$

The Fault output activates during an over current condition. The dual-latch PWM configuration ensures that only one single output conduction pulse occurs during any given oscillator cycle, whether terminated by the output of the error amp or the current limit comparator.

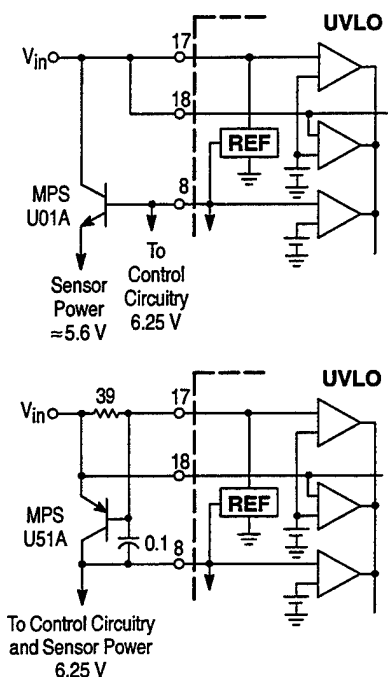
Figure 21. Pulse Width Modulator Timing Diagram



Reference

The on-chip 6.25 V regulator (Pin 8) provides charging current for the oscillator timing capacitor, a reference for the error amplifier, and can supply 20 mA of current suitable for directly powering sensors in low voltage applications. In higher voltage applications, it may become necessary to transfer the power dissipated by the regulator off the IC. This is easily accomplished with the addition of an external pass transistor as shown in Figure 22. A 6.25 V reference level was chosen to allow implementation of the simpler NPN circuit, where $V_{ref} - V_{BE}$ exceeds the minimum voltage required by Hall Effect sensors over temperature. With proper transistor selection and adequate heatsinking, up to one amp of load current can be obtained.

Figure 22. Reference Output Buffers



The NPN circuit is recommended for powering Hall or opto sensors, where the output voltage temperature coefficient is not critical. The PNP circuit is slightly more complex, but is also more accurate over temperature. Neither circuit has current limiting.

Undervoltage Lockout

A triple Undervoltage Lockout has been incorporated to prevent damage to the IC and the external power switch transistors. Under low power supply conditions, it guarantees that the IC and sensors are fully functional, and that there is sufficient bottom drive output voltage. The positive power supplies to the IC (V_{CC}) and the bottom drives (V_C) are each monitored by separate comparators that have their thresholds at 9.1 V. This level ensures sufficient gate drive necessary to attain low $R_{DS(on)}$ when driving standard power MOSFET devices. When directly powering the Hall sensors from the reference, improper sensor operation can result if the reference output voltage falls below 4.5 V. A third comparator is used to detect this condition. If one or more of the comparators detects an undervoltage condition, the Fault Output is activated, the top drives are turned off and the bottom drive outputs are held in a low state. Each of the

comparators contain hysteresis to prevent oscillations when crossing their respective thresholds.

Fault Output

The open collector Fault Output (Pin 14) was designed to provide diagnostic information in the event of a system malfunction. It has a sink current capability of 16 mA and can directly drive a light emitting diode for visual indication. Additionally, it is easily interfaced with TTL/CMOS logic for use in a microprocessor controlled system. The Fault Output is active low when one or more of the following conditions occur:

- 1) Invalid Sensor Input code
- 2) Output Enable at logic [0]
- 3) Current Sense Input greater than 100 mV
- 4) Undervoltage Lockout, activation of one or more of the comparators
- 5) Thermal Shutdown, maximum junction temperature being exceeded

This unique output can also be used to distinguish between motor start-up or sustained operation in an overloaded condition. With the addition of an RC network between the Fault Output and the enable input, it is possible to create a time-delayed latched shutdown for overcurrent. The added circuitry shown in Figure 23 makes easy starting of motor systems which have high inertial loads by providing additional starting torque, while still preserving overcurrent protection. This task is accomplished by setting the current limit to a higher than nominal value for a predetermined time. During an excessively long overcurrent condition, capacitor CDLY will charge, causing the enable input to cross its threshold to a low state. A latch is then formed by the positive feedback loop from the Fault Output to the Output Enable. Once set, by the Current Sense Input, it can only be reset by shorting CDLY or cycling the power supplies.

Drive Outputs

The three top drive outputs (Pins 1, 2, 24) are open collector NPN transistors capable of sinking 50 mA with a minimum breakdown of 30 V. Interfacing into higher voltage applications is easily accomplished with the circuits shown in Figures 24 and 25.

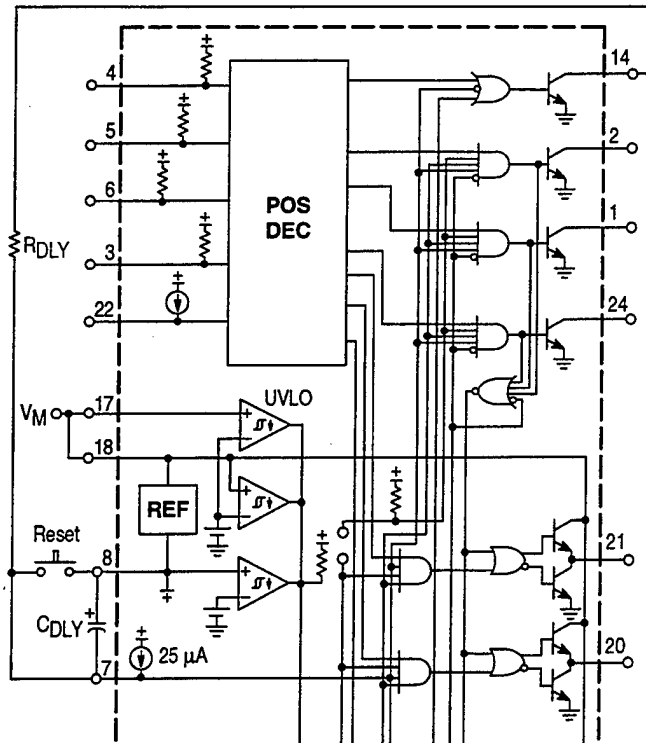
The three totem pole bottom drive outputs (Pins 19, 20, 21) are particularly suited for direct drive of N-Channel MOSFETs or NPN bipolar transistors (Figures 26, 27, 28 and 29). Each output is capable of sourcing and sinking up to 100 mA. Power for the bottom drives is supplied from V_C (Pin 18). This separate supply input allows the designer added flexibility in tailoring the drive voltage, independent of V_{CC} . A zener clamp should be connected to this input when driving power MOSFETs in systems where V_{CC} is greater than 20 V so as to prevent rupture of the MOSFET gates.

The control circuitry ground (Pin 16) and current sense inverting input (Pin 15) must return on separate paths to the central input source ground.

Thermal Shutdown

Internal thermal shutdown circuitry is provided to protect the IC in the event the maximum junction temperature is exceeded. When activated, typically at 170°C, the IC acts as though the Output Enable was grounded.

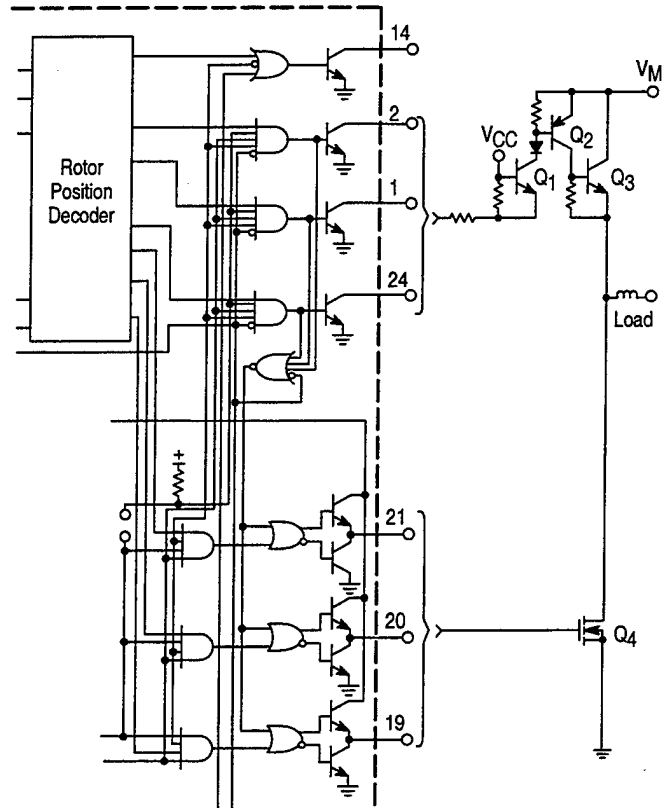
Figure 23. Timed Delayed Latched Over Current Shutdown



$$t_{DLY} \approx R_{DLY} C_{DLY} \ln \left(\frac{V_{ref} - (I_{IL} \text{ enable } R_{DLY})}{V_{th} \text{ enable} - (I_{IL} \text{ enable } R_{DLY})} \right)$$

$$\approx R_{DLY} C_{DLY} \ln \left(\frac{6.25 - (20 \times 10^{-6} R_{DLY})}{1.4 - (20 \times 10^{-6} R_{DLY})} \right)$$

Figure 24. High Voltage Interface with NPN Power Transistors



Transistor Q₁ is a common base stage used to level shift from V_{CC} to the high motor voltage, V_M. The collector diode is required if V_{CC} is present while V_M is low.

Figure 25. High Voltage Interface with N-Channel Power MOSFETs

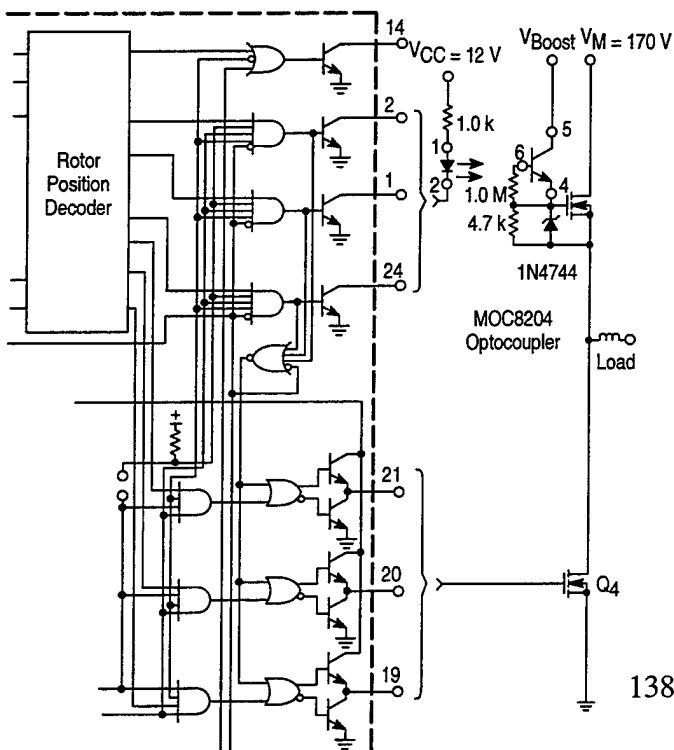
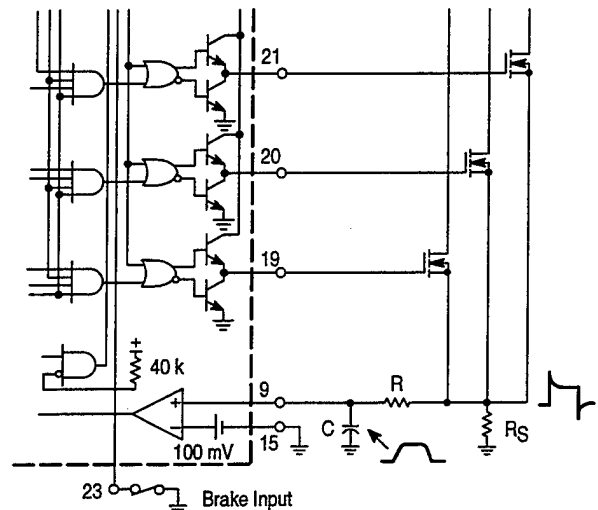
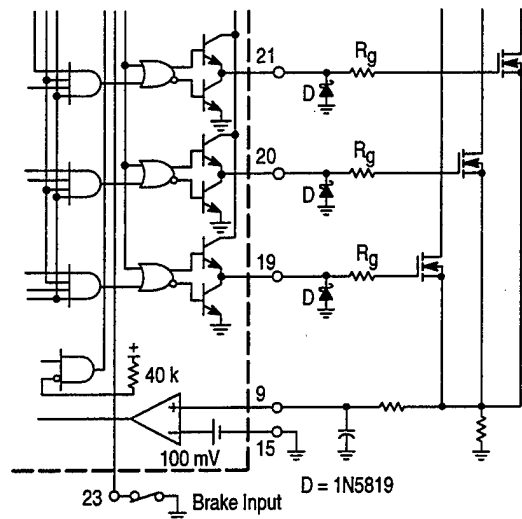


Figure 26. Current Waveform Spike Suppression



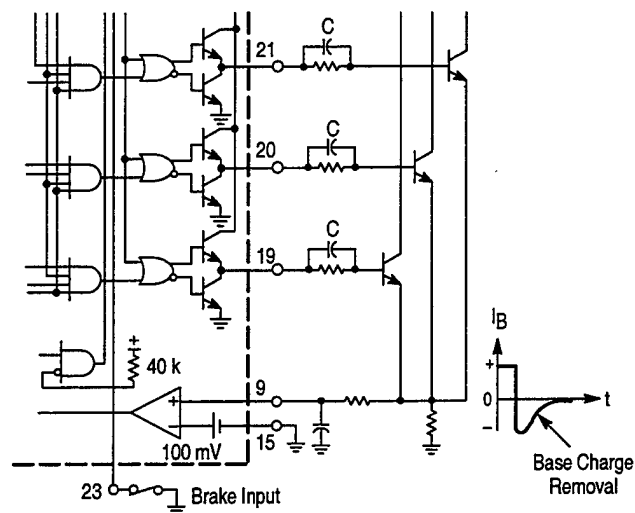
The addition of the RC filter will eliminate current-limit instability caused by the leading edge spike on the current waveform. Resistor R_S should be a low inductance type.

Figure 27. MOSFET Drive Precautions



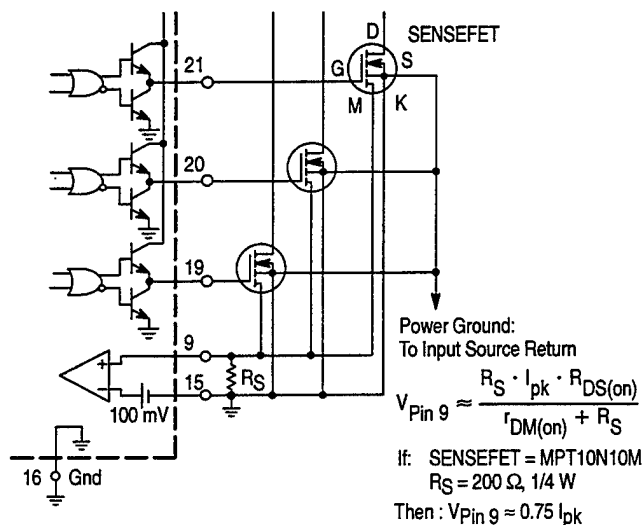
Series gate resistor R_g will dampen any high frequency oscillations caused by the MOSFET input capacitance and any series wiring inductance in the gate-source circuit. Diode D is required if the negative current into the Bottom Drive Outputs exceeds 50 mA.

Figure 28. Bipolar Transistor Drive



The totem-pole output can furnish negative base current for enhanced transistor turn-off, with the addition of capacitor C.

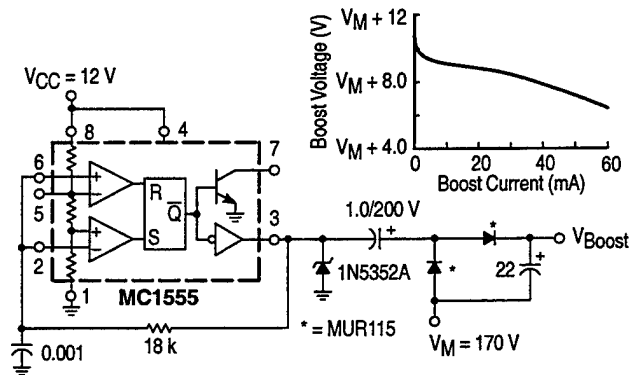
Figure 29. Current Sensing Power MOSFETs



Control Circuitry Ground (Pin 16) and Current Sense Inverting Input (Pin 15) must return on separate paths to the Central Input Source Ground.

Virtually lossless current sensing can be achieved with the implementation of SENSEFET power switches.

Figure 30. High Voltage Boost Supply



This circuit generates V_{Boost} for Figure 25.

Figure 31. Differential Input Speed Controller

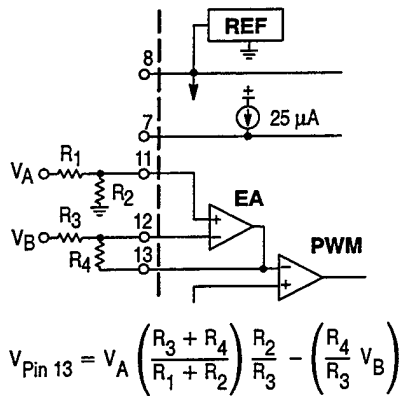
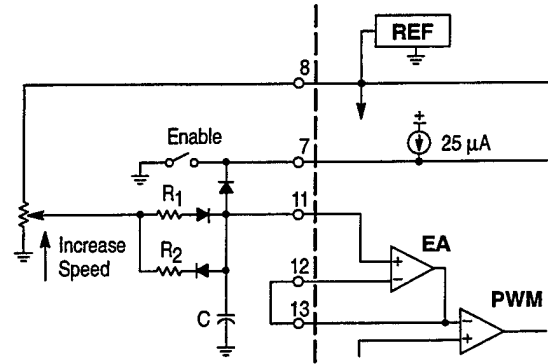
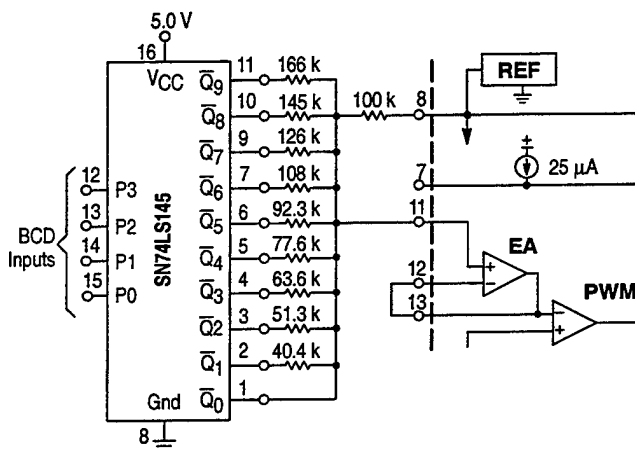


Figure 32. Controlled Acceleration/Deceleration



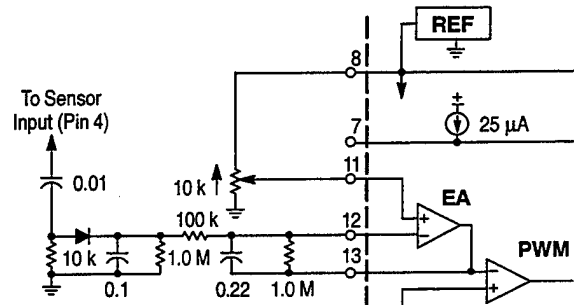
Resistor R_1 with capacitor C sets the acceleration time constant while R_2 controls the deceleration. The values of R_1 and R_2 should be at least ten times greater than the speed set potentiometer to minimize time constant variations with different speed settings.

Figure 33. Digital Speed Controller



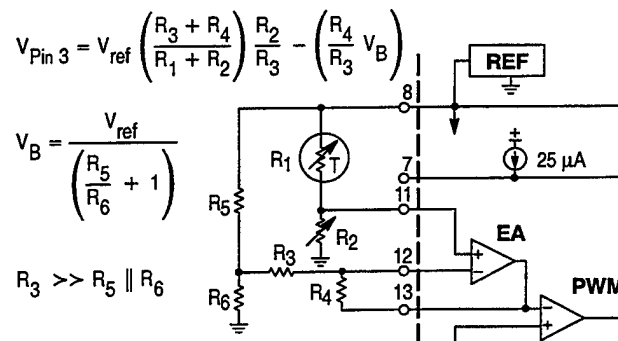
The SN74LS145 is an open collector BCD to One of Ten decoder. When connected as shown, input codes 0000 through 1001 steps the PWM in increments of approximately 10% from 0 to 90% on-time. Input codes 1010 through 1111 will produce 100% on-time or full motor speed.

Figure 34. Closed Loop Speed Control



The rotor position sensors can be used as a tachometer. By differentiating the positive-going edges and then integrating them over time, a voltage proportional to speed can be generated. The error amp compares this voltage to that of the speed set to control the PWM.

Figure 35. Closed Loop Temperature Control



This circuit can control the speed of a cooling fan proportional to the difference between the sensor and set temperatures. The control loop is closed as the forced air cools the NTC thermistor. For controlled heating applications, exchange the positions of R_1 and R_2 .

The three phase application shown in Figure 36 is a full-featured open loop motor controller with full wave, six step drive. The upper power switch transistors are Darlington's while the lower devices are power MOSFETs. Each of these devices contains an internal parasitic catch diode that is used to return the stator inductive energy back to the power supply. The outputs are capable of driving a delta or wye connected stator, and a grounded neutral wye if split supplies are used. At any given rotor position, only one top and one bottom power switch (of different totem poles) is enabled. This configuration switches both ends of the stator winding from supply to ground which causes the current flow to be bidirectional or full wave. A leading edge spike is usually present on the current waveform and can cause a current-limit instability. The spike can be eliminated by adding an RC filter in series with the Current Sense Input. Using a low inductance type resistor for R_S will also aid in spike reduction. Care must be taken in the selection of the

$$I_{\text{peak}} = \frac{V_M + \text{EMF}}{R_{\text{switch}} + R_{\text{winding}}}$$

If the motor is running at maximum speed with no load, the generated back EMF can be as high as the supply voltage, and at the onset of braking, the peak current may approach twice the motor stall current. Figure 37 shows the commutation waveforms over two electrical cycles. The first cycle (0° to 360°) depicts motor operation at full speed while the second cycle (360° to 720°) shows a reduced speed with about 50% pulse width modulation. The current waveforms reflect a constant torque load and are shown synchronous to the commutation frequency for clarity.

[illegible]

Figure 37. Three Phase, Six Step, Full Wave Commutation Waveforms

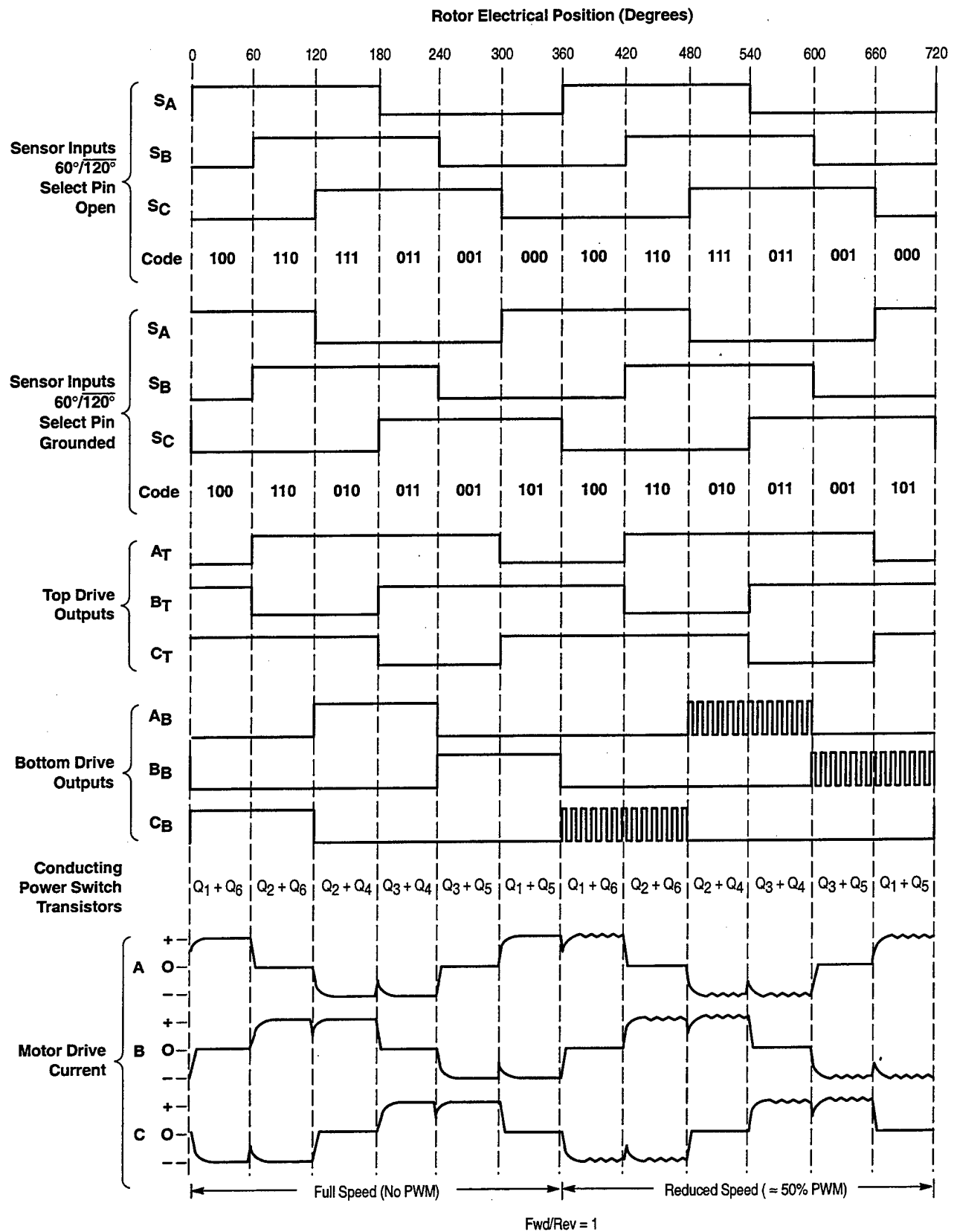
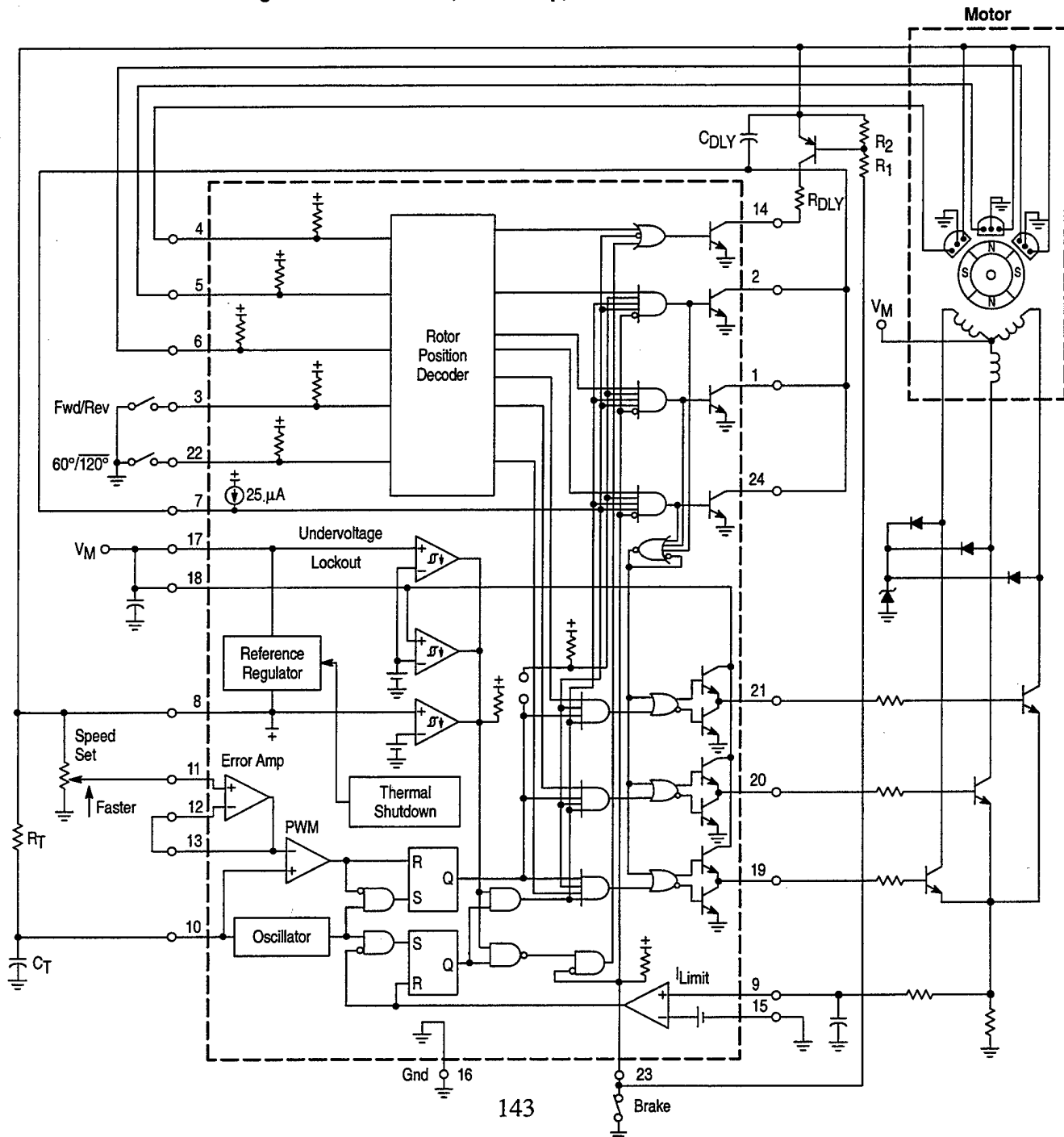


Figure 38 shows a three phase, three step, half wave motor controller. This configuration is ideally suited for automotive and other low voltage applications since there is only one power switch voltage drop in series with a given stator winding. Current flow is unidirectional or half wave because only one end of each winding is switched. Continuous braking with the typical half wave arrangement presents a motor overheating problem since stator current is limited only by the winding resistance. This is due to the lack of upper power switch transistors, as in the full wave circuit, used to disconnect the windings from the supply voltage V_M . A unique

solution is to provide braking until the motor stops and then turn off the bottom drives. This can be accomplished by using the $\overline{\text{Fault}}$ Output in conjunction with the Output Enable as an over current timer. Components R_{DLY} and C_{DLY} are selected to give the motor sufficient time to stop before latching the Output Enable and the top drive AND gates low. When enabling the motor, the brake switch is closed and the PNP transistor (along with resistors R_1 and R_{DLY}) are used to reset the latch by discharging C_{DLY} . The stator flyback voltage is clamped by a single zener and three diodes.

Figure 38. Three Phase, Three Step, Half Wave Motor Controller



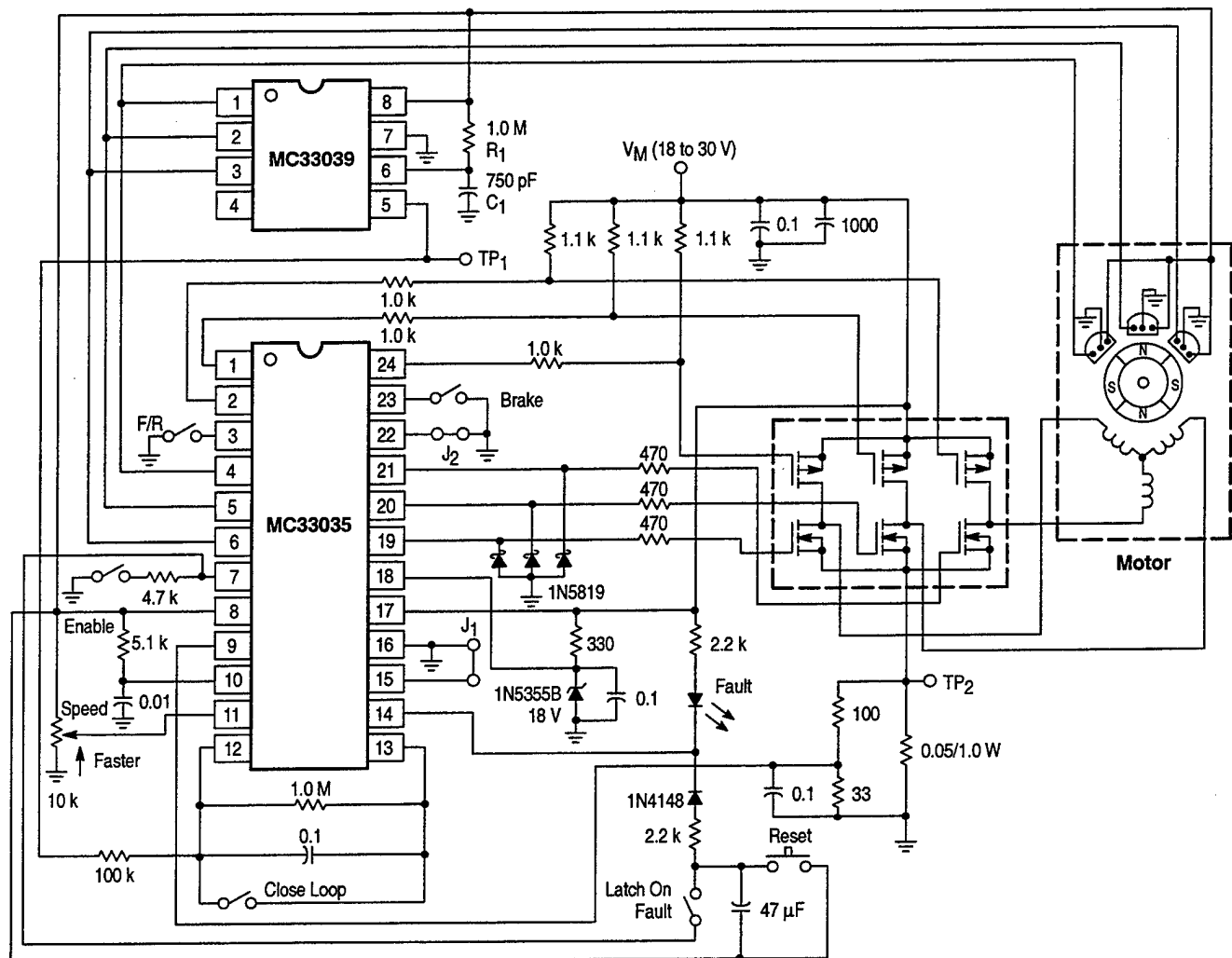
Three Phase Closed Loop Controller

The MC33035, by itself, is only capable of open loop motor speed control. For closed loop motor speed control, the MC33035 requires an input voltage proportional to the motor speed. Traditionally, this has been accomplished by means of a tachometer to generate the motor speed feedback voltage. Figure 39 shows an application whereby an MC33039, powered from the 6.25 V reference (Pin 8) of the MC33035, is used to generate the required feedback voltage without the need of a costly tachometer. The same Hall sensor signals used by the MC33035 for rotor position decoding are utilized by the MC33039. Every positive or negative going transition of the Hall sensor signals on any of the sensor lines causes the MC33039 to produce an output pulse of defined amplitude and time duration, as determined by the external resistor R_1 and capacitor C_1 . The output train

of pulses at Pin 5 of the MC33039 are integrated by the error amplifier of the MC33035 configured as an integrator to produce a DC voltage level which is proportional to the motor speed. This speed proportional voltage establishes the PWM reference level at Pin 13 of the MC33035 motor controller and closes the feedback loop. The MC33035 outputs drive a TMOS power MOSFET 3-phase bridge. High currents can be expected during conditions of start-up, breaking, and change of direction of the motor.

The system shown in Figure 39 is designed for a motor having 120/240 degrees Hall sensor electrical phasing. The system can easily be modified to accommodate 60/300 degree Hall sensor electrical phasing by removing the jumper (J_2) at Pin 22 of the MC33035.

Figure 39. Closed Loop Brushless DC Motor Control Using The MC33035 and MC33039



Sensor Phasing Comparison

There are four conventions used to establish the relative phasing of the sensor signals in three phase motors. With six step drive, an input signal change must occur every 60 electrical degrees; however, the relative signal phasing is dependent upon the mechanical sensor placement. A comparison of the conventions in electrical degrees is shown in Figure 40. From the sensor phasing table in Figure 41, note that the order of input codes for 60° phasing is the reverse of 300°. This means the MC33035, when configured for 60° sensor electrical phasing, will operate a motor with either 60° or 300° sensor electrical phasing, but resulting in opposite directions of rotation. The same is true for the part when it is configured for 120° sensor electrical phasing; the motor will operate equally, but will result in opposite directions of rotation for 120° for 240° conventions.

Figure 40. Sensor Phasing Comparison

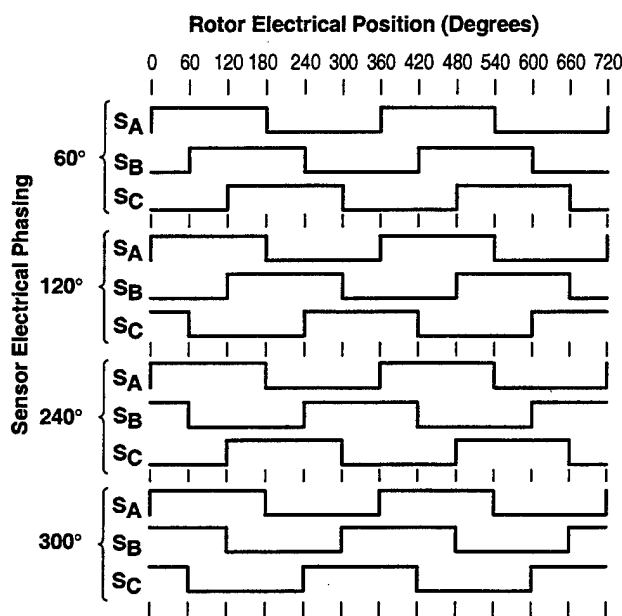


Figure 41. Sensor Phasing Table

Sensor Electrical Phasing (Degrees)											
60°			120°			240°			300°		
SA	SB	SC	SA	SB	SC	SA	SB	SC	SA	SB	SC
1	0	0	1	0	1	1	1	0	1	1	1
1	1	0	1	0	0	1	0	0	1	1	0
1	1	1	1	1	0	1	0	1	1	0	0
0	1	1	0	1	0	0	0	1	0	0	0
0	0	1	0	1	1	0	1	1	0	0	1
0	0	0	0	0	1	0	1	0	0	1	1

In this data sheet, the rotor position is always given in electrical degrees since the mechanical position is a function of the number of rotating magnetic poles. The relationship between the electrical and mechanical position is:

$$\text{Electrical Degrees} = \text{Mechanical Degrees} \left(\frac{\# \text{Rotor Poles}}{2} \right)$$

An increase in the number of magnetic poles causes more electrical revolutions for a given mechanical revolution. General purpose three phase motors typically contain a four pole rotor which yields two electrical revolutions for one mechanical.

Two and Four Phase Motor Commutation

The MC33035 is also capable of providing a four step output that can be used to drive two or four phase motors. The truth table in Figure 42 shows that by connecting sensor inputs S_B and S_C together, it is possible to truncate the number of drive output states from six to four. The output power switches are connected to B_T , C_T , B_B , and C_B . Figure 43 shows a four phase, four step, full wave motor control application. Power switch transistors Q_1 through Q_8 are Darlington type, each with an internal parasitic catch diode. With four step drive, only two rotor position sensors spaced at 90 electrical degrees are required. The commutation waveforms are shown in Figure 44.

Figure 45 shows a four phase, four step, half wave motor controller. It has the same features as the circuit in Figure 38, except for the deletion of speed control and braking.

Figure 42. Two and Four Phase, Four Step, Commutation Truth Table

MC33035 (60°/120° Select Pin Open)						
Inputs			Outputs			
Sensor Electrical Spacing* = 90°			Top Drives		Bottom Drives	
S_A	S_B	F/R	B_T	C_T	B_B	C_B
1	0	1	1	1	0	1
1	1	1	0	1	0	0
0	1	1	1	0	0	0
0	0	1	1	1	1	0
1	0	0	1	0	0	0
1	1	0	1	1	1	0
0	1	0	1	1	0	1
0	0	0	0	1	0	0

*With MC33035 sensor input S_B connected to S_C .

Figure 43. Four Phase, Four Step, Full Wave Motor Controller

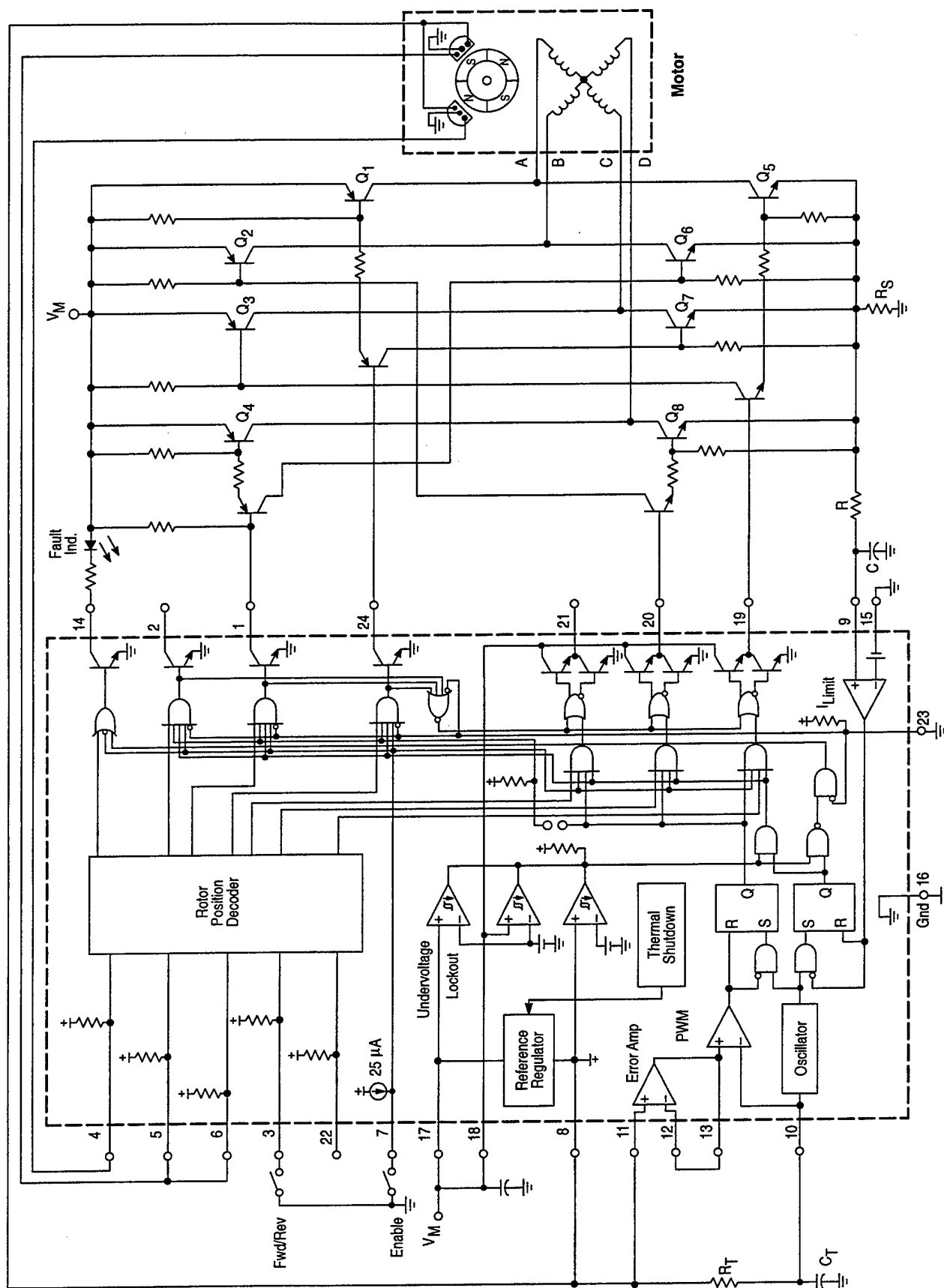


Figure 44. Four Phase, Four Step, Full Wave Motor Controller

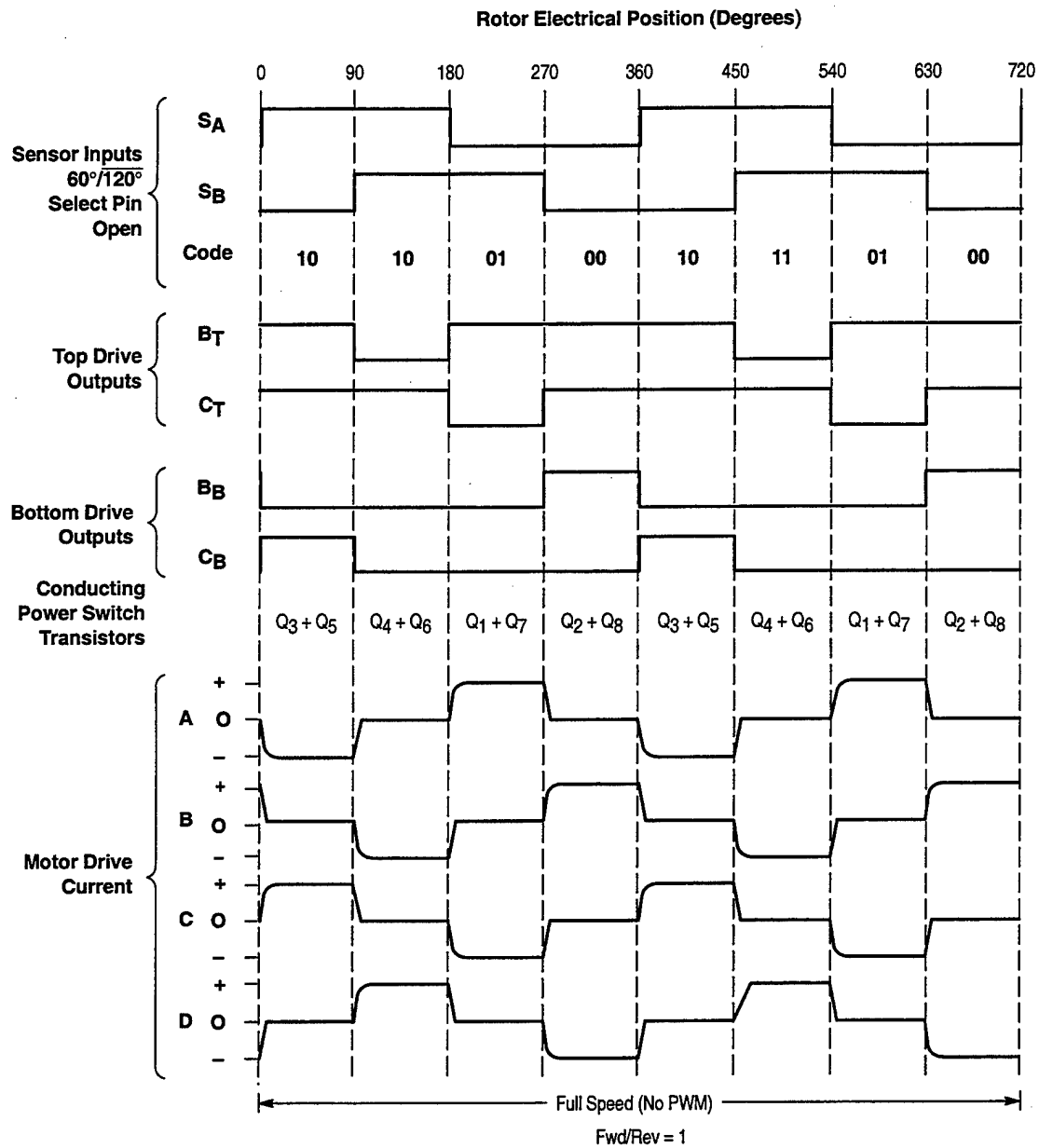
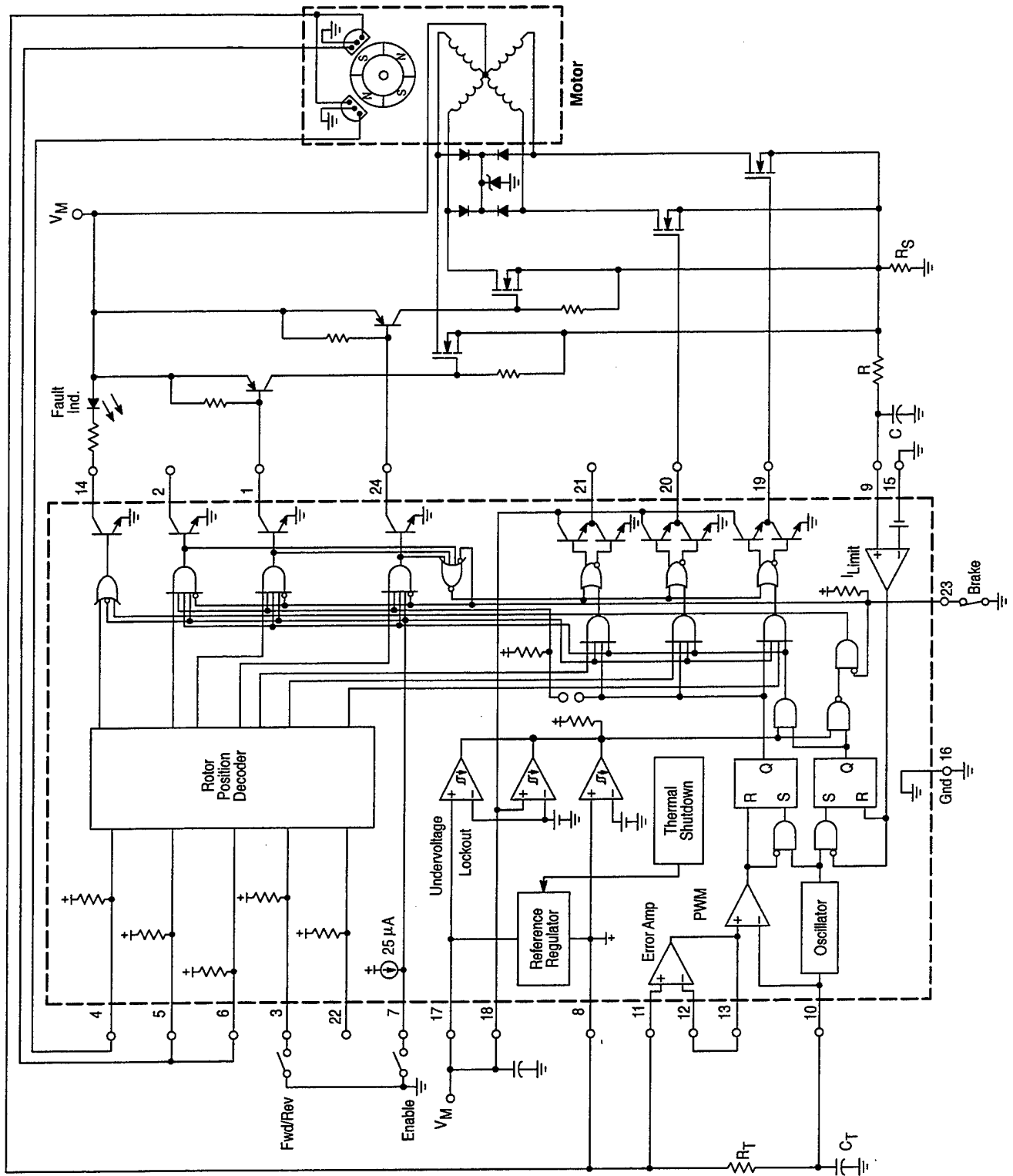


Figure 45. Four Phase, Four Step, Half Wave Motor Controller



Brush Motor Control

Though the MC33035 was designed to control brushless DC motors, it may also be used to control DC brush type motors. Figure 46 shows an application of the MC33035 driving a MOSFET H-bridge affording minimal parts count to operate a brush-type motor. Key to the operation is the input sensor code [100] which produces a top-left (Q_1) and a bottom-right (Q_3) drive when the controller's forward/reverse pin is at logic [1]; top-right (Q_4), bottom-left (Q_2) drive is realized when the Forward/Reverse pin is at logic [0]. This code supports the requirements necessary for H-bridge drive accomplishing both direction and speed control.

The controller functions in a normal manner with a pulse width modulated frequency of approximately 25 kHz. Motor speed is controlled by adjusting the voltage presented to the noninverting input of the error amplifier establishing the PWM's slice or reference level. Cycle-by-cycle current limiting of the motor current is accomplished by sensing the voltage (100 mV) across the R_S resistor to ground of the H-bridge motor current. The over current sense circuit makes it possible to reverse the direction of the motor, using the

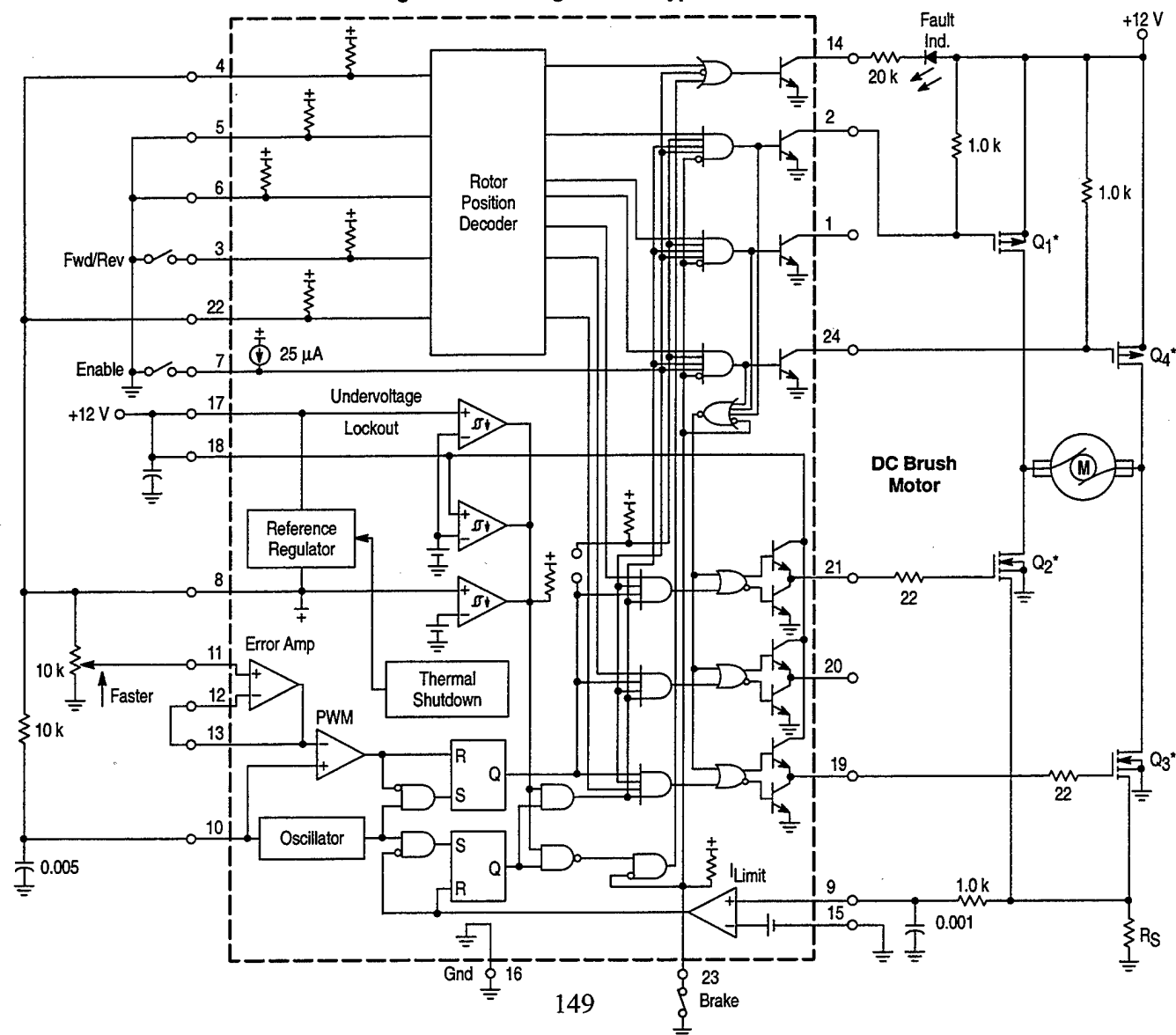
normal forward/reverse switch, on the fly and not have to completely stop before reversing.

LAYOUT CONSIDERATIONS

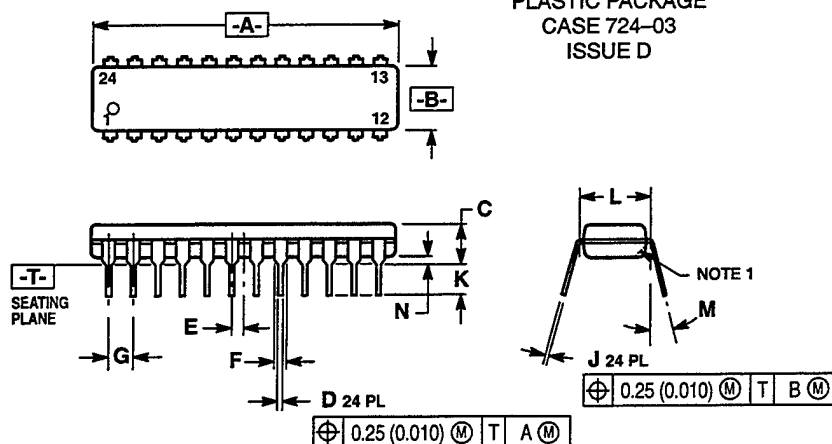
Do not attempt to construct any of the brushless motor control circuits on wire-wrap or plug-in prototype boards. High frequency printed circuit layout techniques are imperative to prevent pulse jitter. This is usually caused by excessive noise pick-up imposed on the current sense or error amp inputs. The printed circuit layout should contain a ground plane with low current signal and high drive and output buffer grounds returning on separate paths to the power supply input filter capacitor V_M . Ceramic bypass capacitors (0.1 μ F) connected

close to the integrated circuit at V_{CC} , V_C , V_{ref} and the error amp noninverting input may be required depending upon circuit layout. This provides a low impedance path for filtering any high frequency noise. All high current loops should be kept as short as possible using heavy copper runs to minimize radiated EMI.

Figure 46. H-Bridge Brush-Type Controller

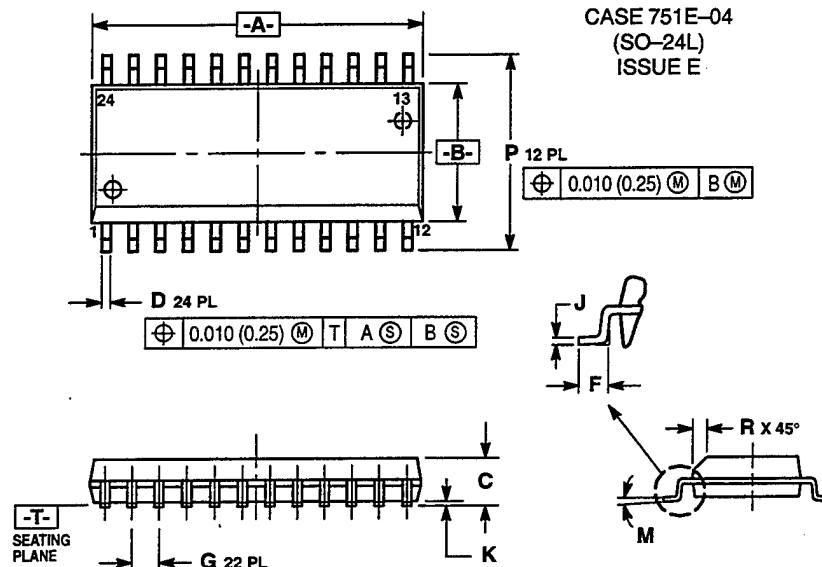


OUTLINE DIMENSIONS

P SUFFIX
PLASTIC PACKAGE
CASE 724-03
ISSUE D


- NOTES:
1. CHAMFERED CONTOUR OPTIONAL.
 2. DIMENSION L TO CENTER OF LEADS WHEN FORMED PARALLEL.
 3. DIMENSIONING AND TOLERANCING PER ANSI Y14.5M, 1982.
 4. CONTROLLING DIMENSION: INCH.

DIM	MIN	MAX	MIN	MAX
A	1.230	1.265	31.25	32.13
B	0.250	0.270	6.35	6.85
C	0.145	0.175	3.69	4.44
D	0.015	0.020	0.38	0.51
E	0.050 BSC		1.27 BSC	
F	0.040	0.060	1.02	1.52
G	0.100 BSC		2.54 BSC	
J	0.007	0.012	0.18	0.30
K	0.110	0.140	2.80	3.55
L	0.300 BSC		7.62 BSC	
M	0°	15°	0°	15°
N	0.020	0.040	0.51	1.01

DW SUFFIX
PLASTIC PACKAGE
CASE 751E-04
(SO-24L)
ISSUE E


- NOTES:
1. DIMENSIONING AND TOLERANCING PER ANSI Y14.5M, 1982.
 2. CONTROLLING DIMENSION: MILLIMETER.
 3. DIMENSIONS A AND B DO NOT INCLUDE MOLD PROTRUSION.
 4. MAXIMUM MOLD PROTRUSION 0.15 (0.006) PER SIDE.
 5. DIMENSION D DOES NOT INCLUDE DAMBAR PROTRUSION. ALLOWABLE DAMBAR PROTRUSION SHALL BE 0.13 (0.005) TOTAL IN EXCESS OF D DIMENSION AT MAXIMUM MATERIAL CONDITION.

DIM	MIN	MAX	MIN	MAX
A	15.25	15.54	0.601	0.612
B	7.40	7.60	0.292	0.299
C	2.35	2.65	0.093	0.104
D	0.35	0.49	0.014	0.019
F	0.41	0.90	0.016	0.035
G	1.27 BSC		0.050 BSC	
J	0.23	0.32	0.009	0.013
K	0.13	0.29	0.005	0.011
M	0°	8°	0°	8°
P	10.05	10.55	0.395	0.415
R	0.25	0.75	0.010	0.029

Motorola reserves the right to make changes without further notice to any products herein. Motorola makes no warranty, representation or guarantee regarding the suitability of its products for any particular purpose, nor does Motorola assume any liability arising out of the application or use of any product or circuit, and specifically disclaims any and all liability, including without limitation consequential or incidental damages. "Typical" parameters which may be provided in Motorola data sheets and/or specifications can and do vary in different applications and actual performance may vary over time. All operating parameters, including "Typicals" must be validated for each customer application by customer's technical experts. Motorola does not convey any license under its patent rights nor the rights of others. Motorola products are not designed, intended, or authorized for use as components in systems intended for surgical implant into the body, or other applications intended to support or sustain life, or for any other application in which the failure of the Motorola product could create a situation where personal injury or death may occur. Should Buyer purchase or use Motorola products for any such unintended or unauthorized application, Buyer shall indemnify and hold Motorola and its officers, employees, subsidiaries, affiliates, and distributors harmless against all claims, costs, damages, and expenses, and reasonable attorney fees arising out of, directly or indirectly, any claim of personal injury or death associated with such unintended or unauthorized use, even if such claim alleges that Motorola was negligent regarding the design or manufacture of the part. Motorola and are registered trademarks of Motorola, Inc. Motorola, Inc. is an Equal Opportunity/Affirmative Action Employer.

Mfax is a trademark of Motorola, Inc.

How to reach us:

USA/EUROPE/Locations Not Listed: Motorola Literature Distribution;
P.O. Box 5405, Denver, Colorado 80217. 1-303-675-2140 or 1-800-441-2447

JAPAN: Motorola Japan Ltd.; SPD, Strategic Planning Office, 141,
4-32-1 Nishi-Gotanda, Shinagawa-ku, Tokyo, Japan. 81-3-5487-8488

Customer Focus Center: 1-800-521-6274

Mfax™: RMFA00@email.sps.mot.com – TOUCHTONE 1-602-244-6609
Motorola Fax Back System – US & Canada ONLY 1-800-774-1848
– http://sps.motorola.com/mfax/

ASIA/PACIFIC: Motorola Semiconductors H.K. Ltd.; 8B Tai Ping Industrial Park,
51 Ting Kok Road, Tai Po, N.T., Hong Kong. 852-26629298

HOME PAGE: http://motorola.com/sps/

***So, just what
is a
Fuel Cell,
anyway????***

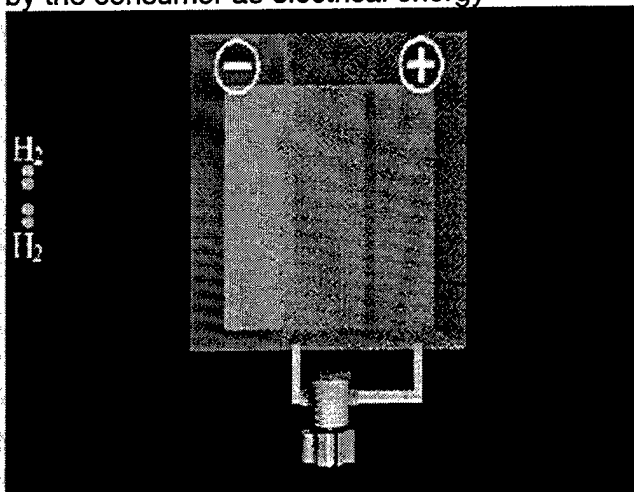
A fuel cell converts chemical energy to electrical energy. It is a device that uses the electrochemical reaction of hydrogen and an oxidant such as oxygen to produce electrical energy silently, without combustion.

The fuel cell was invented in 1839 by Sir William Grove; however, it wasn't until 1950 that Francis T. Bacon demonstrated a practical, working fuel cell.

Fuel Cells were further developed by the US in the 1960's for use in the Gemini and Apollo missions. Today fuel cells provide the Space Shuttle with ALL its needs for electric power, as well as its pure drinking water.

The initial advancements in fuel cell technology have come from the space program. H Power has advanced that technology by reducing fuel cell size and weight, while increasing its power output. H Power's proprietary technologies now make mass production of fuel cell systems commercially feasible.

Here you see the internal workings of H Power's Hydrogen Fuel Cell. The hydrogen fuel (H_2) enters the fuel cell which, like a battery, has a negative and a positive electrode. As the hydrogen molecules come into contact with the negative electrode, they split into two atoms and then react electrochemically, forming **PROTONS** and **ELECTRONS**. The electrons flow out of the cell to be used by the consumer as electrical energy



Meanwhile, the protons pass across the **PROTON EXCHANGE MEMBRANE** (or PEM) to the positive electrode where they combine with atomic Oxygen, split from oxygen molecules brought into the fuel cell from the air and with the electrons from the external circuit, to form water molecules.

Other than water, the only by-product of this process is heat, which may be reclaimed to increase the already high efficiency of the fuel cell even further.

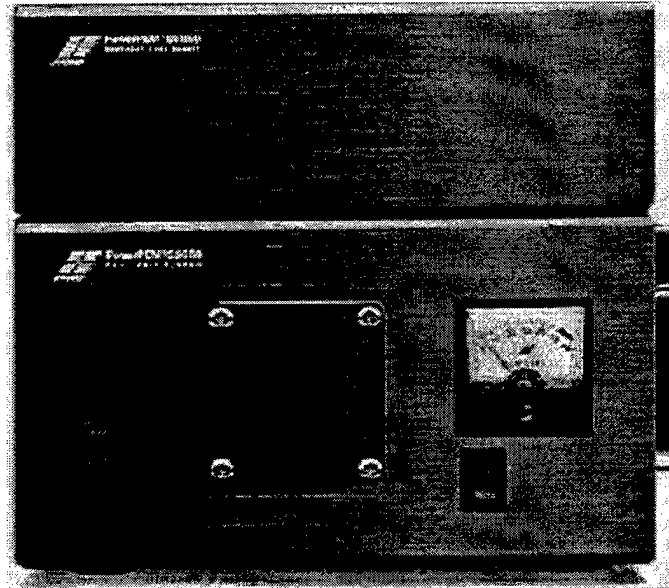
Batteries store their energy in the power-producing electrodes which are consumed as power is delivered. When the chemical energy in the electrodes is depleted, the battery must either be discarded (primary type) or recharged using an external energy source (secondary type). Fuel cells, on the other hand, have the distinct advantage of being able to store their energy external to the fuel cell stack. This advantage allows the fuel cell to produce electricity continuously as long as fuel is supplied.

The World's Most Advanced Portable Generator Uses the Most Abundant Energy in the Universe.

-HYDROGEN-

PowerPEM™-SSG50

**Fuel Cell Power Source
for Portable Power Applications**



The new H Power **PowerPEM™-SSG50** provides highly efficient, and continuous 12 volt power to any DC electrical device, from a module smaller than a shoe box. The run time at the maximum 50 Watt power rating is 4 hours on one "fill-up."

(above - top view with cover removed)
(below - left and right side views)

In fact, the **PowerPEM™-SSG50** is so clean and convenient, the only thing more impressive than the unit itself, is all that you can do with it.

Main Specifications:

Fuel Cell System: Module

Type:

Solid-state Proton-Exchange Membrane (PEM) fuel cell system operating on oxygen from ambient air and clean hydrogen fuel, with auxiliaries and electronic controls

Dimensions:

10.5 (W) x 5.5 (H) x 7.0 (D)

[267 (W) x 140 (H) x 175 (D) mm]

Weight:

Approx. 7.5 lb [3.41 kg]

Energy Source:

Metal-Hydride hydrogen cartridges

Power Output:

Regulated 11.5 VDC to 14.0 VDC

Power Rating:

50 watts DC

Hydrogen Fuel Supply Module:

Dimensions:

10.0 (W) x 2.8 (H) x 6.5 (D)

[254 (H) x 71 (H) x 165 (D) mm]

Weight:

Approx. 7.0 lb [3.2 kg]

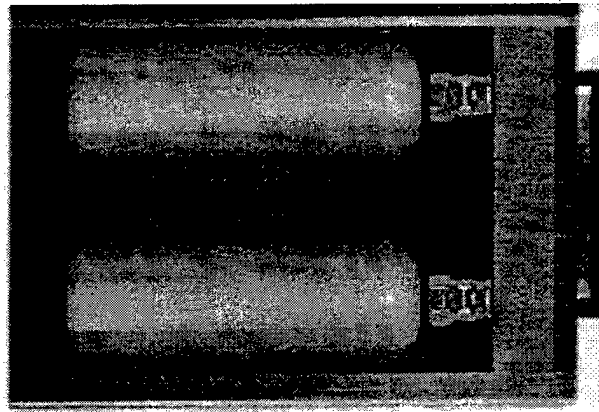
with metal-hydride cartridges installed

Operating Environment:

Normal ambient conditions

Temperature range:

32°F - 105°F [0°C - 40°C]



TYPES OF FUEL CELLS

Phosphoric Acid

Proton Exchange Membrane or Solid Polymer

Molten Carbonate

Solid Oxide

Alkaline

Other Fuel Cells

Phosphoric Acid. This is the most commercially developed type of fuel cell. It is already being used in such diverse applications as hospitals, nursing homes, hotels, office buildings, schools, utility power plants, and an airport terminal. Phosphoric acid fuel cells generate electricity at more than 40% efficiency -- and nearly 85% if steam this fuel cell produces is used for co-generation compared to 30% for the most efficient internal combustion engine. Operating temperatures are in the range of 400 degrees F. These fuel cells also can be used in larger vehicles, such as buses and locomotives.

Proton Exchange Membrane. These cells operate at relatively low temperatures (about 200 degrees F), have high power density, can vary their output quickly to meet shifts in power demand, and are suited for applications, -- such as in automobiles where quick startup is required. According to the U.S. Department of Energy, "they are the primary candidates for light-duty vehicles, for buildings, and potentially for much smaller applications such as replacements for rechargeable batteries in video cameras."

Molten Carbonate. Molten carbonate fuel cells promise high fuel-to-electricity efficiencies and the ability to consume coal-based fuels. This cell operates at about 1,200 degrees F. The first full-scale molten carbonate stacks have been tested, and demonstration units are being readied for testing in California in 1996.

Solid Oxide. Another highly promising fuel cell, the solid oxide fuel cell could be used in big, high -power

applications including industrial and large-scale central electricity generating stations. Some developers also see solid oxide use in motor vehicles. A 100-kilowatt test is being readied in Europe. Two small, 25-kilowatt units are already on line in Japan. A solid oxide system usually uses a hard ceramic material instead of a liquid electrolyte, allowing operating temperatures to reach 1,800 degrees F. Power generating efficiencies could reach 60%. One type of solid oxide fuel cell uses an array of meter-long tubes. Other variations include a compressed disc that resembles the top of a soup can.

Alkaline. Long used by NASA on space missions, these cells can achieve power generating efficiencies of up to 70 percent. They use alkaline potassium hydroxide as the electrolyte. Until recently they were too costly for commercial applications, but several companies are examining ways to reduce costs and improve operating flexibility.

Other Fuel Cells. Direct methanol fuel cells (DMFC) are a relatively new member of the fuel cell family. These cells are similar to the PEM cells in that they both use a polymer membrane as the electrolyte. However, in the DMFC, the anode catalyst itself draws the hydrogen from the liquid methanol, eliminating the need for a fuel Reformer. Efficiencies of about 40% are expected with this type of fuel cell, which would typically operate at a temperature between 120-190 degrees F. Higher efficiencies are achieved at higher temperatures. Regenerative fuel cells. Still a very young member of the fuel cell family, regenerative fuel cells would be attractive as a closed-loop form of power generation. Water is separated into hydrogen and oxygen by a solar-powered electrolyser. The hydrogen and oxygen are fed into the fuel cell which generates electricity, heat and water. The water is then recirculated back to the solar-powered electrolyser and the process begins again. These types of fuel cells are currently being researched by NASA and others worldwide.

LIST OF REFERENCES

1. Finbar Sheehy, *The Hang Gliders Technical Notebook*, Faoilean Press, Pasadena, CA, 1992
2. Thomas J. Sokira and Wolfgang Jaffe, *Brushless DC Motors, Electronic Commutation and Controls*, TAB BOOKS Inc., Blue Ridge Summit, PA, 1990
3. David Halliday, Robert Resnick, and Jearl Walker, *Fundamentals of Physics*, Extended, Fourth Edition, John Wiley and Sons, Inc., New York, NY 1993
4. *GM Sunraycer Case History*, Society of Automotive Engineers, Inc., Warrendale, PA, 1992
5. Fuel Cells 2000,
<http://www.fuelcells.org/fuel/fctypes.shtml>
6. Mark Drela, Professor of Aerodynamics, Massachusetts Institute of Technology, XROTOR User Guide
7. Charles N. Adkins and Robert H. Liebeck, "Design of Optimum Propellers," *Journal of Propulsion and Power*, Vol 10, No 5, Sept-Oct 1994
8. <http://mot-sps.com/documentation/>, Motorola Technical Manual, MC33035 Brushless Motor Controller.
9. John D. Anderson, Jr, *Fundamentals of Aerodynamics*, Second Edition, McGraw-Hill, Inc., New York, NY, 1991
10. John D. Anderson, Jr, *Introduction to Flight*, Third Edition, McGraw-Hill, New York, NY, 1989
11. Dennis Pagen, *Hang Gliding Training Manual*, Sport Aviation Publications, Mingoville, PA, 1995
12. Barnes W McCormick, Jr., *Aerodynamics of V/STOL Flight*, Academic Press, New York, London, 1967
13. AA 2036 *Performance and Static Stability Workbook*, Naval Postgraduate School, 1997
14. Generic Battery Technology Comparsion,
m.t.thompson@ieee.org
15. Ultralife Batteries Inc., Product Data,
<http://www2.ulbi.com/ssss.html>
16. Yardney Technology Products, Inc., *Rechargeable Silver*

Cells, Pawcatuck, CT, 1999

17. So Just What is a Fuel Cell Anyway???,
http://www.HPower.com/What_is.htm
18. Fisher Electric Inc., <http://www.fisherelectric.com>
19. Wills Wing,
http://www.willswing.com/Hgliders/falcon_review.htm
20. Nargafly, <http://www.avnet.co.uk/bmaa/mf97/mfjf97h.htm>
21. French Ultralight,
http://perso.clubinternet.fr/ulmdev/pages_individuelles//asso_et_prolpulms/frame.html
22. Mosquito, <http://homepages.enterprise.net/skysufer/>
23. Twin Motor Design, tschupsk@nwl.com
24. Airwave Hang Glider,
<http://www.airwavegliders.co.uk/home/Products/products.html>

INITIAL DISTRIBUTION LIST

1. Defense Technical Information Center 2
8725 John J. Kingman Rd., STE 0944
Ft. Belvoir, Virginia 22060-6218
2. Dudley Knox Library 2
Naval Postgraduate School
411 Dyer Rd.
Monterey, California 93943-5101
3. Chairman, Code EC 1
Department of Electrical and Computer Engineering
Naval Postgraduate School
Monterey, California 93943-5121
4. Professor Xiaoping Yun, Code EC/YX 2
Department of Electrical and Computer Engineering
Naval Postgraduate School
Monterey, California 93943-5121
5. Professor Jovan Lebaric, Code EC/LJ 2
Department of Electrical and Computer Engineering
Naval Postgraduate School
Monterey, California 93943-5121
6. Professor, Conrad Newberry, Code AA/NC 1
Department of Electrical and Computer Engineering
Naval Postgraduate School
Monterey, California 93943-5106
7. Professor John Ciezki, Code EC/CY 1
Department of Electrical and Computer Engineering
Naval Postgraduate School
Monterey, California 93943-5121
8. Professor Mike Shields, Code EC/SM 1
Department of Electrical and Computer Engineering
Naval Postgraduate School
Monterey, California 93943-5121
9. J (PL-TS) 1
Mr. Chuck Mirabile
SPAWARSYSCEN D13541
49275 ELECTRON DR, BLDG 33, RM 2526
San Diego, California 92152-5435
10. MAJOR Rodney S. Nolan, USMC 2
9 Burns Rd.
Stafford, Virginia 22554